ACOUSTIC CHARACTERISTICS OF PERFORATED DISSIPATIVE AND HYBRID SILENCERS

DISSERTATION

Presented in Partial Fulfillment of the Requirements for

the Degree Doctor of Philosophy in the Graduate

School of The Ohio State University

By

Iljae Lee, M.S.

* * * * *

The Ohio State University
2005

Dissertation Committee:

Professor Ahmet Selamet, Adviser

Professor Rajendra Singh

Professor Mohammad Samimy

Dr. Norman T. Huff

Approved by

_____

Adviser

Graduate Program in Mechanical Engineering

ABSTRACT

Acoustic characteristics of silencers filled with fibrous material (hence dissipative) are investigated. Following a theoretical and experimental analysis of a single-pass, perforated, dissipative concentric silencer, the study is extended to a hybrid silencer designed by combining dissipative and reflective (Helmholtz resonator) components. The ability to model these silencers relies heavily on the understanding of the acoustic behavior of the fibrous material and the perforations. Therefore, the present study has developed two experimental setups to measure: (a) the complex characteristic impedance and the wavenumber of the fibrous material with varying filling density and texturization conditions, and (b) the acoustic impedance of perforations in contact with the fibrous material, and with and without the mean flow. New empirical expressions are then provided for the acoustic impedance of perforations with varying porosity, hole diameter, wall thickness, mean flow rate, and the fiber characteristics. The experimental results illustrate that the presence of absorbent significantly increases both the resistance and reactance of the perforation impedance. The addition of mean flow is also shown in general to increase the resistance, while decreasing the reactance particularly at low porosities.

The empirical expressions for the fiber acoustic properties and the perforation impedance are then integrated into the predictions of transmission loss. These predictions are based primarily on a three-dimensional boundary element method (BEM) developed in the present study, due to its ability to treat silencers with complex internals, in addition to one- and two-dimensional analytical approaches also introduced. Comparisons of predictions with the acoustic attenuation experiments support the proposed relationships for the properties of fibrous material and the perforation impedance. The influence of the internal geometry modifications of dissipative silencers, such as baffles and extended inlet/outlet, and the impact of connecting duct length between a pair of silencers, are investigated with BEM. Hence, the contributions of the present study include the development of methodologies for the measurement of acoustic properties of the fibrous material and the impedance of perforations, particularly in contact with the absorbent along with the resulting empirical expressions, thereby assisting towards analytical and computational design tools for the dissipative and hybrid silencers.

Dedicated to my parents and wife

ACKNOWLEDGMENTS

I truly thank my adviser, Professor Ahmet Selamet, for his guidance and support during my Ph.D. studies, as well as his patience in correcting this dissertation. I hope that I reflect, in this work, his enthusiasm for and dedication to scientific truth. I am also in debt to Professor Ahmet Selamet for giving me opportunities to disseminate the findings through publications and presentations.

I would like to thank Owens Corning and Dr. Norman T. Huff for providing the financial support for this work. I am grateful to Dr. Norman T. Huff for many productive discussions and his gracious personality.

I also wish to express thanks to my committee members, Professors Rajendra Singh and Mohammad Samimy, and Dr. Norman T. Huff, for their valuable feedback and suggestions on this dissertation.

I am grateful to the current and former members of the research group who helped me: Dr. Nolan Dickey, Dr. Emel Selamet, Dr. Mubing Xu, Adam Christian, Don Williams, Cam Giang, Lauren Lecuru, Yuesheng He, Jacques Paul, Vincent Mariucci, and Yale Jones. I particularly thank Dr. Nolan Dickey for discussing with me various aspects of this investigation.

Finally, this dissertation is dedicated to my parents and wife, Jungmi. Thank you for your unconditional love, support, and understanding.

VITA

March 19, 1969 .....Born – Seoul, Korea

1999.....M.S.M.E., The Ohio State University

1995.....B.S.M.E., Yonsei University, Korea

1997 – present .....Graduate Research Associate,
The Ohio State University

JOURNAL PUBLICATIONS

1. Selamet, A., Xu, M. B., Lee, I.-J., and Huff, N. T., 2005, "Analytical approach for sound attenuation in perforated dissipative silencers with inlet/outlet extensions," *Journal of the Acoustical Society of America* **117**, 2078-2089.

2. Selamet, A., Xu, M. B., Lee, I.-J., and Huff, N. T., 2005, "Helmholtz resonator lined with absorbing material," *Journal of the Acoustical Society of America* **117**, 725-733.

3. Selamet, A., Xu, M. B., Lee, I.-J., and Huff, N. T., 2004, "Analytical approach for sound attenuation in perforated dissipative silencers," *Journal of the Acoustical Society of America* **115**, 2091-2099.

4. Xu, M. B., Selamet, A., Lee, I.-J., and Huff, N. T., 2004, "Sound attenuation in dissipative expansion chambers," *Journal of Sound and Vibration* **272**, 1125-1133.

5. Selamet, A. and Lee, I.-J., 2003, "Helmholtz resonator with extended neck," *Journal of the Acoustical Society of America* **113**, 1975-1985.

6. Selamet, A., Lee, I.-J., and Huff, N. T., 2003, "Acoustic attenuation of hybrid silencers," *Journal of Sound and Vibration* **262**, 509-527.

FIELD OF STUDY

Mechanical Engineering

TABLE OF CONTENTS

Page

LIST OF TABLES

LIST OF FIGURES

CHAPTER 1

INTRODUCTION

1.1 Background

Due to its significant acoustic attenuation characteristics at high frequencies, fibrous material has been used in interior sound absorption and silencers of machinery that generates high frequency noise while operating at low temperature and flow velocities, for example, heating, ventilation and air-conditioning (HVAC) systems, or fans. In spite of their desirable acoustic characteristics, the use of traditional absorbing material in the intake and exhaust systems of internal combustion engines has been limited, due to environmental concerns such as blowout of fibers due to flow and mechanical/chemical failure of the fibers at high temperatures. However, recent developments in materials and the demand for improved silencer performance in industry have led to a renewed interest in dissipative silencers. The blowout has been practically eliminated by the use of continuous strand fiber, such as the Advantex® fiber developed by Owens Corning, coupled with the perforated tubes. In addition to desirable acoustic characteristics, dissipative silencers may offer additional advantages such as improved flow efficiency and thermal insulation. For example, in internal combustion engines, lower backpressure from higher flow efficiency will improve the engine performance,

and lower muffler skin temperatures due to thermal insulation may reduce the thermal fatigue.

A simple dissipative silencer consists of a perforated main duct and an outer chamber filled with absorbing material. Attenuation of acoustic waves in the absorbing material is mainly due to viscous and thermal dissipation. Therefore, the acoustic properties of absorbing material are essential to understand the noise control by dissipative silencers. In general, the complex numbers of characteristic impedance and wavenumber are employed to account for the dissipation of wave through the absorbing material. Due to the complex structure of absorbing material, these acoustic properties are often determined experimentally (Delany and Bazley, 1970). Perforated ducts are used in reactive silencers to improve the acoustic performance at low frequencies, to reduce flow losses, and to minimize generation of flow noise from abrupt cross-sectional area changes. In dissipative silencers, perforated ducts are also used to protect the absorbing material and to control the acoustic behavior of the silencers by adding mainly reactance to the impedance. While the acoustic characteristics of a perforated duct within a reactive silencer is relatively well established primarily by experiments (refer, for example, to Sullivan and Crocker [1978]), the effect of a perforated duct in contact with absorbing material remains to be investigated.

The exhaust systems of internal combustion engines generate noise with a wide frequency range, including particularly strong low frequency components. In such applications, dissipative silencers can be enhanced at low frequencies by reactive acoustic elements such as Helmholtz or quarter wave resonators. The combination of dissipative and reactive components defines the hybrid silencer, which is an effective noise

attenuator over a wide range of frequencies. Hybrid silencers commonly have multiple chambers connected to each other by ducts. The interactions among these chambers may substantially affect the overall performance of hybrid silencers. Thus, the design of hybrid silencers requires understanding of acoustic characteristics of individual dissipative and reactive elements, as well as the interactions among them. The significance of such interactions for reactive chambers and resonators was demonstrated by Davis *et al.* (1953). However, interactions between dissipative and reactive components remain to be investigated.

1.2 Objective

The objective of the present study is to analytically, computationally and experimentally investigate the acoustic behavior of hybrid silencers that consist of dissipative and reactive components including mean flow effect. First, the acoustic performance of uniformly perforated cylindrical dissipative silencers is explored with varying duct porosity, hole diameter, and filling density. The transmission loss predictions from analytical and computational approaches for these configurations are compared with the experiments. Finally, the analytical and numerical approaches are utilized to illustrate the effect of both individual chamber configuration and the connecting tubes (or the relative location of the chambers) on the acoustic performance of the hybrid silencers.

One-dimensional decoupled and two-dimensional analytical approaches and three-dimensional boundary element method (BEM) are developed to predict the transmission loss of silencers. Two experimental setups are developed in the present

study to determine the acoustic properties of absorbing material, the perforation impedance, and the transmission loss. The first setup is used to measure the acoustic properties of absorbing materials, the impedance of perforations facing absorbent or air, and the transmissions loss in the absence of mean flow. The second setup is designed to measure, in the presence of mean flow: (1) the acoustic impedance of perforations facing absorbing material, and (2) the transmission loss of silencers. Based on these experimental results, the characteristic impedance and the wavenumber of absorbing material are presented along with an empirical formulation for the acoustic impedance of perforations in contact with the absorbent with and without the mean flow.

The study has assumed that (1) the absorbing material is homogeneous, isotropic, and rigid frame; (2) temperature is held constant at ambient conditions; (3) the thickness of the perforated duct is much smaller than the wavelength; and (4) the effect of finite amplitudes is negligible.

1.3 Outline

Following this introduction, Chapter 2 presents a review of pertinent works from literature. Chapter 3 describes the analytical methods and the boundary element method. Experimental setups for acquiring the acoustic characteristics of absorbing material, perforation impedance, and transmission loss with and without mean flow are described in Chapter 4. Experimental results for the acoustic properties of absorbing materials, complex characteristic impedance and wavenumber, are presented in Chapter 5. Chapter 6 provides new empirical formulations for the acoustic impedance of perforations in contact with absorbing material with and without mean flow. Using the acoustic

properties of absorbing material and the perforation impedance developed in Chapters 5 and 6, Chapter 7 compares the predicted transmission loss of single-pass dissipative silencers with experiments followed by hybrid silencer. Based on the computational method, parametric studies are also provided in this chapter to illustrate the effect of variation in the acoustic properties of absorbing material and the perforation impedance. Finally, Chapter 8 presents a summary and concluding remarks along with suggestions for future works.

CHAPTER 2

LITERATURE REVIEW

This chapter gives an overview of existing literature on predominantly dissipative and hybrid silencers in the frequency domain. First, examples of hybrid silencers are introduced, followed by the examination of studies related to dissipative silencers. Analytical and numerical approaches to predict the acoustic behavior of dissipative silencers are reviewed. Experimental methods to determine the acoustic properties of absorbing material and the impedance of perforations in contact with this material are also presented. Finally, only a brief review of literature on Helmholtz resonators is provided due to the fact that the acoustic characteristics of Helmholtz resonators have been widely investigated.

2.1 Hybrid silencers

The idea of combining dissipative and reactive chambers, hence comprising the hybrid silencers, dates back to 1930s. An early example is a three-pass muffler by Peik (1935) with a main chamber packed by absorbing material, and a recent one is a pair of hybrid silencer designs suggested by Sterrett *et al.* (1998), which involve a single dissipative chamber and multiple reactive chambers envisioned as Helmholtz resonators.

The use of absorbing material on silencers can be found from numerous patents (Nelson, 1937; Schmidt, 1937; Manning, 1939; Wolfhugel, 1983; Fukuda, 1986; Tanaka *et al*., 1987; Hetherington, 1989; Udell, 1990; Hisashige *et al*., 1991; Kraai *et al*., 1994). Yet, no analytical or experimental guidance has been provided to determine the acoustic characteristics of particularly hybrid configurations. Recently, Selamet *et al*. (2003) predicted the transmission loss of a hybrid silencer consisting of two dissipative chambers and a reactive resonator using BEM. They demonstrated computationally the effectiveness of hybrid silencers over a wide frequency range, while not detailing the interaction among the elements or providing validation.

2.2 Dissipative silencers

One- and two-dimensional analytical approaches and three-dimensional numerical methods have been widely used to predict the acoustic behavior of dissipative silencers. Analytical approaches may be suitable for simple geometries, while numerical methods need to be used for silencers with complex configurations or inhomogeneous absorbing material properties. The acoustic properties of absorbing material are usually obtained by experiments due to their complex structures. Thus, this section summarizes the available analytical and numerical approaches for dissipative silencers, as well as the experimental methods to acquire the acoustic properties of absorbing material. In addition, studies on the acoustic impedance of perforations backed by absorbing material are reviewed.

2.2.1 Analytical models

Depending on the dimensions of silencers and frequencies of interest, a lumped model, one-dimensional decoupled, and two-dimensional analytical approaches can be utilized to predict the acoustic behavior of dissipative silencers in the frequency domain. A simple lumped model may be useful to approximate the resonance frequencies of perforated dissipative silencers and Helmholtz resonators with small dimensions compared to the wavelength of interest. One-dimensional decoupled approach may be used to predict the transmission loss of perforated reactive and dissipative silencers at low frequencies. Two-dimensional analysis is used to account for higher order modes.

One-dimensional decoupled models

One-dimensional decoupling model for unfilled perforated silencers was introduced by Jayaraman and Yam (1981) with the assumption of equal mean flow in the main duct and outer chamber. The method was extended by Peat (1988) and Munjal (1987) to unfilled perforated multiple duct silencers. Wang (1999) and Selamet *et al*. (2001) applied the same method to dissipative perforated silencers. One-dimensional decoupling approach may be accurate at low frequencies. Such a method, however, shows numerical instability for large duct porosities or long chambers (Peat, 1988).

Multi-dimensional analytical models

Absorbing material of dissipative silencers can be modeled as either locally or bulk reacting depending on the geometry of silencers and the acoustic properties of the material. For the locally reacting model, the wave is assumed to propagate only in the

normal direction of the material surface, and the normal surface impedance of the material is applied as boundary conditions to the main ducts of the silencers. Therefore, only the surface impedance of the absorbing material is important in this model. Such a model can be appropriate for the absorbing material with high flow resistivity or small thickness, and for partitioned silencers (Mechel, 1990a). Morse (1939b) used the locally reacting model to investigate wave propagation inside infinitely long ducts lined with absorbing material. Later, Mechel (1990a, 1990b) developed a theoretical analysis and provided the transmission loss of baffled finite length of dissipative silencers. However, the locally reacting model may not be appropriate for low flow resisitivity.

On the other hand, the bulk reacting model considers wave propagation in multiple directions within the absorbing material, thus yielding more accurate predictions than the locally reacting approach. Typically, a modal analysis is used to describe the wave propagation within both the main duct and dissipative chamber. In this analysis, eigenvalues (wavenumbers) and eigenfunctions (modes) for an infinite length of a silencer are calculated first. Numerical schemes are generally used to calculate the common wavenumbers in two domains of the silencer. Then, boundary conditions at inlet and outlet endplates are applied to obtain overall acoustic performance such as transmission loss. Transfer matrix methods may be applied for multi-chamber silencers after using the modal analysis for each chamber. Scott (1946c) provided a theoretical analysis in the frequency domain for infinite lengths of rectangular and circular ducts lined with homogeneous and isotropic absorbing materials. He used wave equation with complex wavenumber and effective density to account for the wave dissipation through the absorbing material. Scott's analytical results were compared and verified by Bokor

(1969), Wassilieff (1987), and Kurze and Ver (1972). Bokor (1969) experimentally obtained the wavenumber and the characteristic impedance using a standing wave method for various sample thickness and compared them with the theoretical work of Scott (1946c). Kurze and Ver (1972) suggested a more generalized model of Scott's method including non-isotropic absorbing material, and compared their results with those from Scott (1946c) and Bokor (1969). Wassilieff (1987) also verified the homogeneous isotropic model of Scott (1946c) and the non-isotropic model of Kurze and Ver (1972). While these studies focused on constant rectangular or circular cross-sectional areas, Glav (1996a, 1996b) used point matching and null-field methods to find eigenvalues and eigenfunctions of infinite length of dissipative silencers with arbitrary constant cross-sectional areas. Aly and Badawy (2001) developed a theoretical approach including the effect of variable duct cross-sectional area, as well as liner length, porosity, and flow resistivity. The overall behavior of dissipative silencers with finite length is associated with inlet and outlet boundary conditions. Cummings and Chang (1988) used a match of sound field at the interface between chamber and inlet/outlet pipe. Glav (2000) extended his previous works (null-field and mode-matching) to finite length of dissipative silencers with arbitrary cross-sectional areas using a transfer matrix method.

For many applications of dissipative silencers, mean flow exists in the main duct, which may change the acoustic characteristics of the silencers. Thus many theoretical and experimental efforts have been made for dissipative silencers with mean flow. The wave propagation in infinite length of dissipative silencers in the presence of mean flow has been investigated using either locally or bulk reacting assumptions. Ko (1972) developed a theoretical method for the prediction of acoustic behavior of infinitely long

duct lined with absorbing material using the locally reacting model in the presence of mean flow. He demonstrated the effect of Mach number, boundary layer refraction, and acoustic impedance; and concluded, in particular, that the fundamental mode was not necessarily the least attenuated in the lined duct. Accordingly, a simple one-dimensional model that includes only the fundamental mode may not provide accurate results even at low frequencies. The effect of mean flow on infinite length of bulk reacting materials has been investigated by Cummings and Chang (1987a, 1987b), Bies *et al*. (1991), Gogate and Munjal (1993), and Cummings and Sormaz (1993). Cummings and Chang (1987a, 1987b) investigated anisotropic bulk reacting liners including mean flow within the material and concluded that the induced mean flow inside the absorbing material can increase the effective flow resisitivity. However, their assumption of uniform mean flow profile within the absorbing material may be valid for limited cases. Cummings and Chang (1988) extended their earlier works on infinite lengths to finite-length silencers by incorporating boundary conditions at the inlet and outlet ducts. They obtained then the transmission loss of dissipative silencers, again including the internal uniform mean flow within the absorbing material.

2.2.2 Numerical models

Hybrid silencers may involve complex geometries due to a combination of reactive and dissipative elements. Multi-dimensional numerical methods such as finite element method (FEM) and BEM are effective for the silencers with such complicated configurations, inhomogeneous acoustic field, or acoustic-structure interactions. FEM is useful for the silencers with structure interaction or inhomogeneous acoustic field.

However, FEM requires a large number of nodes and elements for the silencers with large dimensions. On the other hand, BEM is appropriate for complex silencers with homogeneous acoustic field or unbounded radiation problems.

FEM has been used for dissipative silencers, for example, by Craggs (1977), Kagawa *et al.* (1977), Astley and Cummings (1987), Cummings and Astley (1996), and Peat and Pathi (1995). Craggs (1977) used FEM and a locally reacting model to predict the behavior of a lined expansion chamber without experimental validation. Kagawa *et al.* (1977) compared their FEM results with the experiments for lined expansion chambers, including temperature gradient. Astley and Cummings (1987), Cummings and Astley (1996), and Peat and Pathi (1995) demonstrated the effect of mean flow in the main duct on the overall behavior of dissipative silencers.

BEM has been employed for reactive silencers, for example, by Wang *et al.* (1993), Ji *et al.* (1994, 1995), Wang and Liao (1998), and Wu and Zhang (1998). Wang *et al.* (1993) used BEM to demonstrate the higher order modes for simple expansion chambers with offset inlet and outlet. Ji *et al.* (1994) predicted the transmission loss of simple expansion chambers using the direct Green function solution (that is, without the coordinate transformation) and the substructure method in the presence of mean flow. In particular, a transfer matrix can be acquired from only one BEM run in their approach. Later, they also illustrated velocity and pressure distribution inside simple expansion chambers using BEM (Ji *et al*., 1995). Wang and Liao (1998) used a coordinate transformation to predict the transmission loss of straight-through perforated reactive silencers in the presence of mean flow. Wu and Zhang (1998) also used BEM to obtain the transfer matrix of a perforated silencer. They argued that their method was more

efficient than conventional transfer matrix and three-point approaches. However, it still required two BEM runs. BEM was also applied to dissipative silencers by Cheng and Wu (1999), Selamet *et al.* (2001), and Wu *et al.* (2002, 2003). Cheng and Wu (1999) and Wu *et al.* (2002) developed a direct-mixed BEM, where multi-domains were integrated into a single domain. Recently, Wu *et al.* (2003) incorporated perforated interface along with fibrous mats into BEM for bulk reacting dissipative silencers. Selamet *et al.* (2001) employed BEM for the predictions of single-pass dissipative silencers, including the effect of absorbing material on the perforation impedance.

2.2.3 Acoustic properties of absorbing material

Wave propagation through an absorbing material is dissipated into heat by the viscous boundary layer effect. Thus, in order to predict the acoustic behavior of dissipative silencers, accurate acoustic properties of absorbing material are necessary. Surface properties such as surface impedance and absorption coefficient are used as boundary conditions for locally reacting models. On the other hand, wave propagation through an absorbing material can be described by the complex characteristic impedance and the wavenumber, which are employed for a bulk reacting model. Due to their complexity, the acoustic properties of absorbing material are usually obtained by experiments. Standing wave and two-microphone methods are commonly used for the measurements of the wave pattern reflected from the absorbing material, from which the acoustic properties can be acquired. Recently, multi-microphone techniques were examined to reduce the error (Jang and Ih, 1998). Jones and Stiede (1997) summarized

the experimental methods for different number of microphones and type of sound sources in terms of accuracy and time efficiency.

Surface impedance and absorption coefficient

The absorption coefficient or surface impedance represents the acoustic behavior at the surface of the absorbing material. While the absorption coefficient represents only the acoustic characteristics of the material itself with a real number, the surface impedance can be incorporated into silencer analyses with a complex number. The measurements of these two surface acoustic properties can be performed using an impedance tube setup. A classical standing wave method and a two-microphone approach are examples of such impedance tube setups. The classical standing wave method was used until 1980s, for example by Beranek (1940a, 1940b, 1942, 1947a, 1947b) and Scott (1946b). The method locates pressure maximum and minimum (standing wave pattern) using a movable microphone at each frequency in order to calculate the surface impedance. Though it gives a reasonable accuracy, the standing wave method may not be appropriate in the presence of mean flow. In addition, it requires a measurement at each frequency and needs a long pipe at low frequencies.

On the other hand, the two-microphone method (transfer function method), which was introduced by Seybert and Ross (1977) and standardized by ASTM in 1985, has been used extensively since it can obtain surface properties for a wide frequency range with a single experiment using signal processing. Normal incident sound absorption coefficient and normal specific impedance of absorbing materials can be determined by this method, which uses an impedance tube, two microphones, a digital frequency analysis, and a

broadband random sound source. The wave inside the impedance tube is assumed planar. Two microphones are used to decompose the standing wave into two traveling waves. The standard two-microphone test method with broadband random excitation is described in ASTM E1050-98, and the detailed theory, including the transmission loss calculation, were presented by Seybert and Ross (1977) and Chung and Blaser (1980a, 1980b).

Error in the two-microphone method can be caused by inaccurate distances between microphones or sample, non-identical microphone characteristics, and the wave attenuation inside the impedance tube. Efforts have been made to reduce the error by Chung and Blaser (1980a), Seybert and Soenarko (1981), Boden and Åbom (1986), Åbom and Boden (1988), and Katz (2000). Chung and Blaser (1980a) demonstrated the effectiveness of the use of a third microphone and a microphone switching technique for calibration. Seybert and Soenarko (1981) claimed that bias error could be reduced by locating microphones close to a sample. Boden and Åbom (1986) concluded that, in addition to a close microphone location to a sample, non-reflective termination and high coherence between microphones reduced the error. Later, Åbom and Boden (1988) extended their previous error analysis to measurements with mean flow and the attenuation of wave inside the ducts. Furthermore, they suggested the use of a high signal-to-noise ratio, large microphone spacing, and signal averaging in order to minimize the error due to mean flow. Recently, a multi-microphone technique in the presence of mean flow was presented by Jang and Ih (1998) using a least squares method. The method may provide accurate results, but requires more than two microphones or their movement. Katz (2000) suggested a technique to determine the precise distance from a sample and spacing between microphones using a third microphone.

Characteristic impedance and wavenumber

The surface acoustic characteristics of absorbing material do not provide enough information to describe the wave propagation through the absorbing material. Thus the complex wavenumber and the characteristic impedance of absorbing materials are introduced to account for both propagation and dissipation of wave through the absorbing material. In general, these two values are frequency-dependent complex numbers and are acquired by impedance tube experiments. The standing wave pattern inside the absorbing material was measured earlier by Scott (1946b) to determine the wavenumber. However, this direct measurement inevitably disturbs the acoustic field resulting in inaccuracies.

Alternatively, the surface impedance obtained by indirect methods can be used to determine the wavenumber and the characteristic impedance of the absorbing material. Two different measurements of the surface impedance at one side of a sample are required with a different end condition (two-cavity method) or material thickness (two-thickness method). The two-cavity method with a ¼-wave cavity backing was adopted by Delany and Bazley (1970) and Yaniv (1973). Two different cavity backings generate zero and infinite acoustic impedance at each frequency. That is, this method requires two experiments at each frequency. Two-thickness method proved to be more accurate and efficient than the two-cavity method with ¼-wave cavity backing depth (Smith and Parrott, 1983; Woodcock and Hodgson, 1992). However, the two-thickness method requires two identical samples, which may be difficult to produce. Furthermore, adding the second sample to the first one may generate an interface between the two samples,

consequently leading to an error. Thus the improved two-cavity method by employing the transfer function approach and arbitrary backing space depth has been widely used, for example by Utsuno *et al.* (1989) and Nice and Godfrey (2000). Especially, Utsuno *et al.* (1989) discussed the selection of an appropriate set of backing space depth.

The two-thickness and two-cavity methods necessitate two measurements on one side of a sample with two different conditions on the other, which may be impractical for a high density or long sample. Therefore using impedances at both sides of a sample in a single experiment becomes a simple and effective alternative for high as well as low material density. For example, Song and Bolton (2000) provided a simple method that utilizes the reciprocal characteristics of transfer matrix for homogeneous material with a single experiment. The method can be also used for low density material. Recently, Tao *et al.* (2003) proposed a two-source method to measure the characteristic impedance and the wavenumber. The two-source method was shown to be advantageous compared to the two-cavity approach for the materials with absorption coefficients below 0.4. However, the two-source method exhibits, in their experiment, unstable characteristic impedance for high absorption coefficient at high frequencies, and requires an exchange of speaker locations.

Flow resistivity

Flow resistivity, defined as the ratio of pressure difference across a unit length of sample to flow velocity, is one of the important acoustic properties of absorbing material. This quantity has been used, for example by Delany and Bazley (1970), as a parameter in determining the characteristic impedance and wavenumber of the absorbing material.

Because of the complexity related to the material structure (size and shape), filling density, and types of construction (random or layered) of material, the flow resistivity is usually determined by experiments. A steady-state flow method uses an air-flow measurement, which obtains the flow resistivity first with mean flow and then applies an extrapolation for zero mean flow. Since this method neglects the inertia effect, the flow resistivity is a real number. Nichols (1947) presented a useful empirical formulation of flow resistance, which is closely related to the flow resistivity, for the materials with high porosity (0.9-1.0). According to Nichols, perpendicular filling to flow has higher flow resistance than random filling for the same thickness. In addition, the flow resistance is inversely proportional to the square of fiber diameter. Recently, the anisotropic effect of flow resistivity was explored by Tarnow (2002), who claimed that the resisitivity perpendicular to the fiber layers was doubled relative to that of the parallel direction.

2.2.4 Acoustic impedance of perforations in contact with absorbing material

Perforated ducts in silencers without absorbing material are commonly used to enhance the acoustic performance at low frequencies, to reduce the flow separation, thereby reducing the energy losses and the noise generated by flow, and to redirect the flow path. The perforation impedance without backing by absorbing material has been extensively investigated, for example, by Ingard (1953), Sullivan and Crocker (1978), Melling (1973), Dickey *et al*. (2000, 2001), Dean (1974), Rao and Munjal (1986), Cummings (1986), Jing *et al*. (2001), Lee and Ih (2003), Sun *et al*. (2002), and Salikuddin *et al*. (1994). An empirical formulation of the perforation impedance by Sullivan and Crocker (1978) has also been widely used in the linear regime in the

absence of mean flow. Melling (1973) and Dickey *et al*. (2000) considered the impact of high amplitudes on the perforation impedance. In the nonlinear regime, the perforation impedance is dependent on the acoustic velocity. The resistance and reactance increase and decrease, respectively, as the acoustic velocity increases in the nonlinear regime. The effect of grazing mean flow on the impedance was included by Dean (1974), Rao and Munjal (1986), Cummings (1986), Dickey *et al*. (2001), and Jing *et al*. (2001). According to these studies, grazing flow generally decreases the reactance and increases the resistance of the perforation impedance.

A perforated duct or screen is used also in dissipative silencers to prevent absorbing material from being blown out by flow. The backing by absorbing material can alter the perforation impedance and consequently the overall characteristics of dissipative silencers. Perforation impedance with backing in the absence of mean flow has been studied by Bolt (1947), Ingard and Bolt (1951a, 1951b), Ingard (1954a), Callaway and Ramer (1952), Davern (1977), Takahashi (1997), and Chen *et al.* (2000). Bolt (1947) analytically considered the mass reactance of perforations facing the absorbing material. He concluded that the addition of perforations to the absorbing material generally increased the absorption coefficient at low frequencies at the cost of a loss at high frequencies. Later, Ingard and Bolt (1951b) also indicated the effectiveness of perforations at low frequencies and discussed an increase of resistance of the impedance. They concluded that a combination of absorbing material and perforations established a Helmholtz resonator. Ingard (1954a) emphasized the increase of resistance by the addition of perforations and the effect of an air gap between the perforations and absorbing material. His analysis showed that the air gap between the perforations and

facing material narrowed the effective frequency range of absorption coefficients. Callaway and Ramer (1952) also considered the perforations facing absorbing material as a Helmholtz resonator. They showed that the air gap between the perforations and absorbing material increased the absorption coefficients for a very low duct porosity (1.23%). Davern (1977) experimentally illustrated the effect of porosity and wall thickness of the perforations, absorbing material density, air space between perforations and absorbing material, and impervious layer between the perforations and absorbing material on the absorption coefficient. Chen *et al*. (2000) used FEM to predict the absorption coefficients for perforations facing various surface shapes in the absence of mean flow.

Cummings (1976) suggested a theoretical perforation impedance facing absorbing material in the presence of mean flow. He incorporated the wavenumber and characteristic impedance of the facing material into the perforation impedance. However, the mean flow effect was simplified by ignoring the end correction on the flow side when the flow speed was greater than 1 m/s. Kirby and Cummings (1998) presented a semi-empirical formulation for the perforation impedance backed by absorbing material in the presence of grazing mean flow. They concluded that the absorbing material increased the perforation impedance and the results were strongly dependent on the density of absorbing material immediately adjacent to perforations. They also argued that the interaction among holes could be neglected and thus the formulation for single hole could be used for a multi-hole perforation. This semi-empirical formulation is employed in the literature (Kirby, 2001, 2003). However, Kirby (2001) concluded that the use of semi-

empirical expression of Kirby and Cummings (1998) might overestimate the perforation impedance.

2.3 Helmholtz resonators

Given its low-frequency attenuation characteristics, Helmholtz resonators may be desirable reactive elements to use in a hybrid silencer. For simple geometries with small dimensions compared to wavelength of interest, lumped models can be applied to estimate the resonance frequency. However, multi-dimensional analyses may be required for Helmholtz resonators in hybrid silencers since they may have relatively long necks or complex geometry as a result of the combination with dissipative chambers. Helmholtz resonators are well understood compared to dissipative silencers. Ingard (1953) investigated the effect of neck geometry such as cross-sectional area shape, location, and size on the resonance frequency of such a resonator with circular or rectangular cross-sectional area for the volume. He developed end corrections for both single and double holes to account for the higher order modes at the interface between neck and cavity. Chanaud (1994) examined the effect of both orifice and cavity geometry on the resonance frequency of a Helmholtz resonator using the end corrections suggested by Ingard (1953). He presented the limitations of simple lumped and transcendental models based on the predictions, and concluded that for a fixed volume and orifice size, the orifice position changed the resonance frequency substantially, while the orifice shape was not significant. Both references (Ingard, 1953; Chanaud, 1994) considered only very short neck length compared to wavelength. Tang and Sirignano (1973) studied a Helmholtz resonator with a neck comparable to wavelength as an application to reduce combustion

instability. They developed a general formulation and applied to quarter wave and Helmholtz resonators with various neck lengths.

Recently, Selamet and his coworkers (Dickey and Selamet, 1996; Selamet *et al*., 1997; Selamet and Ji, 2000) have employed several approaches to examine the effect of cavity volumes and neck locations. They illustrated the effect of length-to-diameter ratio of the volume on the resonance frequency and the transmission loss characteristics using lumped and one-dimensional approaches (Dickey and Selamet, 1996). Earlier works have been extended further by studying a number of circular concentric configurations with lumped, radial and axial one-dimensional models, two-dimensional analytical approaches, and a three-dimensional boundary element method (Selamet *et al.*, 1997). They also developed a three-dimensional analytical approach to investigate the effect of neck offset on the behavior of circular asymmetric Helmholtz resonators (Selamet and Ji, 2000).

CHAPTER 3

THEORETICAL MODELS

To predict the acoustic behavior of dissipative and hybrid silencers, different approaches can be used depending on their geometries and applications. Lumped model is suitable for the silencers with dimensions small compared to the wavelength of interest in order to approximate resonance frequencies and transmission losses. One-dimensional analysis may be appropriate for the silencers with relatively small diameters leading to planar wave propagation. A decoupled one-dimensional analytical approach is applied in this study for both unfilled and dissipative perforated silencers. However, the neglect of higher order mode propagation may lead to inaccuracies for the silencers with large diameters or at high frequencies. The effect of higher order modes can be effectively accounted for by using multi-dimensional methods. In this study, a two-dimensional analytical approach is developed for axisymmetric, cylindrical, unfilled and dissipative silencers to incorporate the higher order modes. Finally, the three-dimensional BEM is also employed for the acoustic prediction of silencers with generic geometries with and without absorbing material.

The lumped, one-dimensional decoupled, and two-dimensional analytical approaches and the three-dimensional boundary element method used in the present study

are introduced in this chapter. In addition, the acoustic properties of absorbing material and the acoustic impedance of perforations facing absorbing material are also discussed.

3.1 Lumped model

The lumped approach can be applied to resonators and silencers when their dimensions are so small ($k\ell \ll 1$, k is the wavenumber and ℓ is the characteristic dimension) that the spatial parameters can be ignored. The estimations of resonance frequencies and transmission losses for Helmholtz resonators are typical examples of the lumped model applications. Unfilled and dissipative perforated silencers are also can be modeled as undamped and damped Helmholtz resonators.

3.1.1 Simple Helmholtz resonator

In terms of acoustic resistance R_{ac}, acoustic inertance L_{ac}, and acoustic compliance C_{ac}, the acoustic impedance of the unfilled Helmholtz resonator depicted in Fig 3.1 is defined as,

$$Z_H = \frac{p_H}{S_k u_H} = R_{ac} + i\omega L_{ac} + \frac{1}{i\omega C_{ac}}, \tag{3.1}$$

where

$$L_{ac} = \frac{\rho_0 \left(\ell_k + \delta_k \right)}{S_k}, \tag{3.2}$$

$$C_{ac} = \frac{V_c}{\rho_0 c_0^2}, \tag{3.3}$$

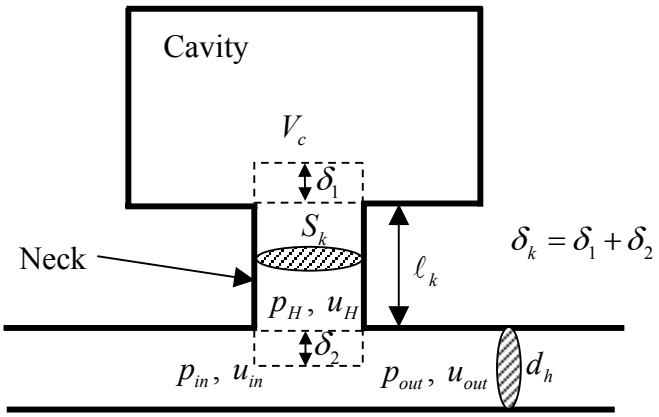

Figure 3.1: The schematic of a simple Helmholtz resonator.

p_H and u_H are the acoustic pressure and particle velocity at the neck, respectively, S_k the neck cross-sectional area, ω the angular velocity, ρ_0 the air density, c_0 the speed of sound, ℓ_k the neck length, V_c the cavity volume, and δ_k the end correction to account for higher modes excited at the discontinuities, which may be determined by the geometry and location of the neck relative to the volume and main duct. The acoustic resistance R_{ac} due to viscous friction and radiation is generally neglected for simple Helmholtz resonators except for very small neck diameters.

The resonance frequency of the Helmholtz resonator can be calculated when the impedance in Eq. (3.1) is minimum, that is $Z_H = 0$ ignoring the acoustic resistance, thus

$$\omega_r = 2\pi f_r = \sqrt{\frac{1}{L_{ac} C_{ac}}} . \tag{3.4}$$

Substitution of Eqs. (3.2) and (3.3) into Eq. (3.4) yields the resonance frequency of the resonator as

$$f_r = \frac{c_0}{2\pi} \sqrt{\frac{S_k}{V_c \left(\ell_k + \delta_k \right)}} . \tag{3.5}$$

The transmission loss of the Helmholtz resonator can be also estimated from the lumped analysis. The transfer matrix relating the acoustic pressure and particle velocity at the inlet and outlet of the main duct is given by

$$\begin{bmatrix} p_{in} \\ \rho_0 c_0 u_{in} \end{bmatrix} = \begin{bmatrix} 1 & 0 \\ \dfrac{\rho_0 c_0}{Z_H} \dfrac{S_k}{S_d} & 1 \end{bmatrix} \begin{bmatrix} p_{out} \\ \rho_0 c_0 u_{out} \end{bmatrix} = \begin{bmatrix} T_{11} & T_{12} \\ T_{21} & T_{22} \end{bmatrix} \begin{bmatrix} p_{out} \\ \rho_0 c_0 u_{out} \end{bmatrix}, \tag{3.6}$$

where S_d is the cross-sectional area of the main duct, and subscripts *in* and *out* indicate the inlet and outlet of the silencer, respectively. The transmission loss of the resonator can be then calculated, assuming the same cross-sectional areas for the inlet and outlet, as

$$TL = 20\log_{10}\left|\frac{1}{2}\left(T_{11}+T_{12}+T_{21}+T_{22}\right)\right| = 20\log_{10}\left|\frac{1}{2}\frac{\rho_0 c_0}{Z_H}\frac{S_k}{S_d}+1\right| \tag{3.7}$$

and thus

$$TL = 20\log_{10}\left|\frac{1}{2}\frac{\dfrac{\rho_0 c_0}{R_{ac}+i\omega\dfrac{\rho_0\left(\ell_k+\delta_k\right)}{S_k}+\dfrac{\rho_0 c_0^2}{i\omega V_c}}}{}\frac{S_k}{S_d}+1\right|. \tag{3.8}$$

Thus, the transmission loss is dependent on the impedance of the resonator and the cross-sectional area ratio of the neck to the main duct.

3.1.2 Perforated silencers

An empty (unfilled) perforated silencer depicted in Fig. 3.2 may be simplified as a combination of an expansion chamber and a Helmholtz resonator. The perforations and the outer chamber can be considered as a neck and a cavity, respectively. Sullivan and Crocker (1978) expressed the resonance frequency of a perforated duct silencer as follows:

$$f_{r,P} = \frac{c_0}{\pi}\sqrt{\frac{\phi d_1}{\left(d_2^2-d_1^2\right)\left(t_w+\delta_k\right)}}; \quad k_0 L < \frac{\pi}{4}, \tag{3.9}$$

where ϕ is the duct porosity, t_w the perforated duct wall thickness, L the silencer length, d_1 and d_2 the diameter of the main duct and the outer chamber, respectively.

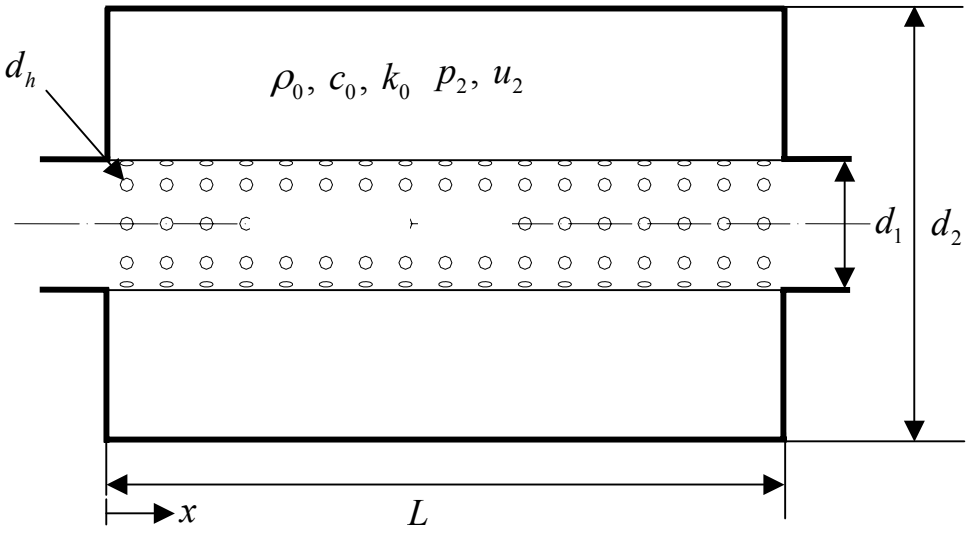

Figure 3.2: The schematic of a perforated reactive single-pass straight silencer.

Equation (3.9) can be obtained by substituting the neck area, cavity volume, and neck length given by

$$S_k = \phi \pi d_1 L\,, \tag{3.10}$$

$$V_c = \frac{\pi}{4}\left(d_2^2 - d_1^2\right) L\,, \tag{3.11}$$

$$\ell_k = t_w \tag{3.12}$$

into Eq. (3.5). Equation (3.9) may be valid for low duct porosities since the unfilled perforated silencer with high duct porosity may act as rather an expansion chamber than a combination of a Helmholtz resonator and an expansion chamber. Sullivan and Crocker (1978) argued that Helmholtz resonator model for the perforated silencer shows 27% error from the experiments for the given dimension in the literature.

3.1.3 Dissipative perforated silencers

The perforated dissipative silencer depicted in Fig. 3.3 also can be approximated as a damped Helmholtz resonator as shown in Fig. 3.4. The acoustic inertance and compliance of the damped Helmholtz resonator can be expressed, using complex density ($\tilde{\rho}$) and speed of sound ($\tilde{c}$), as

$$C_{ac,D} = \frac{V_c}{\tilde{\rho}\tilde{c}^2} \tag{3.13}$$

and

$$L_{ac,D} = \frac{\rho_0\left(t_w + \tilde{\delta}_k\right)}{S_k}\,, \tag{3.14}$$

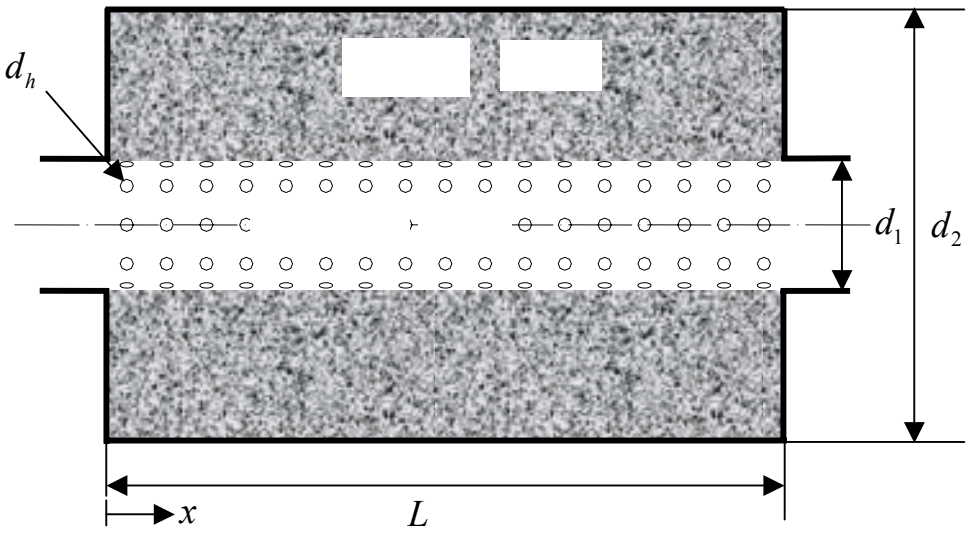

Figure 3.3: The schematic of a perforated dissipative single-pass straight silencer.

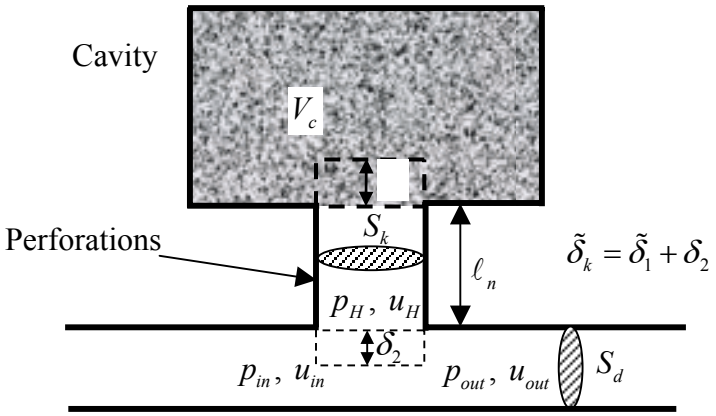

Figure 3.4: Helmholtz resonator model of the dissipative silencer in Fig. 3.3.

where $\tilde{\delta}_k$ is the total end correction of perforations facing air and absorbing material at each side as shown in Fig. 3.4. Since the acoustic inertance and compliance are complex numbers and frequency-dependent, Eq. (3.4) may not be utilized to calculate the resonance frequencies for dissipative silencers. However, the transmission loss can be obtained from Eqs. (3.1), (3.7), (3.13), and (3.14), and then the frequency at which the transmission loss is maximum can be viewed as the resonance frequency of the resonator.

3.2 One-dimensional decoupled model

Assuming harmonic planar wave propagation in both the main duct and the filled outer chamber (Fig. 3.3), the continuity and momentum equations yield, in the absence of mean flow (Munjal, 1987; Wang, 1999),

$$\frac{d^2 p_1}{dx^2} + \left(k_0^2 - \frac{4}{d_1} \frac{ik_0}{\tilde{\zeta}_p} \right) p_1 + \left(\frac{4}{d_1} \frac{ik_0}{\tilde{\zeta}_p} \right) p_2 = 0 \tag{3.15}$$

and

$$\frac{d^2 p_2}{dx^2} + \left(\frac{4d_1}{{d_2}^2 - {d_1}^2} \frac{\tilde{\rho}}{\rho_0} \frac{ik_0}{\tilde{\zeta}_p} \right) p_1 + \left(\tilde{k}^2 - \frac{4d_1}{{d_2}^2 - {d_1}^2} \frac{\tilde{\rho}}{\rho_0} \frac{ik_0}{\tilde{\zeta}_p} \right) p_2 = 0 , \tag{3.16}$$

where k_0 denote the wavenumber in air, p_1 and p_2 is the acoustic pressure in the main duct (domain 1) and the outer chamber (domain 2), respectively, and $\tilde{\zeta}_p$ the acoustic impedance of the perforated duct, which can be defined as

$$\tilde{\zeta}_p = \frac{p_1 - p_2}{\rho_0 c_0 u_1} , \tag{3.17}$$

where u_1 is the particle velocity in the main duct. Equation (3.17) is to be further elaborated later in Section 3.6. Equations (3.15) and (3.16) may be rearranged as,

$$\begin{Bmatrix} p_1' \\ \left(\frac{dp_1}{dx}\right)' \\ p_2' \\ \left(\frac{dp_2}{dx}\right)' \end{Bmatrix} = \begin{bmatrix} 0 & 1 & 0 & 0 \\ -\left(k_0^2 - \frac{4}{d_1}\frac{ik_0}{\tilde{\zeta}_p}\right) & 0 & -\frac{4}{d_1}\frac{ik_0}{\tilde{\zeta}_p} & 0 \\ 0 & 0 & 0 & 1 \\ -\frac{4d_1}{{d_2}^2-{d_1}^2}\frac{\tilde{\rho}}{\rho_0}\frac{ik_0}{\tilde{\zeta}_p} & 0 & -\left(\tilde{k}^2 - \frac{4d_1}{{d_2}^2-{d_1}^2}\frac{\tilde{\rho}}{\rho_0}\frac{ik_0}{\tilde{\zeta}_p}\right) & 0 \end{bmatrix} \begin{Bmatrix} p_1 \\ \frac{dp_1}{dx} \\ p_2 \\ \frac{dp_2}{dx} \end{Bmatrix}, \quad (3.18)$$

where $(\,)'$ indicates derivative with respect to x. Using the linearized momentum equation, Eq. (3.18) can be rearranged as

$$\begin{Bmatrix} p_1' \\ \rho_0 c_0 u_1' \\ p_2' \\ \tilde{\rho}\tilde{c}u_2' \end{Bmatrix} = \begin{bmatrix} 0 & -ik_0 & 0 & 0 \\ -ik_0 - \frac{4}{d_1}\frac{1}{\tilde{\zeta}_p} & 0 & \frac{4}{d_1}\frac{1}{\tilde{\zeta}_p} & 0 \\ 0 & 0 & 0 & -i\tilde{k} \\ \frac{4d_1}{{d_2}^2-{d_1}^2}\frac{\tilde{\rho}}{\rho_0}\frac{k_0}{\tilde{k}}\frac{1}{\tilde{\zeta}_p} & 0 & -i\tilde{k} - \frac{4d_1}{{d_2}^2-{d_1}^2}\frac{\tilde{\rho}}{\rho_0}\frac{k_0}{\tilde{k}}\frac{1}{\tilde{\zeta}_p} & 0 \end{bmatrix} \begin{Bmatrix} p_1 \\ \rho_0 c_0 u_1 \\ p_2 \\ \tilde{\rho}\tilde{c}u_2 \end{Bmatrix}. \quad (3.19)$$

$$= [TA] \begin{Bmatrix} p_1 \\ \rho_0 c_0 u_1 \\ p_2 \\ \tilde{\rho}\tilde{c}u_2 \end{Bmatrix}$$

The solution of Eq. (3.19) may be expressed in terms of eigenvalues and eigenvectors as

$$\begin{Bmatrix} p_1(x) \\ \rho_0 c_0 u_1(x) \\ p_2(x) \\ \tilde{\rho}\tilde{c}u_2(x) \end{Bmatrix} = [\Psi] \begin{Bmatrix} c_1 e^{\lambda_1 x} \\ c_2 e^{\lambda_2 x} \\ c_3 e^{\lambda_3 x} \\ c_4 e^{\lambda_4 x} \end{Bmatrix}, \quad (3.20)$$

where λ_n is the eigenvalue of the matrix $[TA]$ and $[\Psi]$ the modal matrix whose columns are the eigenvectors. Equation (3.20) can be rewritten as

$$\begin{Bmatrix} p_1(x) \\ \rho_0 c_0 u_1(x) \\ p_2(x) \\ \tilde{\rho}\tilde{c}u_2(x) \end{Bmatrix} = [\Psi'(x)] \begin{Bmatrix} c_1 \\ c_2 \\ c_3 \\ c_4 \end{Bmatrix}, \tag{3.21}$$

which leads to a relationship between the acoustic pressure and the particle velocity at the inlet ($x = 0$) and outlet ($x = L$) as

$$\begin{Bmatrix} p_1(0) \\ \rho_0 c_0 u_1(0) \\ p_2(0) \\ \tilde{\rho}\tilde{c}u_2(0) \end{Bmatrix} = [TB] \begin{Bmatrix} p_1(L) \\ \rho_0 c_0 u_1(L) \\ p_2(L) \\ \tilde{\rho}\tilde{c}u_2(L) \end{Bmatrix}, \tag{3.22}$$

where

$$[TB] = [\Psi'(0)][\Psi'(L)]^{-1}. \tag{3.23}$$

For the outer chamber, the boundary conditions at $x = 0$ and $x = L$ may be written as

$$u_2(0) = 0 \tag{3.24}$$

and

$$u_2(L) = 0. \tag{3.25}$$

Finally, combining Eqs. (3.22), (3.24) and (3.25) yields the transfer matrix of the dissipative silencer as

$$\begin{bmatrix} p_1(0) \\ \rho_0 c_0 u_1(0) \end{bmatrix} = \begin{bmatrix} T_{11} & T_{12} \\ T_{21} & T_{22} \end{bmatrix} \begin{bmatrix} p_1(L) \\ \rho_0 c_0 u_1(L) \end{bmatrix}, \tag{3.26}$$

where

$$T_{11} = TB_{11} - \frac{TB_{13}TB_{41}}{TB_{43}}, \tag{3.27}$$

$$T_{12} = TB_{12} - \frac{TB_{13}TB_{42}}{TB_{43}}, \tag{3.28}$$

$$T_{21} = TB_{21} - \frac{TB_{23}TB_{41}}{TB_{43}}, \tag{3.29}$$

$$T_{22} = TB_{22} - \frac{TB_{23}TB_{42}}{TB_{43}}. \tag{3.30}$$

Assuming the main duct with a constant cross-sectional area, the transmission loss of the silencer can be then calculated from the transfer matrix as follows:

$$TL = 20\log_{10}\left(\frac{1}{2}\left|T_{11} + T_{12} + T_{21} + T_{22}\right|\right). \tag{3.31}$$

3.3 Two-dimensional analytical model

A two-dimensional analytical approach is introduced next to determine the acoustic characteristics of the cylindrical, concentric dissipative silencer of length *L,* main duct radius r_1, and filled outer chamber radius r_2 (Fig. 3.5). For two-dimensional axisymmetric and harmonic wave propagation in a circular, the governing equation duct in the cylindrical coordinates (r, x) can be expressed by

$$\nabla^2 p(r,x) + k^2 p(r,x) = 0 \tag{3.32}$$

or

$$\frac{\partial^2 p}{\partial r^2} + \frac{1}{r}\frac{\partial p}{\partial r} + \frac{\partial^2 p}{\partial x^2} + k^2 p = 0. \tag{3.33}$$

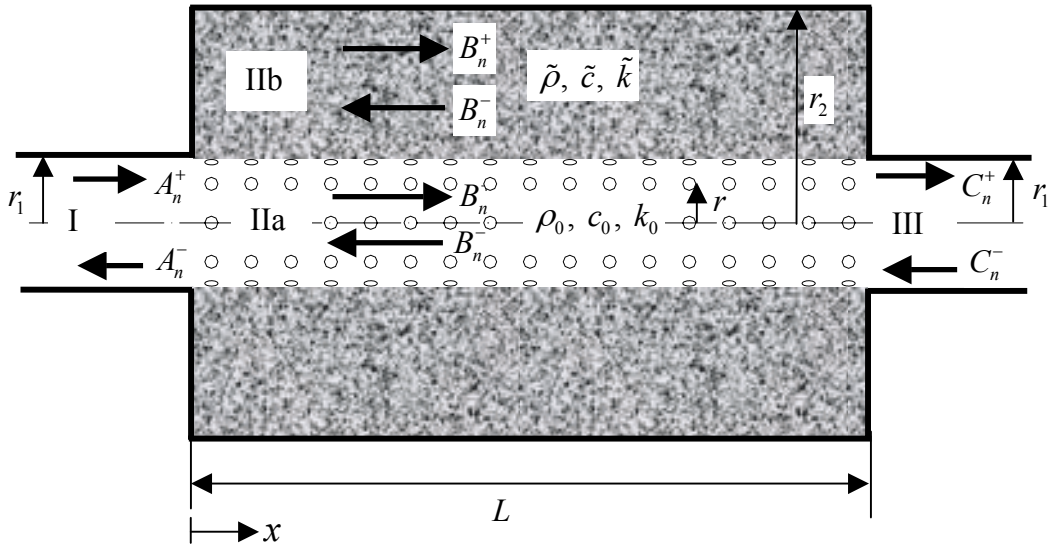

Figure 3.5: Wave propagation in a perforated dissipative silencer in axisymmetric two-dimension.

The solution of Eq. (3.33) in domain I or inlet duct (Fig. 3.5) can be written as

$$p_A(r,x) = \sum_{n=0}^{\infty} \left(A_n^+ e^{-ik_{A,x,n}x} + A_n^- e^{ik_{A,x,n}x} \right) \psi_{A,n}(r), \tag{3.34}$$

where subscript A denotes domain I, p_A is the acoustic pressure, A_n^+ and A_n^- the modal amplitudes corresponding to components traveling in the positive and negative x directions in domain I, respectively, $k_{A,x,n}$ the axial wavenumber, and $\psi_{A,n}(r)$ the eigenfunctions. For the circular duct, the eigenfunctions are given by

$$\psi_{A,n}(r) = J_0\left(k_{A,r,n} r\right), \tag{3.35}$$

where J_0 is the Bessel function of the first kind of order zero, and $k_{A,r,n}$ (radial wavenumber) the roots satisfying the rigid wall boundary condition at $r = r_1$ of

$$J_0'\left(k_{A,r,n} r_1\right) = J_1\left(k_{A,r,n} r_1\right) = 0. \tag{3.36}$$

The relationship between axial and radial wavenumbers is given by

$$k_{A,x,n} = \begin{cases} \sqrt{k_0^2 - k_{A,r,n}^2}\ ; & k_0 > k_{A,r,n} \\ -\sqrt{k_0^2 - k_{A,r,n}^2}\ ; & k_0 < k_{A,r,n} \end{cases}, \tag{3.37}$$

where the negative sign in Eq. (3.37) is assigned so that $e^{-ik_{A,x,n}x}$ decays exponentially in x direction. The particle velocity in the axial direction may then be written, in terms of the linearized momentum equation, as

$$u_{A,x}(r,x) = \frac{1}{\rho_0 \omega} \sum_{n=0}^{\infty} k_{A,x,n} \left[A_n^+ e^{-ik_{A,x,n}x} - A_n^- e^{ik_{A,x,n}x} \right] \psi_{A,n}(r). \tag{3.38}$$

The outlet acoustic pressure and particle velocity in the axial direction (domain III) are similar to those at the inlet duct and are expressed as

$$p_C(r,x) = \sum_{n=0}^{\infty} \left(C_n^+ e^{-ik_{C,x,n}(x-L)} + C_n^- e^{ik_{C,x,n}(x-L)} \right) \psi_{C,n}(r) \tag{3.39}$$

and

$$u_{C,x}(r,x) = \frac{1}{\rho_0 \omega} \sum_{n=0}^{\infty} k_{C,x,n} \left[C_n^+ e^{-ik_{C,x,n}(x-L)} - C_n^- e^{ik_{C,x,n}(x-L)} \right] \psi_{C,n}(r), \tag{3.40}$$

where subscript C denotes domain III, and C_n^+ and C_n^- the modal amplitudes corresponding to components traveling in the positive and negative x directions in domain III, respectively, and $k_{C,x,n}$ the axial wavenumber. The eigenfunctions $\psi_{C,n}(r)$ are given by

$$\psi_{C,n}(r) = J_0\left(k_{C,r,n} r\right), \tag{3.41}$$

and $k_{C,r,n}$ (radial wavenumber) the roots satisfying the rigid wall boundary condition at $r = r_1$ of

$$J_0'\left(k_{C,r,n} r_1\right) = J_1\left(k_{C,r,n} r_1\right) = 0\,. \tag{3.42}$$

The sound propagation in domain II is given by

$$\frac{\partial^2 p}{\partial r^2} + \frac{1}{r}\frac{\partial p}{\partial r} + \frac{\partial^2 p}{\partial x^2} + \kappa^2 p = 0\,, \tag{3.43}$$

where

$$\kappa = \begin{cases} k_0; & 0 \le r \le r_1 \\ \tilde{k}; & r_1 \le r \le r_2 \end{cases}. \tag{3.44}$$

The solutions to Eq. (3.43) are given by for domain IIa (air)

$$p_{Ba}(r,x) = \sum_{n=0}^{\infty} \left(B_n^+ e^{-ik_{B,x,n}x} + B_n^- e^{ik_{B,x,n}x} \right) \psi_{Ba,n}(r); \quad 0 \le r \le r_1; \tag{3.45}$$

and for domain IIb (absorbing material)

$$p_{Bb}(r,x)=\sum_{n=0}^{\infty}\left(B_n^{+}e^{-ik_{B,x,n}x}+B_n^{-}e^{ik_{B,x,n}x}\right)\psi_{Bb,n}(r);\quad r_1\le r\le r_2; \tag{3.46}$$

subscript *Ba* and *Bb* denote domain IIa and IIb, respectively, B_n^{+} and B_n^{-} the modal amplitudes corresponding to components traveling in the positive and negative x directions in domain II, respectively, $k_{B,x,n}$ the common wavenumber in the axial direction for both air and absorbing material, and $\psi_{Ba,n}$ and $\psi_{Ba,n}$ the eigenfunctions in domain IIa and IIb, respectively. The radial wavenumbers for air and absorbing material are different and is related by

$$k_{B,r,n}=\sqrt{k_0{}^2-k_{B,x,n}^2} \tag{3.47}$$

and

$$\tilde{k}_{B,r,n}=\sqrt{\tilde{k}^2-k_{B,x,n}^2}\,. \tag{3.48}$$

Using momentum equation, the acoustic velocities in the radial directions are expressed by

$$u_{Ba,r}=-\frac{1}{i\rho_0\omega}\sum_{n=0}^{\infty}\left(B_n^{+}e^{-ik_{B,x,n}x}+B_n^{-}e^{ik_{B,x,n}x}\right)\frac{\partial\psi_{Ba,n}(r)}{\partial r};\quad 0\le r\le r_1 \tag{3.49}$$

and

$$u_{Bb,r}=-\frac{1}{i\tilde{\rho}\omega}\sum_{n=0}^{\infty}\left(B_n^{+}e^{-ik_{B,x,n}x}+B_n^{-}e^{ik_{B,x,n}x}\right)\frac{\partial\psi_{Bb,n}(r)}{\partial r};\quad r_1\le r\le r_2 \tag{3.50}$$

for domain IIa and IIb, respectively. The transverse modal eigenfunctions in Eqs. (3.45) and (3.46) can be expressed as

$$\psi_{Ba,n}(r)=B_{1,n}J_0\left(k_{B,r,n}r\right)+B_{2,n}Y_0\left(k_{B,r,n}r\right);\quad 0\le r\le r_1; \tag{3.51}$$

and

$$\psi_{Bb,n}(r) = B_{3,n} J_0\left(\tilde{k}_{B,r,n} r\right) + B_{4,n} Y_0\left(\tilde{k}_{B,r,n} r\right); \quad r_1 \le r \le r_2; \tag{3.52}$$

where Y_0 denotes Bessel function of the second kind of order zero, $B_{1,n} - B_{4,n}$ the coefficients related by the following four boundary conditions at $r = 0$, r_1, and r_2:

(1) At $r = 0$, the pressure is finite, thus Eq. (3.51) yields

$$B_{2,n} = 0. \tag{3.53}$$

(2) At $r = r_2$, the rigid wall boundary condition, $u_{B,b,r}\left(x, r_2\right) = 0$, gives

$$B_{3,n} J_1\left(\tilde{k}_{B,r,n} r_2\right) + B_{4,n} Y_1\left(\tilde{k}_{B,r,n} r_2\right) = 0 \tag{3.54}$$

where Y_1 and J_1 are Bessel functions of the first and second kind of order one, respectively.

(3) At $r = r_1$, the continuity of radial particle velocity, $u_{Ba,r}\left(x, r_1\right) = u_{Bb,r}\left(x, r_1\right)$, and Eq. (3.53) yield

$$\frac{k_{B,r,n}}{\rho_0} B_{1,n} J_1\left(k_{B,r,n} r_1\right) = \frac{\tilde{k}_{B,r,n}}{\tilde{\rho}}\left[B_{3,n} J_1\left(\tilde{k}_{B,r,n} r_1\right) + B_{4,n} Y_1\left(\tilde{k}_{B,r,n} r_1\right)\right]. \tag{3.55}$$

(4) At $r = r_1$, the difference of acoustic pressure across the perforated duct yields

$$p_{Ba}\left(x, r_1\right) - p_{Bb}\left(x, r_1\right) = \rho_0 c_0 \tilde{\zeta}_p u_{Ba,r}\left(x, r_1\right) \tag{3.56}$$

and thus

$$B_{1,n} J_0\left(k_{B,r,n} r_1\right) - \left[B_{3,n} J_0\left(\tilde{k}_{B,r,n} r_1\right) + B_{4,n} Y_0\left(\tilde{k}_{B,r,n} r_1\right)\right] = \frac{\tilde{\zeta}_p k_{B,r,n}}{i k_0} B_{1,n} J_1\left(k_{B,r,n} r_1\right). \tag{3.57}$$

The coefficients $B_{3,n}$ and $B_{1,n}$ in Eqs. (3.54) and (3.55) are expressed in terms of the coefficient $B_{4,n}$ as,

$$B_{3,n} = -B_{4,n} \frac{Y_1\left(\tilde{k}_{B,r,n} r_2\right)}{J_1\left(\tilde{k}_{B,r,n} r_2\right)} \tag{3.58}$$

and

$$B_{1,n} = \frac{\tilde{k}_{B,r,n}}{k_{B,r,n}} \frac{\rho_0}{\tilde{\rho}} \frac{1}{J_1\left(k_{B,r,n} r_1\right)} \left[-\frac{Y_1\left(\tilde{k}_{B,r,n} r_2\right)}{J_1\left(\tilde{k}_{B,r,n} r_2\right)} J_1\left(\tilde{k}_{B,r,n} r_1\right) + Y_1\left(\tilde{k}_{B,r,n} r_1\right) \right] B_{4,n} . \tag{3.59}$$

Substitution of Eqs. (3.58) and (3.59) into Eq. (3.57) gives the characteristic equation:

$$\begin{aligned} &\frac{\rho_0}{\tilde{\rho}} \frac{\tilde{k}_{B,r,n}}{k_{B,r,n}} \left[\frac{J_0\left(k_{B,r,n} r_1\right)}{J_1\left(k_{B,r,n} r_1\right)} + i\tilde{\zeta}_p \frac{k_{B,r,n}}{k_0} \right] \\ &= \frac{Y_0\left(\tilde{k}_{B,r,n} r_1\right) J_1\left(\tilde{k}_{B,r,n} r_2\right) - Y_1\left(\tilde{k}_{B,r,n} r_2\right) J_0\left(\tilde{k}_{B,r,n} r_1\right)}{Y_1\left(\tilde{k}_{B,r,n} r_1\right) J_1\left(\tilde{k}_{B,r,n} r_2\right) - Y_1\left(\tilde{k}_{B,r,n} r_2\right) J_1\left(\tilde{k}_{B,r,n} r_1\right)} \end{aligned} . \tag{3.60}$$

Equation (3.60) can be expressed, using Eqs. (3.47) and (3.48), as

$$\begin{aligned} &\frac{\rho_0}{\tilde{\rho}} \frac{\sqrt{\tilde{k}^2 - k_{B,x,n}^2}}{\sqrt{k_0^2 - k_{B,x,n}^2}} \left[\frac{J_0\left(\sqrt{k_0^2 - k_{B,x,n}^2} r_1\right)}{J_1\left(\sqrt{k_0^2 - k_{B,x,n}^2} r_1\right)} + i\tilde{\zeta}_p \frac{\sqrt{k_0^2 - k_{B,x,n}^2}}{k_0} \right] \\ &= \frac{Y_0\left(\sqrt{\tilde{k}^2 - k_{B,x,n}^2} r_1\right) J_1\left(\sqrt{\tilde{k}^2 - k_{B,x,n}^2} r_2\right) - Y_1\left(\sqrt{\tilde{k}^2 - k_{B,x,n}^2} r_2\right) J_0\left(\sqrt{\tilde{k}^2 - k_{B,x,n}^2} r_1\right)}{Y_1\left(\sqrt{\tilde{k}^2 - k_{B,x,n}^2} r_1\right) J_1\left(\sqrt{\tilde{k}^2 - k_{B,x,n}^2} r_2\right) - Y_1\left(\sqrt{\tilde{k}^2 - k_{B,x,n}^2} r_2\right) J_1\left(\sqrt{\tilde{k}^2 - k_{B,x,n}^2} r_1\right)} \end{aligned} , \tag{3.61}$$

and the common axial wavenumber $k_{B,x,n}$ can be obtained by solving Eq. (3.61).

Equations (3.51) and (3.52) can be rewritten using Eqs. (3.53), (3.58), and (3.59) as follows:

$$\psi_{Ba,n}(r) = B_{1,n} J_0(k_{B,r,n} r); \quad 0 \le r \le r_1 ; \tag{3.62}$$

and

$$\psi_{Bb,n}(r) = B_{1,n}\frac{k_{B,r,n}}{\tilde{k}_{B,r,n}}\frac{\tilde{\rho}}{\rho_0}\frac{J_1\left(k_{B,r,n}r_1\right)}{D}\left[J_1\left(\tilde{k}_{B,r,n}r_2\right)Y_0\left(\tilde{k}_{B,r,n}r\right)-Y_1\left(\tilde{k}_{B,r,n}r_2\right)J_0\left(\tilde{k}_{B,r,n}r\right)\right];$$

$$r_1 \le r \le r_2, \qquad (3.63)$$

where

$$D = J_1\left(\tilde{k}_{B,r,n}r_2\right)Y_1\left(\tilde{k}_{B,r,n}r_1\right)-Y_1\left(\tilde{k}_{B,r,n}r_2\right)J_1\left(\tilde{k}_{B,r,n}r_1\right). \qquad (3.64)$$

From the linearized momentum equation, the particle velocities in the axial direction are then obtained as

$$u_{Ba,x}(r,x) = \frac{1}{\rho_0\omega}\sum_{n=0}^{\infty}k_{B,x,n}\left(B_n^+e^{-jk_{B,x,n}x}-B_n^-e^{jk_{B,x,n}x}\right)\psi_{Ba,n}(r); \quad 0 \le r \le r_1 \qquad (3.65)$$

and

$$u_{Bb,x}(r,x) = \frac{1}{\tilde{\rho}\omega}\sum_{n=0}^{\infty}k_{B,x,n}\left(B_n^+e^{-jk_{B,x,n}x}-B_n^-e^{jk_{B,x,n}x}\right)\psi_{Bb,n}(r); \quad r_1 \le r \le r_2 \qquad (3.66)$$

The solution of unknown coefficients A_n^+, A_n^-, B_n^+, B_n^-, C_n^+ and C_n^- can be determined from the boundary conditions at the inlet $(x=0)$ and outlet $(x=L)$. Then the coefficients are used to calculate the transmission loss of the silencer. The boundary conditions at the interfaces of the inlet and outlet are

$$p_A = p_B; \qquad 0 \le r \le r_1,\ x = 0, \qquad (3.67)$$

$$u_B = \begin{cases} u_A; & 0 \le r \le r_1,\ \ x = 0 \\ 0; & r_1 \le r \le r_2,\ x = 0 \end{cases}, \qquad (3.68)$$

$$p_C = p_B; \qquad 0 \le r \le r_1,\ \ x = L, \qquad (3.69)$$

$$u_B = \begin{cases} u_C; & 0 \le r \le r_1,\ \ x = L \\ 0; & r_1 \le r \le r_2,\ x = L \end{cases}. \qquad (3.70)$$

In view of the expressions of the pressure and velocity as infinite series of unknown amplitudes in Eqs. (3.34), (3.38), (3.39), (3.40), (3.45), and (3.65), Eqs. (3.67) – (3.70) give

$$\sum_{n=0}^{\infty}\left(A_n^+ + A_n^-\right)\psi_{A,n}(r) = \sum_{n=0}^{\infty}\left(B_n^+ + B_n^-\right)\psi_{Ba,n}(r); \quad 0 \le r \le r_1 \tag{3.71}$$

$$\sum_{n=0}^{\infty} k_{B,x,n}\left(B_n^+ - B_n^-\right)\psi_{Ba,n}(r) = \begin{cases} \sum_{n=0}^{\infty} k_{A,x,n}\left(A_n^+ - A_n^-\right)\psi_{A,n}(r); & 0 \le r \le r_1 \\ 0; & r_1 \le r \le r_2 \end{cases}, \tag{3.72}$$

$$\sum_{n=0}^{\infty}\left(C_n^+ + C_n^-\right)\psi_{C,n}(r) = \sum_{n=0}^{\infty}\left(B_n^+ e^{-jk_{B,x,n}L} + B_n^- e^{jk_{B,x,n}L}\right)\psi_{Ba,n}(r); \quad 0 \le r \le r_1, \tag{3.73}$$

$$\sum_{n=0}^{\infty} k_{B,x,n}\left(B_n^+ e^{-jk_{B,x,n}L} - B_n^- e^{jk_{B,x,n}L}\right)\psi_{Ba,n}(r) = \begin{cases} \sum_{n=0}^{\infty} k_{C,x,n}\left(C_n^+ - C_n^-\right)\psi_{C,n}(r); & 0 \le r \le r_1 \\ 0; & r_1 \le r \le r_2 \end{cases}. \tag{3.74}$$

In order to solve Eqs. (3.71) – (3.74), the infinite series of unknown amplitudes need to be truncated to a suitable number, and then the same number of equations is solved for the amplitudes of the acoustic waves. An approach proposed by Xu *et al*. (1999) is adopted here to match the sound field. Imposing the continuities of the integral of the pressure and axial velocity over discrete zones of the interfaces at the inlet $(x = 0)$ and outlet $(x = L)$, Eqs. (3.71) – (3.74) yield the pressure and velocity matching conditions as

$$\sum_{n=0}^{N}\left(A_n^+ + A_n^-\right)\int_0^{r_{p,m}} \psi_{A,n}(r)\,dr = \sum_{n=0}^{N}\left(B_n^+ + B_n^-\right)\int_0^{r_{p,m}} \psi_{Ba,n}(r)\,dr, \tag{3.75}$$

$$\sum_{n=0}^{N} k_{B,x,n}\left(B_n^+ - B_n^-\right)\int_0^{r_{u,m}} \psi_{Ba,n}(r)\,dr$$

$$= \begin{cases} \sum_{n=0}^{N} k_{A,x,n}\left(A_n^+ - A_n^-\right)\int_0^{r_{u,m}} \psi_{A,n}(r)\,dr; & 0 \le r_{u,m} \le r \\ \sum_{n=0}^{N} k_{A,x,n}\left(A_n^+ - A_n^-\right)\int_0^{r_1} \psi_{A,n}(r)\,dr; & r_1 \le r_{u,m} \le r_2 \end{cases}, \tag{3.76}$$

$$\sum_{n=0}^{N}\left(C_n^+ + C_n^-\right)\int_0^{r_{p,m}} \psi_{C,n}(r)\,dr = \sum_{n=0}^{N}\left(B_n^+ e^{-jk_{B,x,n}L} + B_n^- e^{jk_{B,x,n}L}\right)\int_0^{r_{p,m}} \psi_{B,n}(r)\,dr\,, \tag{3.77}$$

$$\sum_{n=0}^{N} k_{B,x,n}\left(B_n^+ e^{-jk_{B,x,n}L} - B_n^- e^{jk_{B,x,n}L}\right)\int_0^{r_{u,m}} \psi_{B,n}(r)\,dr$$

$$= \begin{cases} \sum_{n=0}^{N} k_{C,x,n}\left(C_n^+ - C_n^-\right)\int_0^{r_{u,m}} \psi_{C,n}(r)\,dr; & 0 \le r_{u,m} \le r_1 \\ \sum_{n=0}^{N} k_{C,x,n}\left(C_n^+ - C_n^-\right)\int_0^{r_1} \psi_{C,n}(r)\,dr; & r_1 \le r_{u,m} \le r_2 \end{cases} \tag{3.78}$$

with

$$r_{p,m} = \frac{m}{N+1} r_1; \quad m = 1, \cdots, N+1 \tag{3.79}$$

and

$$r_{u,m} = \frac{m}{N+1} r_2; \quad m = 1, \cdots, N+1. \tag{3.80}$$

In view of $4(N+1)$ coefficients solved in Eqs. (3.75) – (3.78) and the assumptions that: (1) the incoming wave is planar and A_0^+ the unity, (2) an anechoic termination is imposed at the exit by setting C_n^- to zero, and (3) all transmitted waves in the outlet pipe are non-propagating modes except the first mode C_0^+, the transmission loss is determined as

$$TL = -20\log_{10}\left|C_0^+\right|. \tag{3.81}$$

3.4 Three-dimensional boundary element method

Dissipative silencers can be first divided into unfilled and filled acoustic domains. Impedance matrix for each domain is then obtained using boundary element method. These impedance matrices are then combined by applying the boundary conditions between the two domains. The matrix for filled acoustic domain can be evaluated by using complex acoustic characteristics of absorbing material, such as density and speed of sound. This section describes the BEM for perforated dissipative silencers depicted in Fig. 3.6.

For the perforated main duct (domain 1), the three-dimensional wave equation with uniform mean flow in the x direction is expressed as

$$\nabla^2\varphi + k_0^2\varphi - 2ik_0 Ma\frac{\partial\varphi}{\partial x} - Ma^2\frac{\partial^2\varphi}{\partial x^2} = 0 \tag{3.82}$$

or

$$\frac{\partial^2\varphi}{\partial x^2} + \frac{\partial^2\varphi}{\partial y^2} + \frac{\partial^2\varphi}{\partial z^2} + k_0^2\varphi - 2ik_0 Ma\frac{\partial\varphi}{\partial x} - Ma^2\frac{\partial^2\varphi}{\partial x^2} = 0, \tag{3.83}$$

where φ is the acoustic velocity potential, Ma is the Mach number of the mean flow. The acoustic pressure and particle velocity can be written respectively, in terms of the acoustic velocity potential, as

$$p_1 = \rho_0\left(i\omega\varphi + V_0\frac{\partial\varphi}{\partial x}\right) \tag{3.84}$$

and

$$u_1 = -\nabla\varphi, \tag{3.85}$$

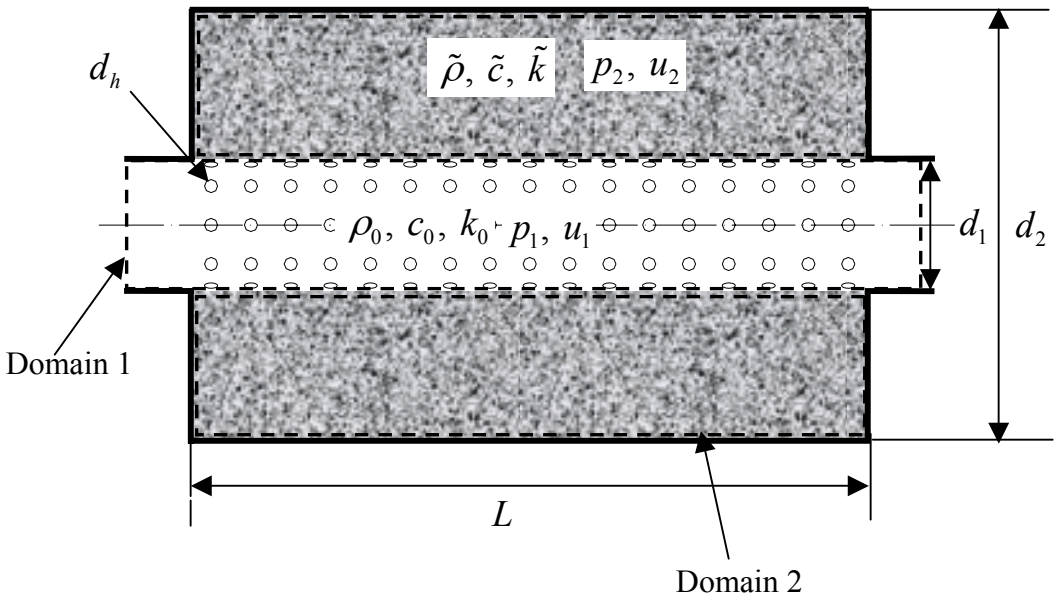

Figure 3.6: Wave propagation in a perforated dissipative silencer in three-dimension.

where V_0 is mean flow velocity and ∇ the del operator. The adjoint of Eq. (3.83) is given by

$$\begin{aligned}&\frac{\partial^2\varphi^*}{\partial x^2}+\frac{\partial^2\varphi^*}{\partial y^2}+\frac{\partial^2\varphi^*}{\partial z^2}+k_0^2\varphi^*+2ik_0Ma\frac{\partial\varphi^*}{\partial x}\\&-Ma^2\frac{\partial^2\varphi^*}{\partial x^2}+\delta(x-x_i)(y-y_i)(z-z_i)=0\end{aligned}\tag{3.86}$$

with its fundamental solution (Green's function) expressed as

$$\varphi^*=\frac{1}{4\pi\sqrt{1-Ma^2}R}e^{-\frac{ik_0Ma}{1-Ma^2}(x-x_i)}e^{-\frac{ik_0}{\sqrt{1-Ma^2}}R},\tag{3.87}$$

where

$$R=\sqrt{\frac{1}{1-Ma^2}(x-x_i)^2+(y-y_i)^2+(z-z_i)^2}\tag{3.88}$$

and δ is the Dirac delta function. The weighted residual integral of Eq. (3.82) is written as

$$\int_V\varphi^*\left(\nabla^2\varphi+k_0^2\varphi-2ik_0Ma\frac{\partial\varphi}{\partial x}-Ma^2\frac{\partial^2\varphi}{\partial x^2}\right)dV=0,\tag{3.89}$$

where V is the acoustic domain volume. Integrating the first term by parts twice and the second term once,

$$\begin{aligned}&\int_V\varphi\left(\nabla^2\varphi^*+k_0^2\varphi^*+2ik_0Ma\frac{\partial\varphi^*}{\partial x}-Ma^2\frac{\partial^2\varphi^*}{\partial x^2}\right)dV\\&+\int_\Gamma\left[\varphi^*\frac{\partial\varphi}{\partial\vec{n}}-\varphi\frac{\partial\varphi^*}{\partial\vec{n}}-2ik_0Ma\varphi\varphi^*\vec{n}_x-Ma^2\left(\varphi^*\frac{\partial\varphi}{\partial x}-\varphi\frac{\partial\varphi^*}{\partial x}\right)\vec{n}_x\right]d\Gamma=0,\end{aligned}\tag{3.90}$$

where Γ is the boundary surface of the acoustic domain, and $\vec{n}$ is the normal vector to the surface and $\vec{n}_x$ is its component in the x direction. Rearranging Eq. (3.90),

$$C_i\varphi_i + \int_\Gamma \left[\frac{\partial \varphi^*}{\partial \vec{n}} + 2ik_0 Ma\varphi^* \vec{n}_x - Ma^2 \frac{\partial \varphi^*}{\partial x} \vec{n}_x \right] \varphi d\Gamma = \int_\Gamma \varphi^* \left[1 - Ma^2 \vec{n}_x^2 \right] \frac{\partial \varphi}{\partial \vec{n}} d\Gamma \ , \quad (3.91)$$

where C_i are the edge or corner point coefficients. Discretizing the boundary surfaces into a number of elements Γ_j, Eq. (3.91) yields

$$C_i\varphi_i + \sum_{j=1}^{N} \int_{\Gamma_j} \left[\frac{\partial \varphi^*}{\partial \vec{n}} + 2ik_0 Ma\varphi^* \vec{n}_x - Ma^2 \frac{\partial \varphi^*}{\partial x} \vec{n}_x \right] \varphi d\Gamma = \sum_{j=1}^{N} \int_{\Gamma_j} \varphi^* \left[1 - Ma^2 \vec{n}_x^2 \right] \frac{\partial \varphi}{\partial \vec{n}} d\Gamma \quad (3.92)$$

which can be expressed in the matrix format as

$$[H']\{\varphi\} = [G']\left\{\frac{\partial \varphi}{\partial \vec{n}}\right\}. \quad (3.93)$$

Using Eqs. (3.84) and (3.85), Eq. (3.93) can be rewritten in terms of pressure and particle velocity as

$$[H]\{p_1\} = [G]\{u_1\}. \quad (3.94)$$

The acoustic pressure and velocity on the boundary can be generally categorized as inlet, outlet, rigid wall, and perforations. Applying rigid boundary condition on the solid wall yields the impedance matrix of the main duct, in terms of inlet, outlet, and perforations, as

$$\begin{Bmatrix} \{p_1^i\} \\ \{p_1^O\} \\ \{p_1^p\} \end{Bmatrix} = \begin{bmatrix} [TC_{11}] & [TC_{12}] & [TC_{13}] \\ [TC_{21}] & [TC_{22}] & [TC_{23}] \\ [TC_{31}] & [TC_{32}] & [TC_{33}] \end{bmatrix} \begin{Bmatrix} \{u_1^i\} \\ \{u_1^O\} \\ \{u_1^p\} \end{Bmatrix}, \quad (3.95)$$

where superscripts *i*, *o* and *p* denote inlet, outlet, and perforations.

Impedance matrix of the dissipative chamber can also be derived by the similar method as explained earlier with complex density and speed of sound. Zero mean flow can be assumed in the dissipative chamber (domain 2), thus $V_0 = Ma = 0$ in Eqs. (3.83)

and (3.84). Applying rigid boundary condition at the wall, impedance matrix for the dissipative chamber becomes

$$\left\{p_2^p\right\} = [TD]\left\{u_2^p\right\}. \tag{3.96}$$

The impedance matrices of inner duct $\left([TC]\right)$ and outer chamber $\left([TD]\right)$ may be coupled by the boundary conditions at the perforations interface. The acoustic velocity continuity at the interface yields,

$$\left\{u_1^p\right\} = -\left\{u_2^p\right\}, \tag{3.97}$$

where the negative sign is assigned since u_1 and u_2 are normal outward acoustic velocities for each domain. Assuming the perforation thickness much smaller than the wavelength, pressure difference at the perforations may be expressed as,

$$\left\{p_1^p\right\} - \left\{p_2^p\right\} = \rho_0 c_0 \tilde{\zeta}_p \left\{u_1^p\right\}. \tag{3.98}$$

Combining Eqs. (3.95) – (3.98) yields the impedance matrix $[TI]$ of the silencer, defined by

$$\begin{Bmatrix} \left\{p_1^i\right\} \\ \left\{p_1^O\right\} \end{Bmatrix} = \begin{bmatrix} [TI_{11}] & [TI_{12}] \\ [TI_{21}] & [TI_{22}] \end{bmatrix} \begin{Bmatrix} \left\{u_1^i\right\} \\ \left\{u_1^O\right\} \end{Bmatrix}, \tag{3.99}$$

where

$$[TI_{11}] = [TC_{11}] + [TC_{13}]\left(\tilde{\zeta}_p [I] - \left([TC_{33}] + [TD]\right)\right)^{-1} [TC_{31}], \tag{3.100}$$

$$[TI_{12}] = [TC_{12}] + [TC_{13}]\left(\tilde{\zeta}_p [I] - \left([TC_{33}] + [TD]\right)\right)^{-1} [TC_{32}], \tag{3.101}$$

$$[TI_{21}] = [TC_{21}] + [TC_{23}]\left(\tilde{\zeta}_p [I] - \left([TC_{33}] + [TD]\right)\right)^{-1} [TC_{31}], \tag{3.102}$$

$$[TI_{22}] = [TC_{22}] + [TC_{23}]\left(\tilde{\zeta}_p [I] - \left([TC_{33}] + [TD]\right)\right)^{-1} [TC_{32}], \qquad (3.103)$$

and $[I]$ is the identity matrix.

For a single-chamber silencer, the average of acoustic pressure and velocity from Eq. (3.99) at nodes on the inlet and outlet planes determine first the transfer matrix of Eq. (3.26), followed by the transmission loss through Eq. (3.31). For a multiple-chamber silencer, the overall impedance matrix is obtained by connecting the impedance matrix of each chamber in terms of acoustic pressure and velocity continuities. The overall impedance matrix then yields the transfer matrix and thus the transmission loss of the silencer in view of Eq. (3.31).

3.5 Physical and acoustic properties of absorbing materials

There are a number of sound absorbing materials including glass fiber, foam, and mineral wool. Understanding their physical and acoustic properties is essential in using such materials in silencers. In this study, glass fiber is considered as an acoustic absorbing material and its physical and acoustical properties are introduced next.

3.5.1 Physical properties of absorbing material

One of the important physical properties of fibrous materials is the flow resistance (or resisitivity). The definitions for and the standard test method to determine them are presented by ASTM C522-87 (1997) and Beranek (1988). The specific flow resistance is defined as

$$R_1 = \frac{\Delta p_f}{u_f} \quad \text{[mks rayl]}, \tag{3.104}$$

where Δp_f and u_f is the pressure difference and the linear flow velocity across the homogeneous sample, respectively. The flow resistivity is then defined as the specific flow resistance per unit thickness of the material as

$$R_f = \frac{R_1}{t_s} = \frac{\Delta p_f}{u_f t_s} \quad \text{[mks rayl/m] or [N·s/m}^4\text{]}, \tag{3.105}$$

where t_s is the sample thickness. The flow resistance (hence resistivity) is mainly dependent on fiber diameter, layer orientation, and material filling density. Nichols (1947) presented an empirical formulation of flow resistance for glass wool as

$$R_1 = \gamma \frac{\rho_f^{(1+\beta)}}{t_s^{\beta} r_f^2}, \tag{3.106}$$

where γ is a constant, ρ_f the filling or bulk density, r_f the fiber radius, and the parameter β is a function of the fiber layer orientation. The flow resistivity of fiber perpendicular to flow direction, in general, is higher than that of random filling. Therefore the value of *b* approaches 0.3 for fibers layered perpendicular to flow direction and 1.0 for a random filling. The effect of fiber orientation on the flow resistivity was also theoretically and experimentally investigated by Tarnow (1997, 2000). He suggests that the flow resistivity for the fiber layered perpendicular to flow direction is twice the value of the one parallel to the flow direction.

Another physical property of absorbing material is the porosity, which is defined as the ratio of the volume of the voids or air (V_a) to the total volume (V_t) as

$$Y = \frac{V_a}{V_t} \tag{3.107}$$

and can be calculated, using bulk or filling density (ρ_f) and the material density of fibers (ρ_m), as

$$Y = 1 - \frac{\rho_f}{\rho_m}. \tag{3.108}$$

According to Nichols (1947), Eq. (3.106) may be valid only for the materials with porosity higher than 0.9. In addition, thermal and chemical properties need to be considered according to the applications of materials. Such properties of various absorbing materials are described in Beranek (1988) and Huff (2001).

3.5.2 Acoustic properties of absorbing material

The absorption of acoustic waves in fibrous material is mainly due to viscous and thermal dissipation, which may be expressed in terms of complex characteristic impedance and wavenumber. The imaginary part of the wavenumber, which is called the attenuation constant, accounts for the decay of the waves. Since the structure of absorbing material is rather complex, the acoustic properties are often determined experimentally. For example, Delany and Bazley (1970) presented empirical expressions for complex characteristic impedance and wavenumber of a fibrous material as follows:

$$\frac{\tilde{Z}}{\rho_0 c_0} = \left[1 + 0.0511\left(f / R_f\right)^{-0.75}\right] + i\left[-0.0768\left(f / R_f\right)^{-0.73}\right] \tag{3.109}$$

and

$$\frac{\tilde{k}}{k_0} = \left[1 + 0.0858\left(f / R_f\right)^{-0.70}\right] + i\left[-0.1749\left(f / R_f\right)^{-0.59}\right], \tag{3.110}$$

where f denotes frequency and R_f the resistivity which is in general experimentally determined.

3.6 Perforation impedance

In Eqs. (3.15), (3.16), (3.56), and (3.98), the acoustic impedance of perforation relates the acoustic waves in the main duct and the outer chamber. The acoustic impedance is the ratio of the pressure difference to the particle velocity. Two existing definitions of impedance differ by the way particle velocity is specified. One is the impedance of a hole using the particle velocity at the hole u_h in Fig. 3.7, and the other is the impedance of a perforated plate applying the velocity in the duct u_1 or u_2. These definitions and the relationship in between are introduced next.

The specific acoustic impedance of a hole is defined as

$$Z_h = \frac{p_1 - p_2}{u_h} = R_S + j\omega L_S = R_S + j\omega\rho_0\ell_{eff} = R_S + jk_0\rho_0 c_0\ell_{eff}, \tag{3.111}$$

where p_1 and p_2 are the acoustic pressures before and after the perforated plate, respectively, as shown in Fig. 3.7, u_h the particle velocity at the hole; R_S the specific resistance; L_S the specific inertance; and ℓ_{eff} the effective length of the hole generally expressed as

$$\ell_{eff} = t_w + \alpha d_h, \tag{3.112}$$

where t_w is the wall thickness, d_h hole diameter, and α end correction coefficient.

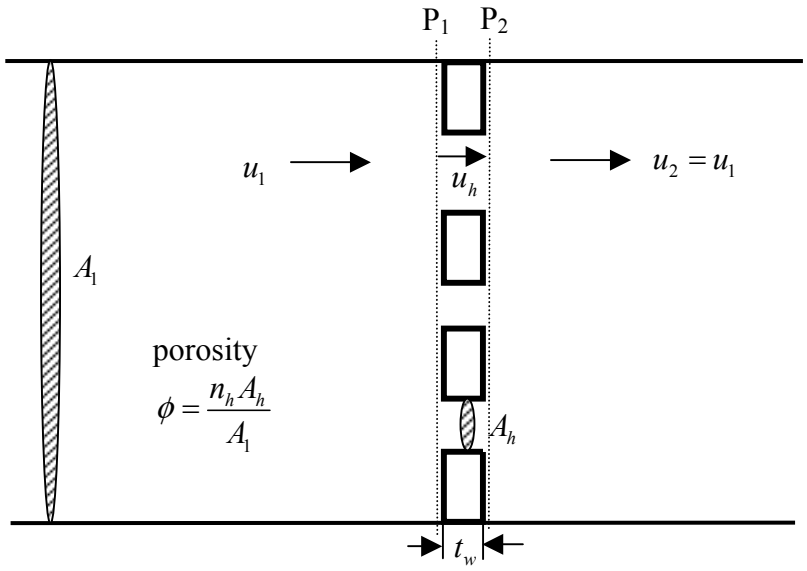

Figure 3.7: Wave propagation through a perforated plate in a duct.

The end correction coefficient α is dependent on hole geometry and the characteristics of medium contacting the hole. The non-dimensional acoustic impedance of a hole is then given by

$$\zeta_h = \frac{p_1 - p_2}{\rho_0 c_0 u_h} = \frac{R_S + jk_0\rho_0 c_0 \ell_{eff}}{\rho_0 c_0} = R + jk_0\left(t_w + \alpha d_h\right), \tag{3.113}$$

where R is the non-dimensional resistance.

The non-dimensional acoustic impedance of a perforated plate can be defined as

$$\zeta_p = \frac{p_1 - p_2}{\rho_0 c_0 u_1}, \tag{3.114}$$

where the particle velocity u_1 in the duct is related to u_h through conservation of mass by

$$u_1 = \frac{n_h A_h}{A_1} u_h = \phi u_h, \tag{3.115}$$

n_h being the number of holes, A_h the area of a hole, and ϕ the porosity. Equations (3.113) – (3.115) yield the relationships between the impedance of a hole and a plate as

$$\zeta_p = \frac{p_1 - p_2}{\rho_0 c_0 u_h \phi} = \frac{\zeta_h}{\phi} = \frac{R + jk_0\left(t_w + \alpha d_h\right)}{\phi}. \tag{3.116}$$

While the impedance of a hole is representative of the acoustic characteristic of perforation itself, the impedance of a plate is usually used in analyses, for example, transmission loss predictions. The impedance of a plate ζ_p is usually obtained first by experiments, and then the impedance of a hole ζ_h are calculated using Eq. (3.116).

CHAPTER 4

EXPERIMENTAL SETUPS

An impedance tube setup was used to measure the acoustic properties of absorbing material, the acoustic impedance of perforations, and the transmission loss of silencers using the two-microphone method in the absence of mean flow. In addition, two new setups were developed to acquire the acoustic impedance of perforations facing the absorbing material and the transmission loss of silencers in the presence of mean flow. This chapter describes foregoing setups with and without mean flow, along with the data reduction procedures to calculate the acoustic characteristics of fibrous material, perforations, and silencers.

4.1 Impedance tube setup in the absence of mean flow

Figure 4.1 shows the schematic of the impedance tube setup used in this study to obtain the characteristic impedance and wavenumber of the absorbing material, the acoustic impedance of perforations, and the transmission loss of silencers in the absence of mean flow. Wide-band white random noise or single frequency sine wave can be generated by a loudspeaker which is enclosed in a wooden box to reduce the radiation

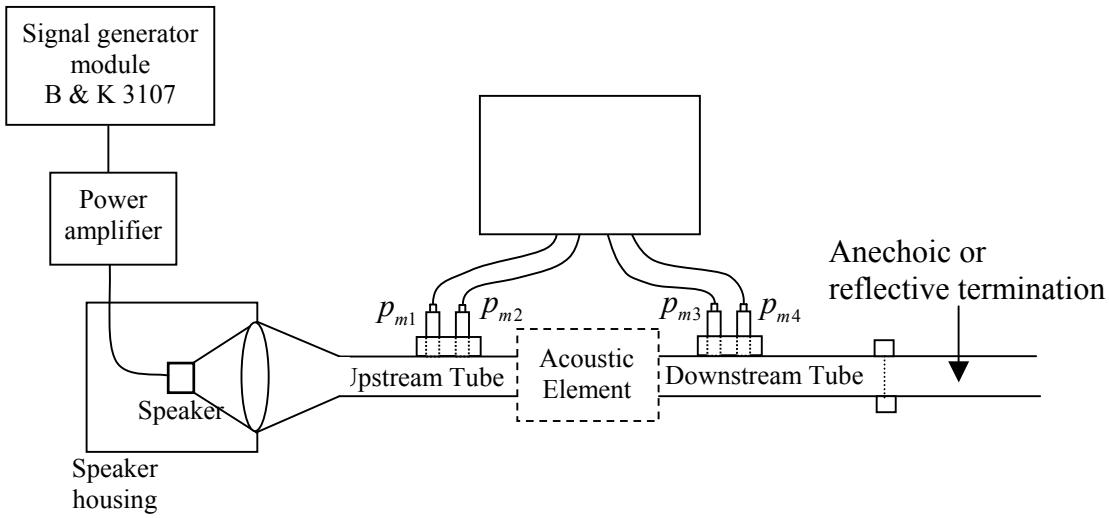

Figure 4.1: The schematic of the impedance tube setup in the absence of mean flow.

noise. The loudspeaker is driven by a signal generator module (B&K 3107) and amplified by a 100 W amplifier. A conical transition of 48 cm long is used to connect the speaker to an upstream PVC with 4.9 cm inner and 5.08 cm nominal outer diameters. The downstream tube is also made of PVC. A reflective or anechoic termination at the end of the downstream tube is employed depending on the measurements. To accomplish the anechoic termination, a 4.5 m long PVC tube filled with absorbing fiber is attached to the downstream of the setup. The reflective termination may be achieved by either placing a rigid block inside the downstream tube or opening the tube.

Each pair of ¼ inch condenser microphones (B&K 4135) are mounted at the upstream and downstream ends of the acoustic element. The signals from these four microphones are processed by a multi-channel analysis system (B&K 3550). Auto- and cross-spectra from microphones are post-processed depending on the purpose of measurement. Ensemble averaging and microphone calibration are employed to reduce the experimental error. Averaging 100 ensembles is applied for each measurement to reduce uncertainties mainly due to signal noise. The mismatches of magnitude and phase among microphones are compensated using a microphone switching technique established by Chung and Blaser (1980a). Next, the methodology is described to determine the characteristic impedance and wavenumber of the absorbing material, acoustic impedance of perforations, and transmission loss of silencers in the absence of mean flow utilizing the impedance tube shown in Fig. 4.1.

4.1.1 Characteristic impedance and wavenumber of absorbing material

A setup depicted in Fig. 4.2 in conjunction with the impedance tube was developed in this study to obtain the complex characteristic impedance and wavenumber of the absorbing material in the absence of mean flow. A sample of absorbing material is mounted inside the main duct bounded by wire screens with a porosity higher than 75 % defining the locations *a* and *b* as shown in Fig. 4.2. Transfer functions among microphones and two measurements with distinctly different terminations are required in the present method to determine the complex characteristic impedance and wavenumber of the absorbing material in the frequency domain. Anechoic and fully reflective boundaries are applied as two different termination conditions.

The transfer matrix, which expresses the relationships between acoustic pressure and velocities at the surfaces *a* and *b* of the sample, is given for the first termination in terms of complex characteristic impedance $\left(\widetilde{\rho c}\right)$, wavenumber $\left(\tilde{k}\right)$, and the length of the sample $\left(\ell_f\right)$ as,

$$\begin{bmatrix} p_a \\ u_a \end{bmatrix} = \begin{bmatrix} \cos\left(\tilde{k}\ell_f\right) & i\widetilde{\rho c}\sin\left(\tilde{k}\ell_f\right) \\ i\dfrac{\sin\left(\tilde{k}\ell_f\right)}{\widetilde{\rho c}} & \cos\left(\tilde{k}\ell_f\right) \end{bmatrix} \begin{bmatrix} p_b \\ u_b \end{bmatrix}, \tag{4.1}$$

and for the second termination (designated by prime)

$$\begin{bmatrix} p'_a \\ u'_a \end{bmatrix} = \begin{bmatrix} \cos\left(\tilde{k}\ell_f\right) & i\widetilde{\rho c}\sin\left(\tilde{k}\ell_f\right) \\ i\dfrac{\sin\left(\tilde{k}\ell_f\right)}{\widetilde{\rho c}} & \cos\left(\tilde{k}\ell_f\right) \end{bmatrix} \begin{bmatrix} p'_b \\ u'_b \end{bmatrix}. \tag{4.2}$$

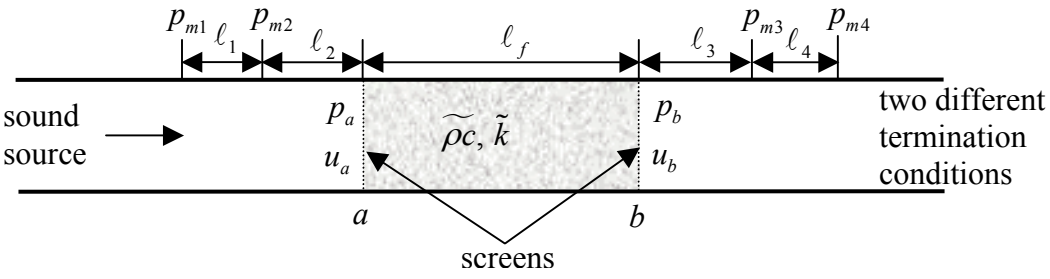

Figure 4.2: The schematic of the experimental setup for obtaining the acoustic properties of absorbing material in the absence of mean flow.

The combination of Eqs. (4.1) and (4.2) yields

$$\begin{bmatrix} p_a \\ u_a \\ p_a' \\ u_a' \end{bmatrix} = \begin{bmatrix} p_b & u_b & 0 & 0 \\ 0 & 0 & p_b & u_b \\ p_b' & u_b' & 0 & 0 \\ 0 & 0 & p_b' & u_b' \end{bmatrix} \begin{bmatrix} \cos\left(\tilde{k}\ell_f\right) \\ i\widetilde{\rho c}\sin\left(\tilde{k}\ell_f\right) \\ i\dfrac{\sin\left(\tilde{k}\ell_f\right)}{\widetilde{\rho c}} \\ \cos\left(\tilde{k}\ell_f\right) \end{bmatrix} \tag{4.3}$$

or

$$\begin{bmatrix} \cos\left(\tilde{k}\ell_f\right) \\ i\widetilde{\rho c}\sin\left(\tilde{k}\ell_f\right) \\ i\dfrac{\sin\left(\tilde{k}\ell_f\right)}{\widetilde{\rho c}} \\ \cos\left(\tilde{k}\ell_f\right) \end{bmatrix} = \begin{bmatrix} p_b & u_b & 0 & 0 \\ 0 & 0 & p_b & u_b \\ p_b' & u_b' & 0 & 0 \\ 0 & 0 & p_b' & u_b' \end{bmatrix}^{-1} \begin{bmatrix} p_a \\ u_a \\ p_a' \\ u_a' \end{bmatrix} = \begin{bmatrix} T_1 \\ T_2 \\ T_3 \\ T_4 \end{bmatrix}. \tag{4.4}$$

In Eq. (4.4), acoustic pressure $\left(p_a, p_b, p_a', p_b'\right)$ and velocities $\left(u_a, u_b, u_a', u_b'\right)$ at the sample surfaces *a* and *b* can be calculated from the pressure measurements at four microphones $\left(p_{m1}, p_{m2}, p_{m3}, p_{m4}, p_{m1}', p_{m2}', p_{m3}', p_{m4}'\right)$. The transfer matrix between the sample surface *a* and microphone #2 is given by, for the first termination,

$$\begin{bmatrix} p_a \\ u_a \end{bmatrix} = \begin{bmatrix} \cos\left(k_0\ell_2\right) & i\rho_0 c_0 \sin\left(k_0\ell_2\right) \\ i\dfrac{1}{\rho_0 c_0}\sin\left(k_0\ell_2\right) & \cos\left(k_0\ell_2\right) \end{bmatrix}^{-1} \begin{bmatrix} p_{m2} \\ u_{m2} \end{bmatrix}. \tag{4.5}$$

The acoustic velocity at microphone #2 $\left(u_{m2}\right)$ can also be expressed in terms of pressure measurements at microphones #1 and #2 $\left(p_{m1}, p_{m2}\right)$ as

$$u_{m2} = \frac{p_{m1} - p_{m2}\cos\left(k_0\ell_1\right)}{i\rho_0 c_0 \sin\left(k_0\ell_1\right)}. \tag{4.6}$$

Substitution of Eq. (4.6) into Eq. (4.5) yields

$$\begin{bmatrix} p_a \\ u_a \end{bmatrix} = \begin{bmatrix} \cos(k_0\ell_2) & i\rho_0 c_0 \sin(k_0\ell_2) \\ i\dfrac{1}{\rho_0 c_0}\sin(k_0\ell_2) & \cos(k_0\ell_2) \end{bmatrix}^{-1} \begin{bmatrix} p_{m2} \\ \dfrac{p_{m1} - p_{m2}\cos(k_0\ell_1)}{i\rho_0 c_0 \sin(k_0\ell_1)} \end{bmatrix}, \tag{4.7}$$

which expresses the acoustic pressure and velocity at the sample surface *a* in terms of only pressure measurements at microphones #1 and #2. Similarly, the acoustic pressure and velocity at the sample surface *a* for the second termination is given by

$$\begin{bmatrix} p'_a \\ u'_a \end{bmatrix} = \begin{bmatrix} \cos(k_0\ell_2) & i\rho_0 c_0 \sin(k_0\ell_2) \\ i\dfrac{1}{\rho_0 c_0}\sin(k\ell_2) & \cos(k_0\ell_2) \end{bmatrix}^{-1} \begin{bmatrix} p'_{m2} \\ \dfrac{p'_{m1} - p'_{m2}\cos(k_0\ell_1)}{i\rho_0 c_0 \sin(k_0\ell_1)} \end{bmatrix}. \tag{4.8}$$

The acoustic pressure and velocity at sample surface *b* can be similarly expressed in terms of pressure measurements at microphones #3 and #4 for the first termination as,

$$\begin{bmatrix} p_b \\ u_b \end{bmatrix} = \begin{bmatrix} \cos(k_0\ell_3) & i\rho_0 c_0 \sin(k_0\ell_3) \\ i\dfrac{1}{\rho_0 c_0}\sin(k_0\ell_3) & \cos(k_0\ell_3) \end{bmatrix} \begin{bmatrix} p_{m3} \\ \dfrac{p_{m3}\cos(k_0\ell_4) - p_{m4}}{i\rho_0 c_0 \sin(k_0\ell_4)} \end{bmatrix}, \tag{4.9}$$

and for the second termination,

$$\begin{bmatrix} p'_b \\ u'_b \end{bmatrix} = \begin{bmatrix} \cos(k_0\ell_3) & i\rho_0 c_0 \sin(k_0\ell_3) \\ i\dfrac{1}{\rho_0 c_0}\sin(k_0\ell_3) & \cos(k_0\ell_3) \end{bmatrix} \begin{bmatrix} p'_{m3} \\ \dfrac{p'_{m3}\cos(k_0\ell_4) - p'_{m4}}{i\rho_0 c_0 \sin(k_0\ell_4)} \end{bmatrix}. \tag{4.10}$$

The complex characteristic impedance and wavenumber of the sample can then be obtained from Eq. (4.4) and Eqs. (4.7) – (4.10). The complex characteristic impedance $\left(\widetilde{\rho c}\right)$ is given, in terms of T_2 and T_3 of Eq. (4.4), by

$$\widetilde{\rho c} = \sqrt{\frac{T_2}{T_3}} \tag{4.11}$$

and the complex wavenumber, in terms of T_1 or T_4 of Eq. (4.4), by

$$\tilde{k} = \frac{1}{\ell_f} \cos^{-1}\left(T_1\right) \tag{4.12}$$

or

$$\tilde{k} = \frac{1}{\ell_f} \cos^{-1}\left(T_4\right). \tag{4.13}$$

Measured T_1 and T_4 of Eq. (4.4) are expected to be the same in ideal experiments. However, they may not be the case in experiments due, for example, to inhomogeneity in the filling and imperfect sample surfaces. Thus, the complex wavenumber may be obtained using an average of T_1 and T_4 as,

$$\tilde{k} = \frac{1}{\ell_f} \cos^{-1}\left(\frac{T_1 + T_4}{2}\right) \tag{4.14}$$

instead of either Eq. (4.12) or (4.13).

4.1.2 Acoustic impedance of perforations

Once the acoustic properties of the absorbing material are obtained, the acoustic impedance of perforations contacting the absorbent on one side can be also determined experimentally. Unlike the measurement of acoustic properties of the absorbing material, only a single experiment with one termination is necessary for the perforation impedance measurement. An anechoic termination is applied in this study to reduce the interferences at microphones by the reflected wave from the termination. The acoustic impedance of perforations shown in Fig. 4.3 is defined as

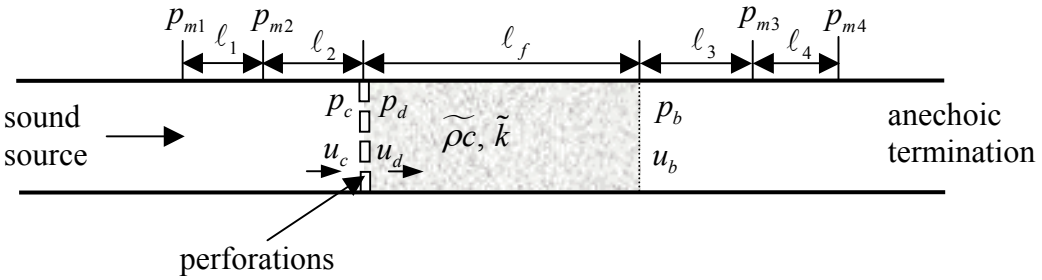

Figure 4.3: The schematic of the experimental setup for obtaining the acoustic impedance of perforations in the absence of mean flow.

$$\zeta_p = \frac{p_c - p_d}{\rho_0 c_0 u_c}, \tag{4.15}$$

where p_c and p_d are the acoustic pressures at the perforation surfaces contacting air and absorbing material, respectively, and $u_c \left(= u_d\right)$ is the acoustic velocity at the perforations. The acoustic pressure and velocity at the perforation surface facing air are obtained in terms of pressures measured at microphones #1 and #2 by using Eqs. (4.5) and (4.6) as

$$\begin{bmatrix} p_c \\ u_c \end{bmatrix} = \begin{bmatrix} \cos\left(k_0 \ell_2\right) & i\rho_0 c_0 \sin\left(k_0 \ell_2\right) \\ i\dfrac{1}{\rho_0 c_0}\sin\left(k_0 \ell_2\right) & \cos\left(k_0 \ell_2\right) \end{bmatrix}^{-1} \begin{bmatrix} p_{m2} \\ \dfrac{p_{m1} - p_{m2}\cos\left(k_0 \ell_1\right)}{i\rho_0 c_0 \sin\left(k_0 \ell_1\right)} \end{bmatrix}. \tag{4.16}$$

The acoustic pressure and velocity at the perforation surface in contact with fiber are expressed in terms of a series of transfer matrices and the pressures measured at microphones #3 and 4 as

$$\begin{bmatrix} p_d \\ u_d \end{bmatrix} = \left[T_{ab}\right]\left[T_{b3}\right] \begin{bmatrix} p_{m3} \\ \dfrac{p_{m3}\cos\left(k_0 \ell_4\right) - p_{m4}}{i\rho_0 c_0 \sin\left(k_0 \ell_4\right)} \end{bmatrix}, \tag{4.17}$$

where

$$\left[T_{ab}\right] = \begin{bmatrix} \cos\left(\tilde{k}\ell_f\right) & i\widetilde{\rho c}\sin\left(\tilde{k}\ell_f\right) \\ i\dfrac{\sin\left(\tilde{k}\ell_f\right)}{\widetilde{\rho c}} & \cos\left(\tilde{k}\ell_f\right) \end{bmatrix} \tag{4.18}$$

is the transfer matrix between surfaces *a* and *b*, and

$$\left[T_{b3}\right] = \begin{bmatrix} \cos\left(k_0 \ell_3\right) & i\rho_0 c_0 \sin\left(k_0 \ell_3\right) \\ i\dfrac{1}{\rho_0 c_0}\sin\left(k_0 \ell_3\right) & \cos\left(k_0 \ell_3\right) \end{bmatrix} \tag{4.19}$$

is the transfer matrix between surface *b* and microphone #3. Finally, the perforation impedance can be determined from Eqs. (4.15) – (4.19) and sound pressure measurements at four microphones. In Eq. (4.15), the experimentally determined acoustic velocities at the perforations may not be exactly identical in experiments. Thus, instead of Eq. (4.15), the averaged value of the two velocities can be used for the calculation of perforation impedance as

$$\zeta_p = \frac{p_c - p_d}{\frac{1}{2}\rho_0 c_0 \left(u_c + u_d\right)}. \tag{4.20}$$

4.1.3 Transmission loss

Transmission loss is used to characterize the acoustic behavior of a silencer, since it is representative of the silencer itself and independent of the source and termination impedances. The transmission loss is defined as the ratio of incident and transmitted power $\left(L_{wi} \text{ and } L_{wt}\right)$ of a silencer and is given under the assumption of anechoic termination and plane wave propagation inside upstream and downstream tubes by

$$TL = L_{wi} - L_{wt} = 10\log\left|\frac{S_{in}A_{in}^2}{2}\frac{2}{S_{out}A_{tr}^2}\right|, \tag{4.21}$$

where S_{in} and S_{out} are the cross-sectional areas of inlet and outlet ducts, and A_{in} and A_{tr} are the magnitudes of incident and transmitted planar waves. When the inlet and outlet pipe diameters are the same, Eq. (4.21) is reduced to

$$TL = 20\log\left|\frac{A_{in}}{A_{tr}}\right|. \tag{4.22}$$

The magnitudes of incident and transmitted waves needed in Eq. (4.22) can be expressed in terms of reflection coefficients at the inlet and outlet surfaces of the silencer $\left(R_a \text{ and } R_b\right)$ as

$$A_{in} = \frac{p_{m2}}{1 + R_a} \tag{4.23}$$

and

$$A_{tr} = \frac{p_{m3}}{1 + R_b}. \tag{4.24}$$

As described in ASTM E1050-98, the reflection coefficients are given by

$$R_a = \frac{H_{12} - e^{-ik_0\ell_1}}{e^{-ik_0\ell_1} - H_{12}} e^{2ik_0(\ell_1+\ell_2)} \tag{4.25}$$

and

$$R_b = \frac{H_{34} - e^{-ik_0\ell_3}}{e^{-ik_0\ell_3} - H_{34}} e^{2ik_0(\ell_3+\ell_4)}, \tag{4.26}$$

where H_{ij} is the transfer function between microphones i and j, which is defined as the ratio of cross-spectrum between microphones i and j $\left(G_{ij}\right)$ and auto-spectrum at microphone i $\left(G_{ii}\right)$:

$$H_{ij} = \frac{G_{ij}}{G_{ii}}. \tag{4.27}$$

Combination of Eqs. (4.22) – (4.27) yields the transmission loss of a silencer.

4.2 Impedance tube setup in the presence of mean flow

An impedance tube setup in the presence of mean flow was designed and fabricated as depicted in Fig. 4.4. The sound source consists of two 8 in speakers with 300 W each, which are connected to the main duct by conical sections. Numerical simulations have shown that the junction where the main duct and conical sections from speakers merge needs to be small to reduce the internal resonances. Such resonances could interfere with the transfer of acoustical energy generated by the speakers to the main duct. In order to suppress the flow noise generated at the inlet, a perforated dissipative silencer of 12×12×18 cm is introduced upstream of the speakers. A perforated duct of 25% porosity is used and the outer chamber is filled with fibrous material.

Anechoic termination is necessary to measure the transmission loss, which may also be beneficial for the perforation impedance measurements since it can reduce the wave reflected from the termination to the acoustic element under consideration. The approach in Fig. 4.1 that places the absorbing material directly within the duct is not suitable when flow is considered. Thus, a termination with two steps of diverging conical sections and a cylindrical chamber is designed based on the numerical simulations of reflection coefficients for various configurations. While an exponential expansion would be ideal to accomplish lower reflection coefficients, the high cost of manufacturing of such an expansion led to the design of a two step (4.5° and 13.0° of half angle) conical sections and a cylindrical chamber of 30.2 cm diameter and 50.8 cm length. The conical sections and the downstream cylindrical chamber, which are separated from the main duct by a perforated tube of 4.9 cm diameter and 25 % duct porosity, are filled with fibrous material of 150 kg/m^3 to suppress of the flow noise and minimize the reflection

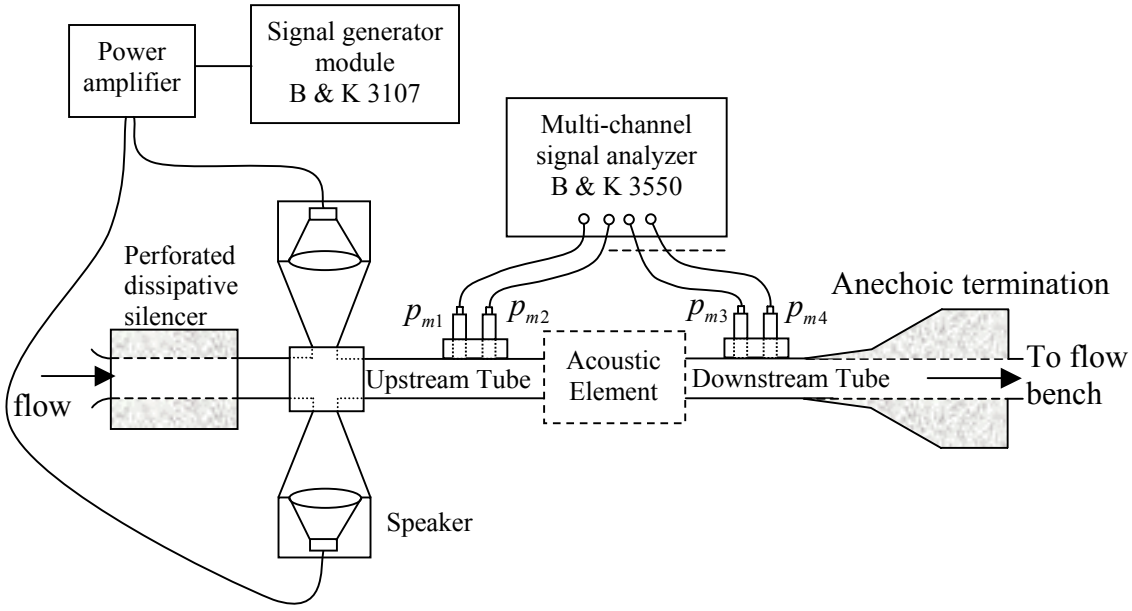

Figure 4.4: The schematic of the impedance tube setup in the presence of mean flow.

coefficient. The downstream end is connected to a flow bench which can pull a maximum air flow rate of 0.63 kg/s at standard conditions with a pressure drop of up to 8.72 kPa.

For transmission loss measurements, two pairs of ¼ inch condenser microphones (B&K 4135) are mounted at upstream and downstream ends of the acoustic element. While random noise can be used as a sound source for low mean flow rates (thus low background noise), a single sine wave is applied at high flow rate due to elevated background noise to ensure at least 10 dB of signal-to-noise ratio as recommended by ASTM E1050-98. This setup can be modified for the measurements of acoustic impedance of perforations in the presence of grazing mean flow, as described next.

4.2.1 Acoustic impedance of perforations

The impedance tube setup of Fig. 4.4 is now modified by introducing a sidebranch as shown in Fig. 4.5 to measure the acoustic impedance of perforations, particularly in contact with the absorbing material, and in the presence of grazing mean flow. The circular sidebranch with an inner diameter of 4.90 cm is perpendicular to the rectangular main duct, with the circular perforated sample plate being placed at the interface of the two. The perforated plate is located 4 m from the inlet of main duct to ensure a fully developed flow at the plate, and its surface is flush with the inner wall of the main duct. The internal dimensions of the main duct is 7.62 × 5.08 cm and the wall thickness is 1.27 cm. An ℓ'_f -long section of the sidebranch starting at the perforations is filled with the fibrous material. Two microphones, one in the main duct and the other

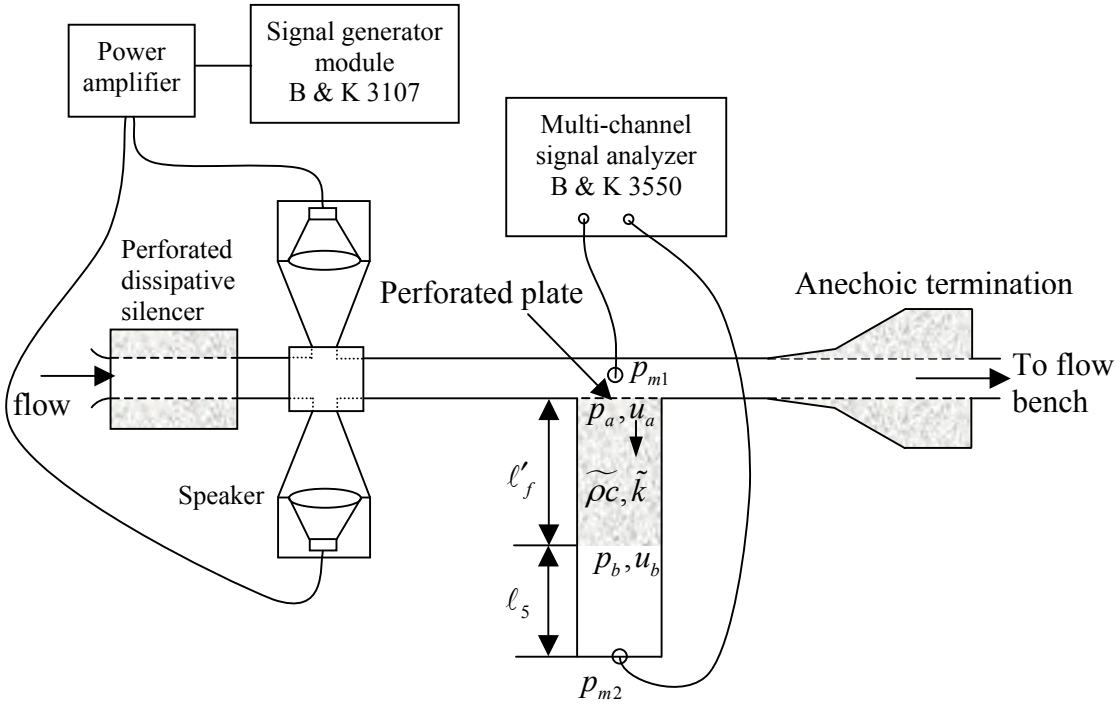

Figure 4.5: The schematic of the experimental setup for obtaining acoustic impedance of perforations in the presence of mean flow.

at the end of sidebranch are mounted, as shown in Fig. 4.5. The pressure measurements (p_{m1} and p_{m2}) from these two microphones are used to calculate the acoustic impedance.

The acoustic impedance of the perforated plate in contact with the absorbing material depicted in Fig. 4.5 is defined as

$$\zeta_p = \frac{p_{m1} - p_a}{\rho_0 c_0 u_a}, \tag{4.28}$$

where p_a and u_a are respectively the acoustic pressure and velocity at the perforation surface contacting the material, specified by

$$\begin{bmatrix} p_a \\ u_a \end{bmatrix} = \begin{bmatrix} \cos\left(\tilde{k}\ell'_f\right) & i\widetilde{\rho c}\sin\left(\tilde{k}\ell'_f\right) \\ i\frac{1}{\widetilde{\rho c}}\sin\left(\tilde{k}\ell'_f\right) & \cos\left(\tilde{k}\ell'_f\right) \end{bmatrix} \begin{bmatrix} \cos\left(k_0\ell_5\right) & i\rho_0 c_0 \sin\left(k_0\ell_5\right) \\ i\frac{1}{\rho_0 c_0}\sin\left(k_0\ell_5\right) & \cos\left(k_0\ell_5\right) \end{bmatrix} \begin{bmatrix} p_{m2} \\ u_{m2} \end{bmatrix}, \tag{4.29}$$

where $\widetilde{\rho c}$ and $\tilde{k}$ are known complex characteristic and wavenumber of the absorbing material. Equation (4.29) can be rewritten, with the rigid wall condition ($u_{m2} = 0$) as

$$\begin{bmatrix} p_a \\ u_a \end{bmatrix} = \begin{bmatrix} T_{11} & T_{12} \\ T_{21} & T_{22} \end{bmatrix} \begin{bmatrix} p_{m2} \\ 0 \end{bmatrix} \tag{4.30}$$

Substitution of Eq. (4.30) into Eq. (4.28) gives the acoustic impedance of perforations as

$$\zeta_p = \frac{\frac{p_{m1}}{p_{m2}} - T_{11}}{\rho_0 c_0 T_{21}}. \tag{4.31}$$

CHAPTER 5

ACOUSTIC PROPERTIES OF ABSORBING MATERIAL

The absorption of acoustic wave in fibrous material may be expressed in terms of complex characteristic impedance and wavenumber as described in Chapter 3. Thus, accurate estimation of such acoustic properties is essential in the use of theoretical approaches and in understanding how the acoustic properties affect transmission loss (to be covered later in Chapter 7.) In addition, the measurement of perforation impedance in contact with absorbing material (to be presented in Chapter 6) requires accurate acoustic properties of the material. Since the structure of absorbing material is rather complex, the acoustic properties are usually determined by experiments as in the present study, which obtained the characteristic impedance and wavenumber of a fibrous material using the impedance tube setup depicted in Figs. 4.1 and 4.2. Advantex® strand glass fiber developed by Owens Corning is used in the experiments. The texturization process separates filament roving strands of fiber glass into individual filaments by turbulent air flow (Silentex™ process). The average diameter of the individual filaments in the roving strand is 24 μm. The degree to which the strands are separated into individual filaments (texturization condition) affects the acoustic properties of the absorbing material. In

addition to the acoustic properties, high thermal and corrosion resistance of the Advantex® glass fiber may also be desirable for particularly exhaust systems. The physical and chemical properties of various absorptive materials and their relative durability in automotive silencer operations have been described by Beranek (1988) and Huff (2001).

This chapter first introduces the selected existing empirical formulations, given by Delany and Bazley (1970) and Mechel (1992), of the complex characteristic impedance and wavenumber in terms of frequency and flow resistivity. Flow resistivity of the fibrous material used in this study is also provided based on the work by Nice (1999). Then, complex characteristic impedance and wavenumber for two different texturization conditions and two filling densities are experimentally determined in the present study and presented along with their comparisons to existing expressions. Finally, the estimated speed of sound in the absorbing material from the measured complex wavenumber is briefly discussed.

5.1 Selected existing formulations

The normalized empirical complex characteristic impedance $\tilde{Z}$ and wavenumber $\tilde{k}$ of Delany and Bazley (1970) for fibrous materials are given in MKS units by

$$\frac{\tilde{Z}}{\rho_0 c_0} = \left[1 + 0.0511\left(f / R_f\right)^{-0.75}\right] + i\left[-0.0768\left(f / R_f\right)^{-0.73}\right] \tag{5.1}$$

$$\frac{\tilde{k}}{k_0} = \left[1 + 0.0858\left(f / R_f\right)^{-0.70}\right] + i\left[-0.1749\left(f / R_f\right)^{-0.59}\right], \tag{5.2}$$

where ρ_0 is the air density, f the frequency, and R_f the flow resistivity which is mainly dependent on fiber diameter, layer orientation, and filling density. The data points used for the curve-fits of Eqs. (5.1) and (5.2) are obtained using a two-cavity method within the range $0.01 < f/R_f < 1$ in MKS units for the homogeneous material with its porosity (Y) close to one. Mechel (1992) also presented similar empirical formulations of characteristic impedance and wavenumber for the glass fiber in MKS units with $\rho_0 f / R_f > 0.25$ as

$$\frac{\tilde{Z}}{\rho_0 c_0} = \left[1 + 0.0235\left(\rho_0 f / R_f\right)^{-0.887}\right] + i\left[-0.0875\left(\rho_0 f / R_f\right)^{-0.770}\right] \tag{5.3}$$

$$\frac{\tilde{k}}{k_0} = \left[1 + 0.102\left(\rho_0 f / R_f\right)^{-0.705}\right] + i\left[-0.179\left(\rho_0 f / R_f\right)^{-0.674}\right]. \tag{5.4}$$

He also provided the coefficients for $\rho_0 f / R_f < 0.25$ and other material, such as mineral and basalt wool.

Equations (5.1) − (5.4) are functions of frequency and flow resistivity. While the negative imaginary part of the wavenumber particularly ensures the dissipation of sound, the real part greater than unity indicates a lower speed of sound through the absorbing material. When the flow resistivity approaches zero, both characteristic impedance and wavenumber approach the values of air.

5.2 Flow resistivity

The flow resistivity for the material used in the present study is experimentally determined by Owens Corning (Nice, 1999) using the standard test method described in the ASTM C522-87 (1997), and given in Table 5.1. The characteristic impedance and wavenumber as proposed by of Delany and Bazley (1970) and Mechel (1992) can then be obtained by substituting the flow resistivity in Table 5.1 into Eqs. (5.1) − (5.4).

Bulk density ρ_f (kg/m^3)	Flow resistivity R_f (mks rayl/m)
100	4,896
200	17,378

Table 5.1 Flow resistivity measured by Owens Corning.

5.3 Characteristic impedance and wavenumber of fibrous material

A transfer function method with two different termination conditions in the impedance tube setup depicted in Fig. 4.2 is developed in this study to acquire the complex characteristic impedance and wavenumber of the fibrous material in the absence of mean flow. The mathematical process for this method is described in Section 4.1.1. The precise measurements of distances between the sample surfaces and microphones or among microphones are critical in the experiments. The accuracy within 0.1 mm for the materials with well defined surfaces is recommended by ASTM 1050-98 (1998).

However, a precise physical measurement may not be possible due, for example, to the difficulty in finding the centers of the microphones with their diameter of 6.35 mm (1/4 inch). Thus, the distances, ℓ_1 through ℓ_4 and ℓ_f, are acoustically estimated using quarter wave resonances as shown in Fig. 5.1. The estimated distances by this method in Fig. 4.2 are as follows: $\ell_1 = \ell_4$= 3.55 cm, ℓ_2=12.81 cm, ℓ_3= 12.71 cm, and ℓ_f=10.16 cm. The sample length ℓ_f is chosen considering two aspects. When the sample length is too short, the impact of inhomogeneous filling may be magnified. On the other hand, too long sample may not transfer sufficient sound energy to the downstream microphones due to wave dissipation through the material, particularly at high frequencies. An accurate estimation of speed of sound is also important for the measurements, which is calculated here by

$$c_0 = 20.047\sqrt{273.15 + T_C} \quad \text{[m/s]}, \tag{5.5}$$

as suggested by ASTM 1050-98 (1998). All experiments were performed at the room temperature, T_C = 19±1 °C.

Existing formulations of Eqs. (5.1) − (5.4) were determined from numerous experiments for various materials and filling densities, and then normalized in terms of flow resistivity and frequency. The present study rather focuses on two filling densities (ρ_f = 100 and 200 kg/m^3; approximate bounds in practical applications), and experimentally determines their acoustic properties. The properties obtained for both filling densities are then directly applied to the measurements of acoustic impedance of perforation in contact with fibrous material as described in Section 4.1.2, and also used for the transmission loss predictions for dissipative silencers.

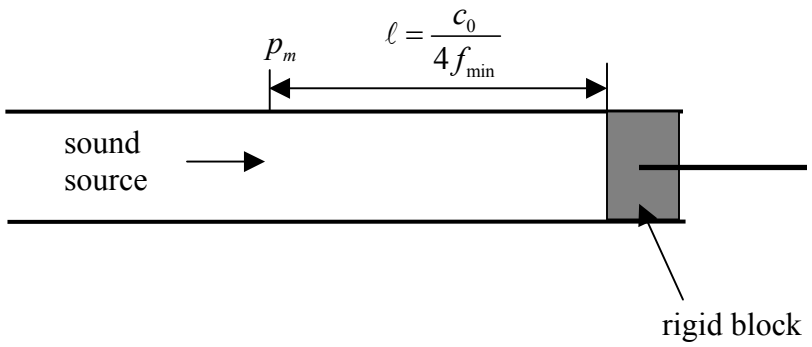

Figure 5.1: Measurement of distance using quarter wave resonance; $f_{\min}$ is the frequency at which the acoustic pressure of p_m is minimum.

5.3.1 Fiber samples

Absorbent samples, 10 cm long and 4.9 cm in diameter and with two different filling densities $\rho_f = 100$ and 200 kg/m^3, are placed in the test tube. Densities significantly lower than $\rho_f = 100$ kg/m^3 may cause the movement of fiber inside silencers and higher than $\rho_f = 200$ kg/m^3 may be undesirable in terms of cost, weight, and in some cases acoustic attenuation, hence the justification for the choices in this study. The material density of the fiber (ρ_m) is 2.62×10^3 kg/m^3 and thus the porosity of the material (Y) for filling or bulk density $\rho_f = 100$ and 200 kg/m^3, with the ideal texturization being calculated as 0.962 and 0.924 using Eq. (3.108), respectively.

The fiber orientation and the texturization condition of samples need to be considered due to their influence on the acoustic properties. Random filling is applied to achieve overall isotropic and homogeneous conditions. However, partially or locally non-isotropic or inhomogeneous fraction may exist due, for example, to the hand filling of the fiber into the test tube. Thus, experiments with five different samples for each filling density are performed to examine the effect of variations of filling conditions. The averaged values from five individual experiments are then used as the final result.

The texturization condition of the fiber, the degree to which the strands are separated into individual filaments, significantly affects the acoustic properties of the material. To illustrate the effect of texturization condition on the acoustic properties of the fibrous material, two set of samples with different texturization conditions were applied in the experiments. Since the texturization condition is difficult to define

quantitavely for the given fibrous material, two qualitative conditions, 'good' and 'normal', are considered in this study. The fiber structures of the two texturization conditions for $\rho_f = 100$ kg/m^3 are shown in Fig. 5.2. While the 'good' texturization reveals mostly individual filaments, the 'normal' texturization exhibits partially bonded strands.

The front surfaces of the fiber samples also need to be well defined in the experiments. The surfaces of the samples perpendicular to the direction of wave propagation are identified by the two screens. The screens have high porosity not to influence the surface properties of the fiber and sufficiently high tension to hold the fiber flat at the surface.

5.3.2 Good texturization

Figures 5.3 and 5.4 show the individual measurements of five different samples and their averaged values for the characteristic impedance and wavenumber at $\rho_f = 100$ kg/m^3 with 'good' texturization condition. Although some scatter is displayed for the characteristic impedance, high repeatability is clearly observed, particularly for the wavenumber. Thus, the effect of locally non-isotropic or inhomogeneous filling is negligible in these experiments. The curve-fitted complex characteristic impedance and wavenumber based on the averaged values of five experiments for 'good' texturization condition are then expressed by

$$\frac{\tilde{Z}}{\rho_0 c_0} = \left[1 + 33.20(f)^{-0.7523}\right] + i\left[-28.32(f)^{-0.6512}\right] \tag{5.6}$$

(a)

(b)

Figure 5.2: Pictures of fiber samples ($\rho_f = 100$ kg/m^3); (a) good texturization and (b) normal texturization.

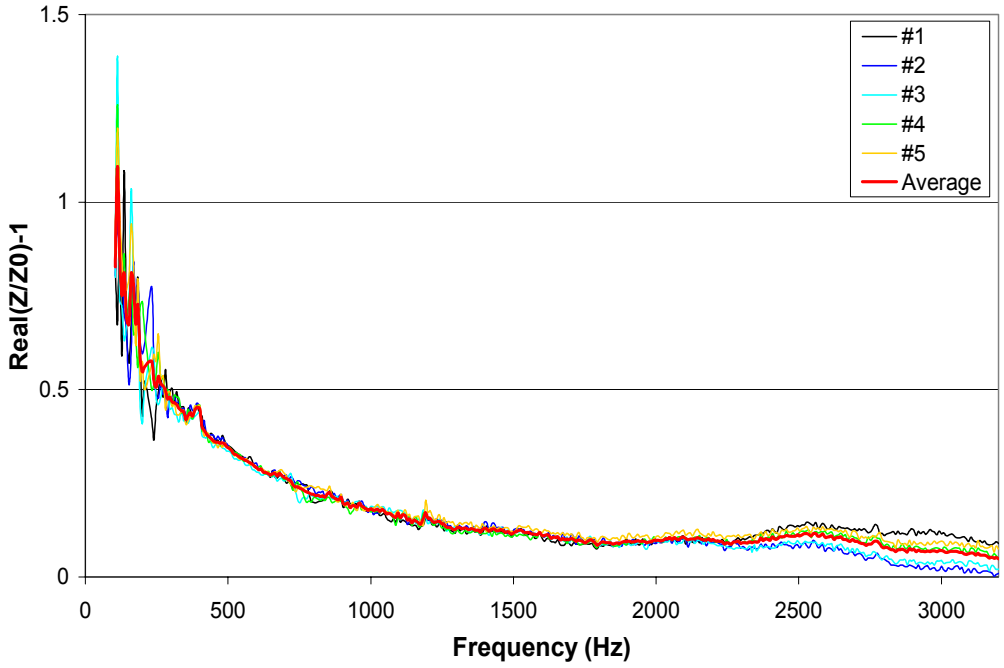

(a)

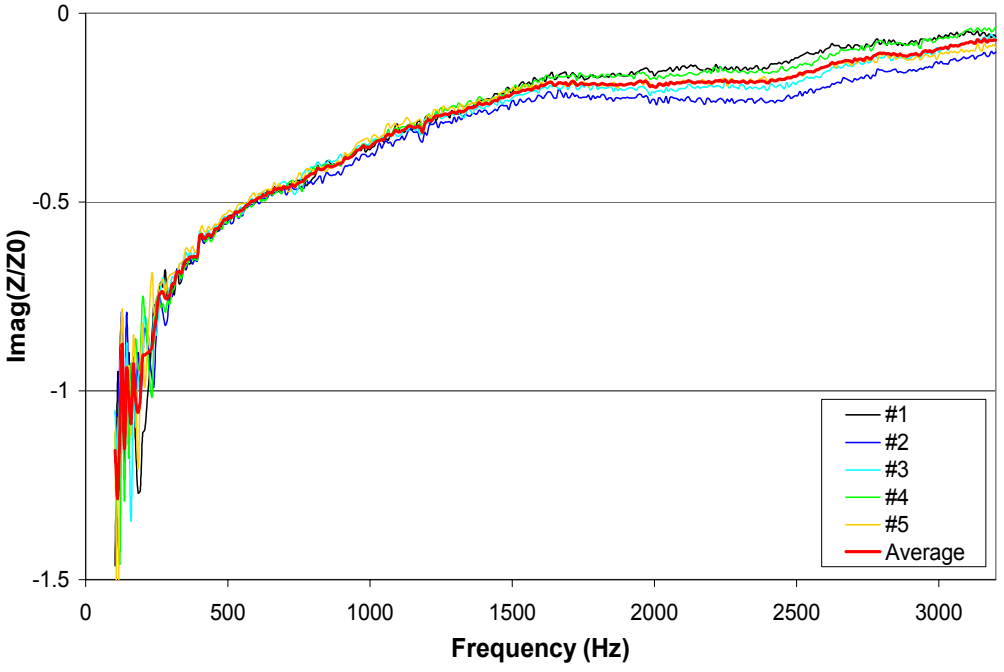

(b)

Figure 5.3: Individual and averaged experimental results of characteristic impedance of fibrous material with good texturization ($\rho_f = 100$ kg/m^3); (a) real part and (b) imaginary part.

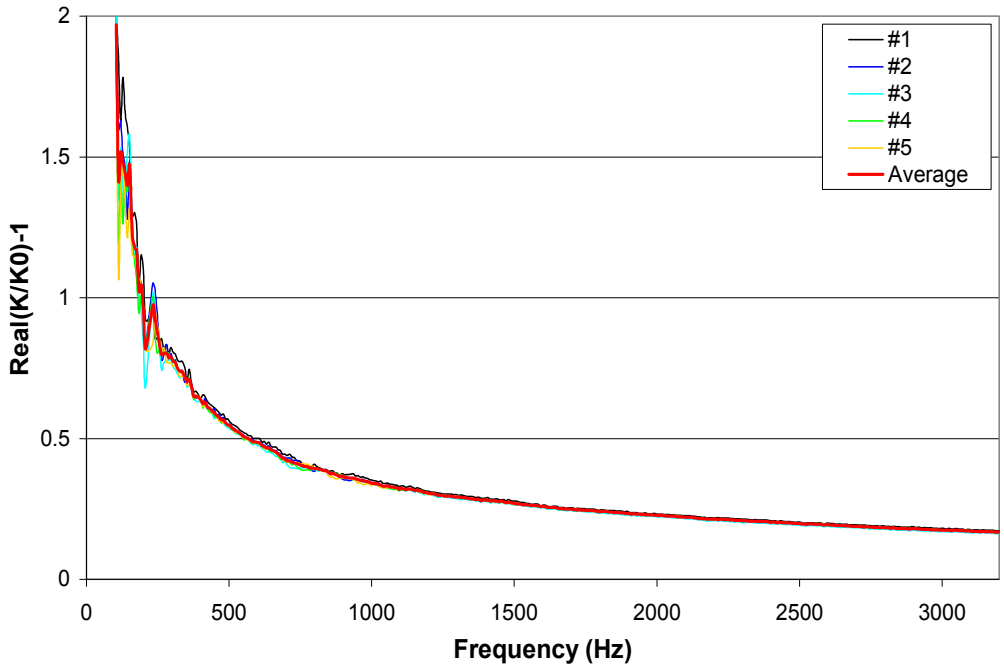

(a)

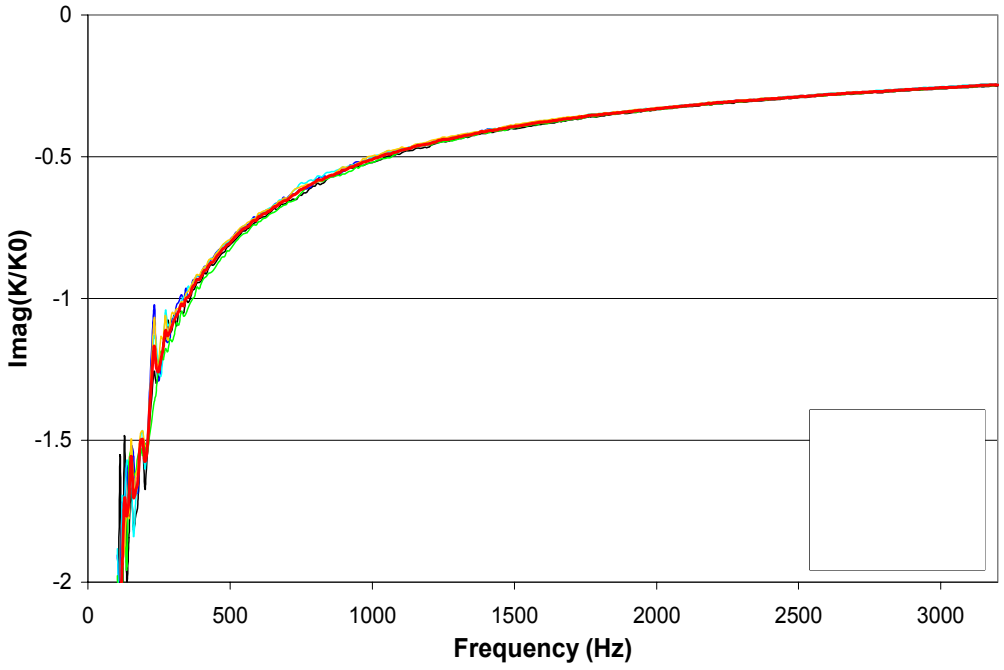

(b)

Figure 5.4: Individual and averaged experimental results of wavenumber of fibrous material with good texturization ($\rho_f = 100$ kg/m^3); (a) real part and (b) imaginary part.

$$\frac{\tilde{k}}{k_0} = \left[1 + 39.20(f)^{-0.6841}\right] + i\left[-38.39(f)^{-0.6285}\right] \tag{5.7}$$

for $\rho_f = 100$ kg/m^3 and

$$\frac{\tilde{Z}}{\rho_0 c_0} = \left[1 + 25.69(f)^{-0.5523}\right] + i\left[-71.97(f)^{-0.7072}\right] \tag{5.8}$$

$$\frac{\tilde{k}}{k_0} = \left[1 + 56.03(f)^{-0.6304}\right] + i\left[-62.05(f)^{-0.5980}\right] \tag{5.9}$$

for $\rho_f = 200$ kg/m^3. The function 'fit' of the MATLAB® is applied for all curve fits in this chapter in the frequency range of 100 – 3200 Hz. At lower frequencies, the anechoic termination condition may not be achieved and thus the two distinct termination conditions, which are necessary for accurate results, may not be applied.

Figures 5.5 − 5.8 show measured and curve-fitted real and imaginary parts of characteristic impedance and wavenumber for both $\rho_f = 100$ [Eqs. (5.6) and (5.7)] and 200 [Eqs. (5.8) and (5.9)] kg/m^3 fillings, along with comparisons to the formulations of Delany and Bazley (1970) and Mechel (1992). The flow resistivity from Table 5.1 is used for the existing formulations [Eqs. (5.1) − (5.4)]. The curve-fits represent most of the data points well, particularly for the wavenumber at both filling densities. The experimental results obtained in this study show trends similar to those of Delany and Bazley, and Mechel, though some deviations exist. For example, the real part of the characteristic impedance of Mechel has lower magnitude compared to the results of Delany and Bazley, and the present study. The impact of each parameter on the transmission loss will be illustrated later in Chapter 7.

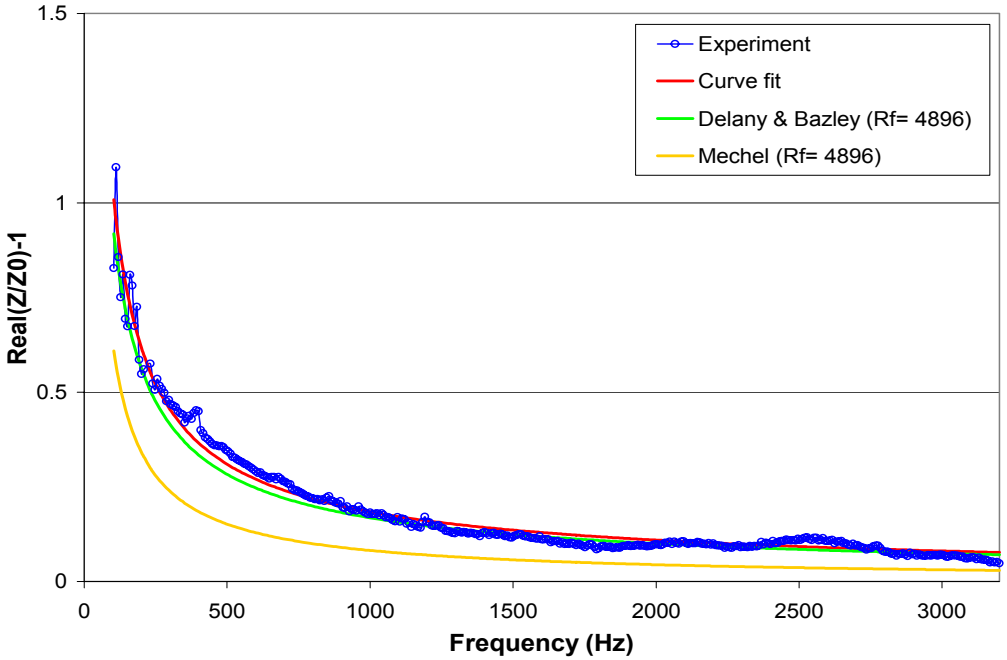

(a)

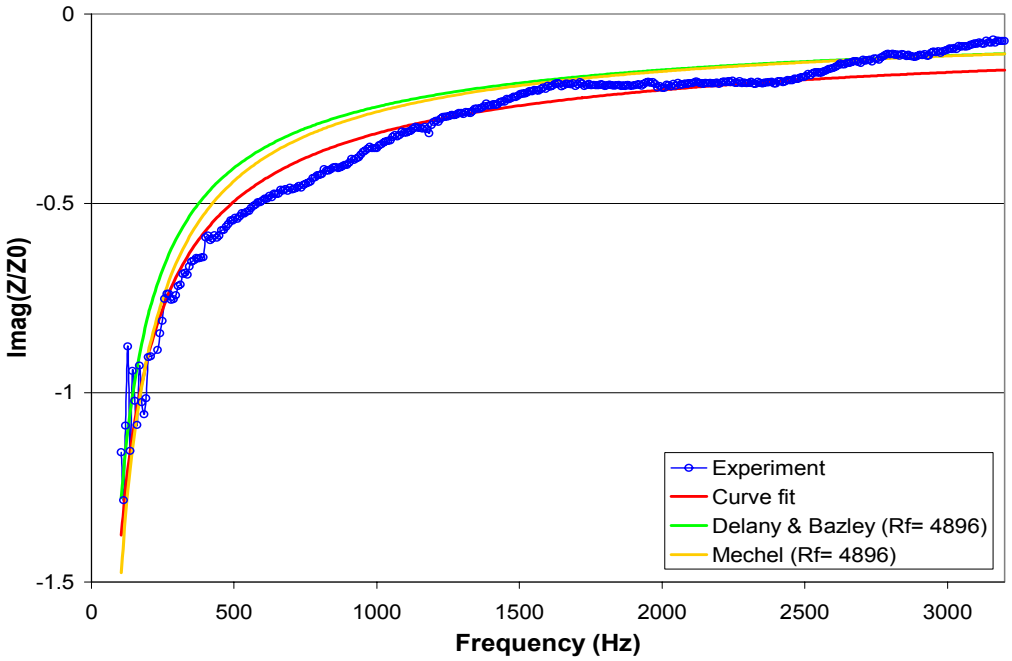

(b)

Figure 5.5: Characteristic impedance of fibrous material with good texturization ($\rho_f = 100$ kg/m^3); (a) real part and (b) imaginary part.

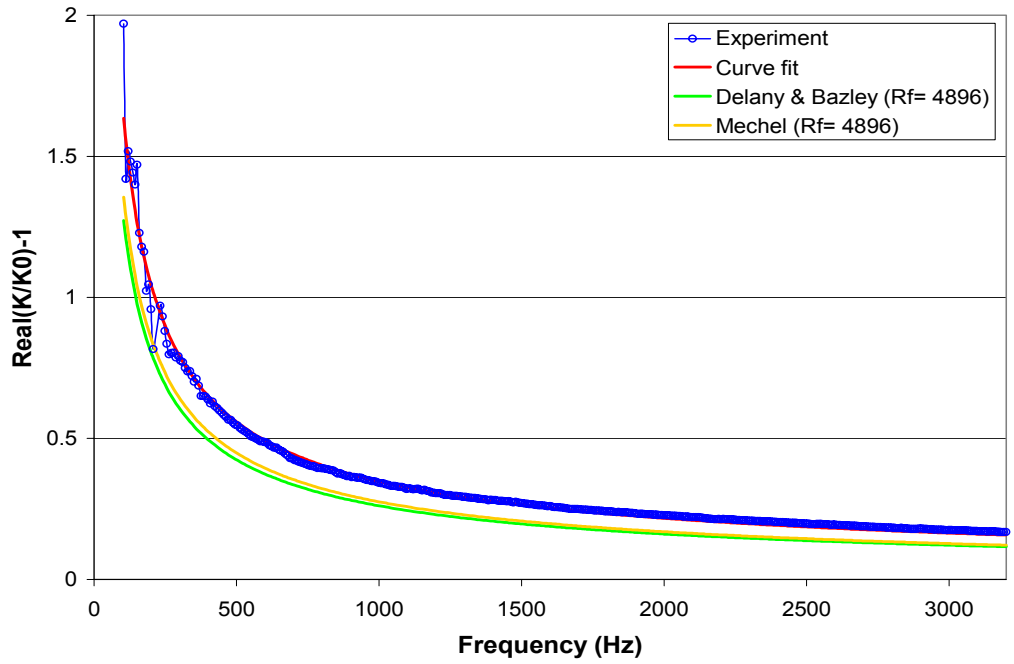

(a)

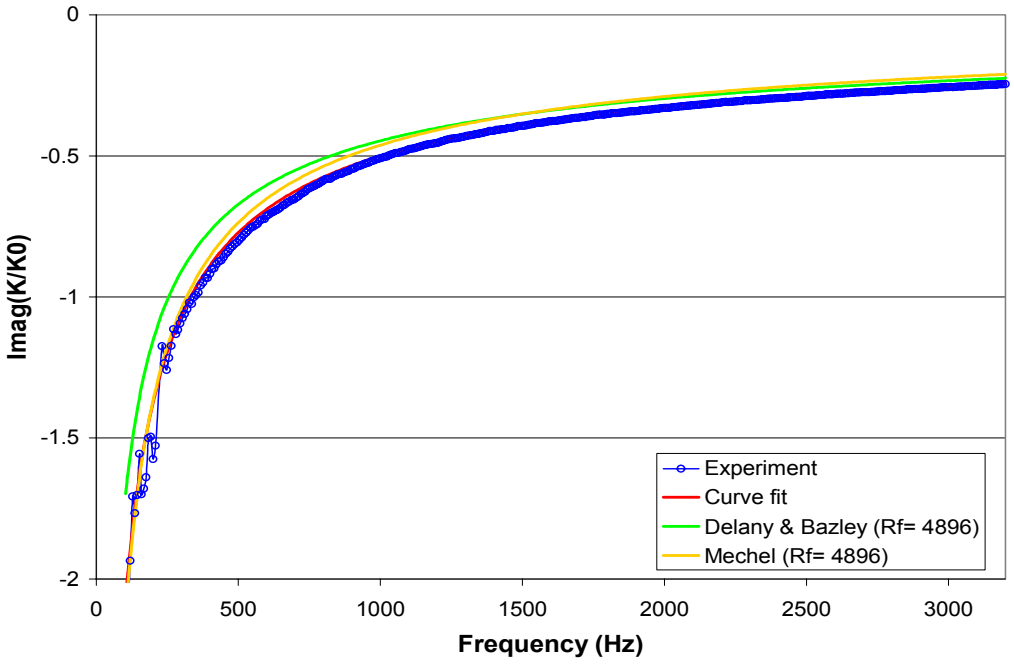

(b)

Figure 5.6: Wavenumber of fibrous material with good texturization ($\rho_f = 100$ kg/m^3); (a) real part and (b) imaginary part.

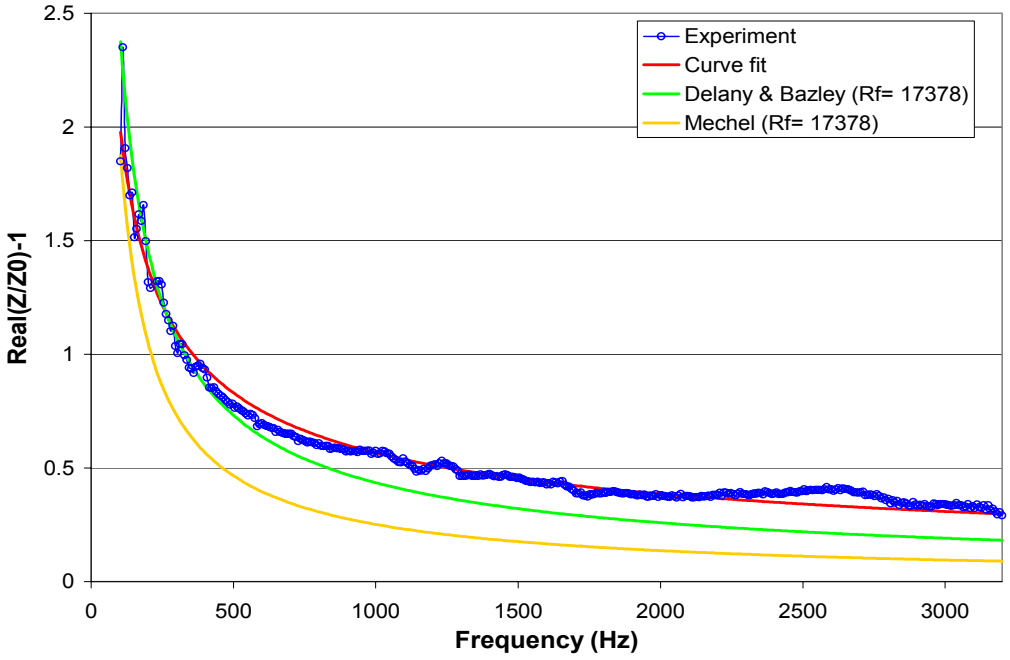

(a)

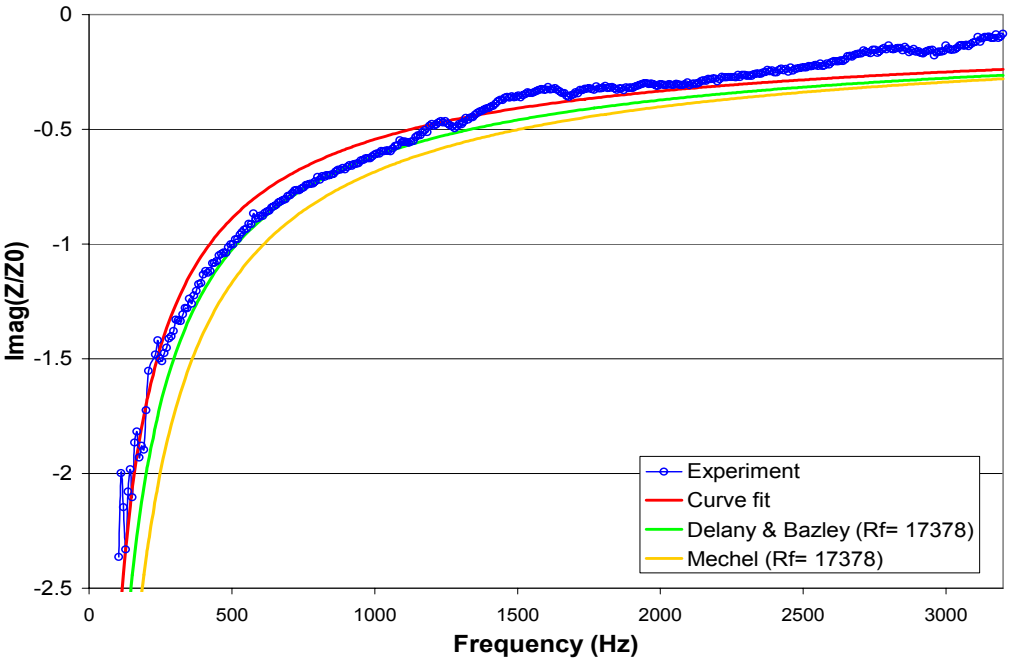

(b)

Figure 5.7: Characteristic impedance of fibrous material with good texturization ($\rho_f = 200$ kg/m^3); (a) real part and (b) imaginary part.

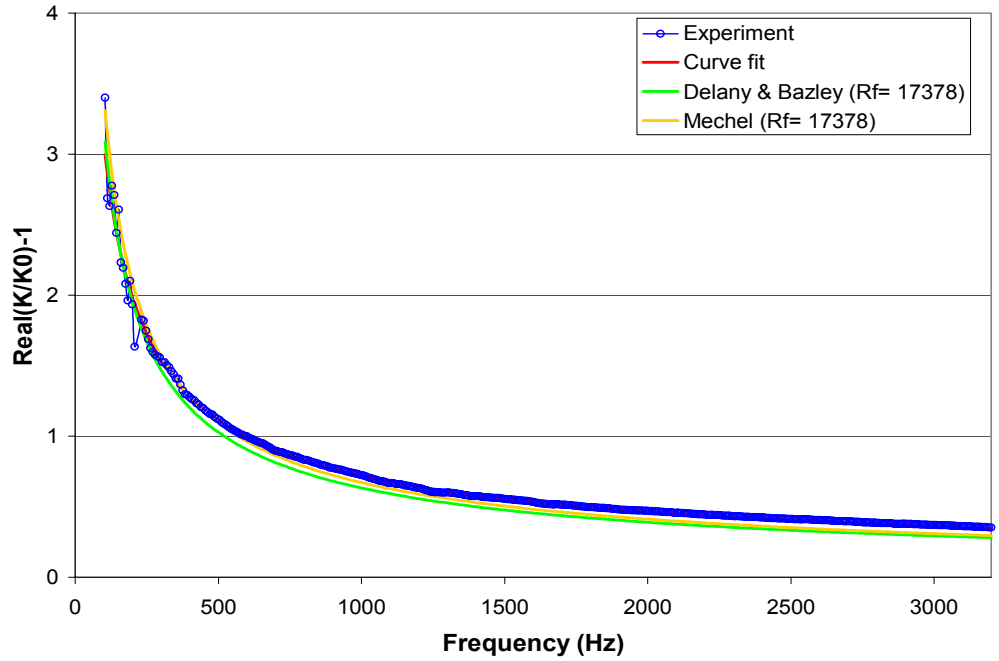

(a)

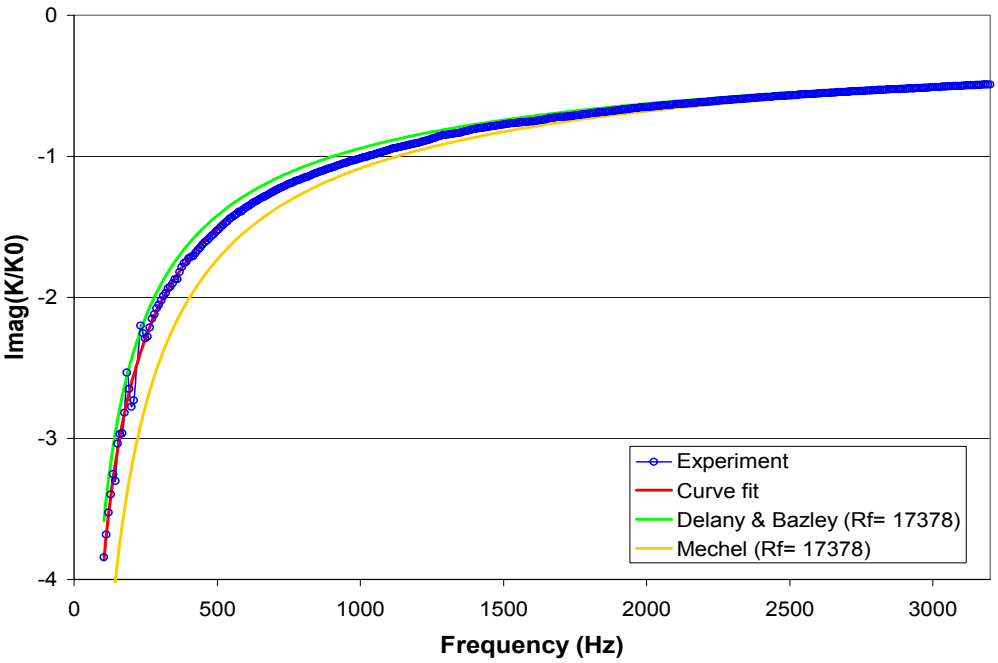

(b)

Figure 5.8: Wavenumber of fibrous material with good texturization ($\rho_f = 200$ kg/m^3); (a) real part and (b) imaginary part.

5.3.3 Normal texturization

The complex characteristic impedance and wavenumber for 'normal' texturization with filling densities of $\rho_f = 100$ and 200 kg/m^3 are also experimentally determined using the same setup and methodology utilized for the 'good' texturization. The curve-fitted properties are given by

$$\frac{\tilde{Z}}{\rho_0 c_0} = \left[1 + 33.46\left(f\right)^{-0.7726}\right] + i\left[-44.51\left(f\right)^{-0.7667}\right] \tag{5.10}$$

$$\frac{\tilde{k}}{k_0} = \left[1 + 23.1\left(f\right)^{-0.6374}\right] + i\left[-26.25\left(f\right)^{-0.6100}\right] \tag{5.11}$$

for $\rho_f = 100$ kg/m^3 and

$$\frac{\tilde{Z}}{\rho_0 c_0} = \left[1 + 17.87\left(f\right)^{-0.5400}\right] + i\left[-152.2\left(f\right)^{-0.8591}\right] \tag{5.12}$$

$$\frac{\tilde{k}}{k_0} = \left[1 + 39.6\left(f\right)^{-0.6081}\right] + i\left[-50.63\left(f\right)^{-0.6050}\right]. \tag{5.13}$$

for $\rho_f = 200$ kg/m^3. Figures 5.9 – 5.12 show the comparisons of acoustic properties of two different texturization conditions. The 'good' texturization shows higher magnitudes of the properties compared to 'normal' texturization. These differences in acoustic properties of material due to the texturization conditions may cause substantial deviations in predicted transmission loss as will be illustrated later in Chapter 7.

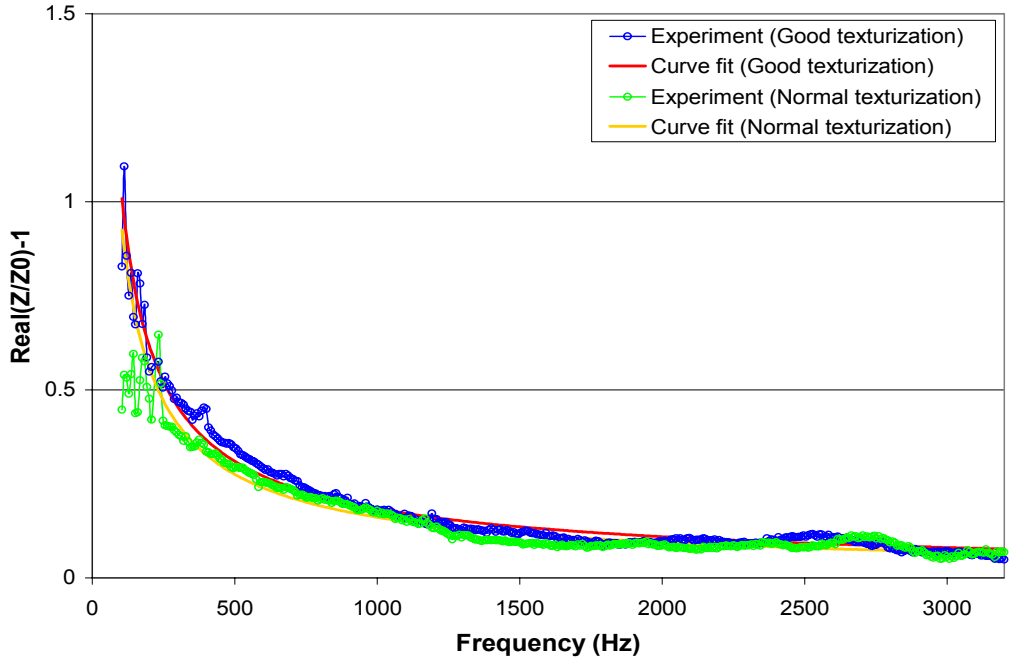

(a)

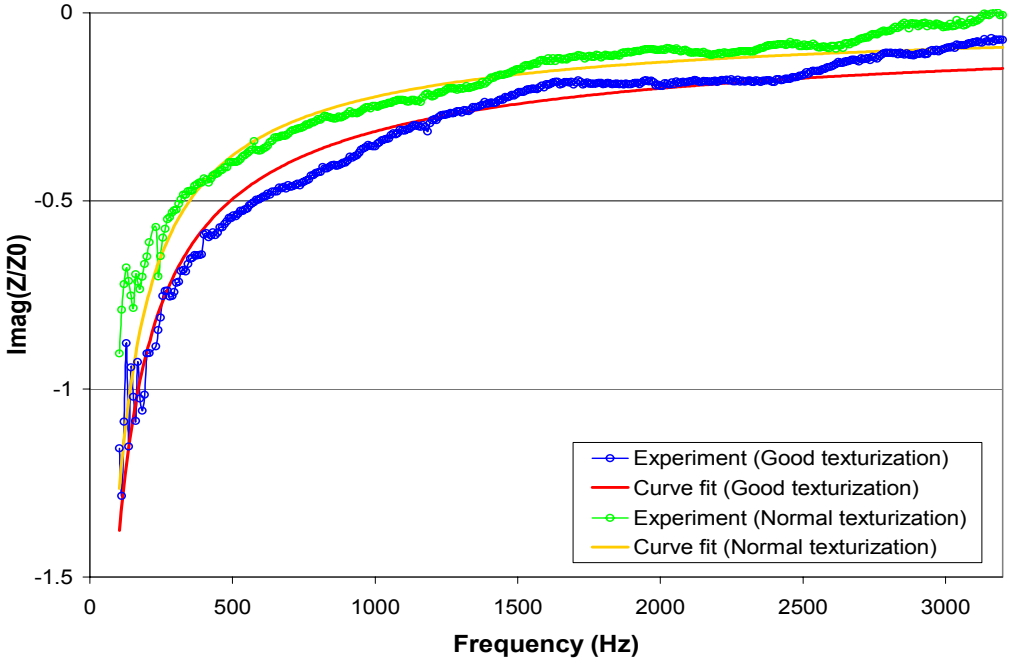

(b)

Figure 5.9: Comparison of characteristic impedance of fibrous material for both texturization conditions ($\rho_f = 100$ kg/m^3); (a) real part and (b) imaginary part.

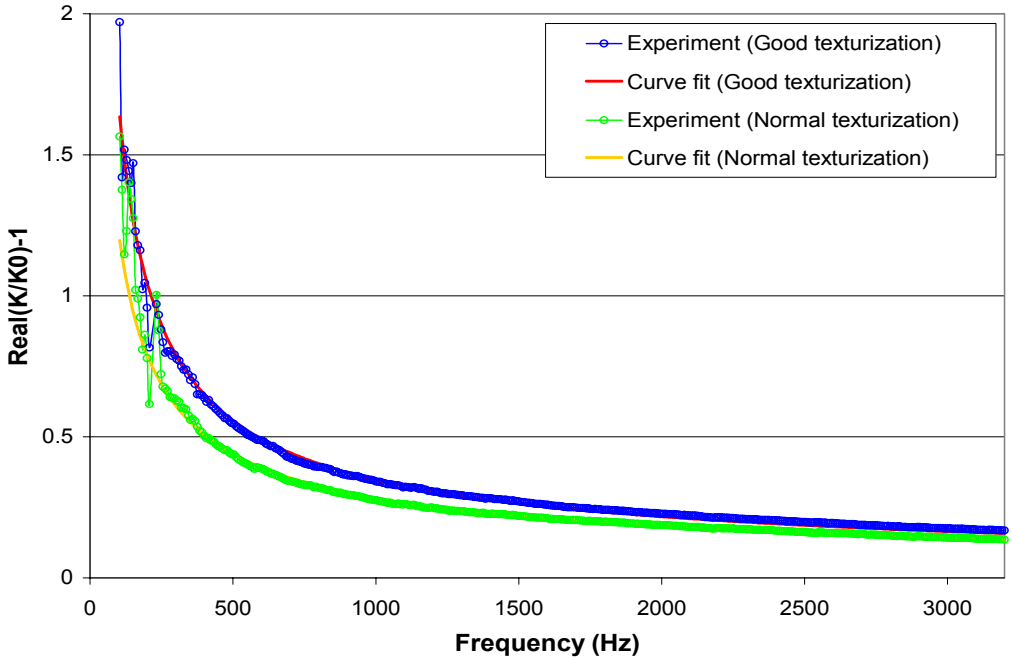

(a)

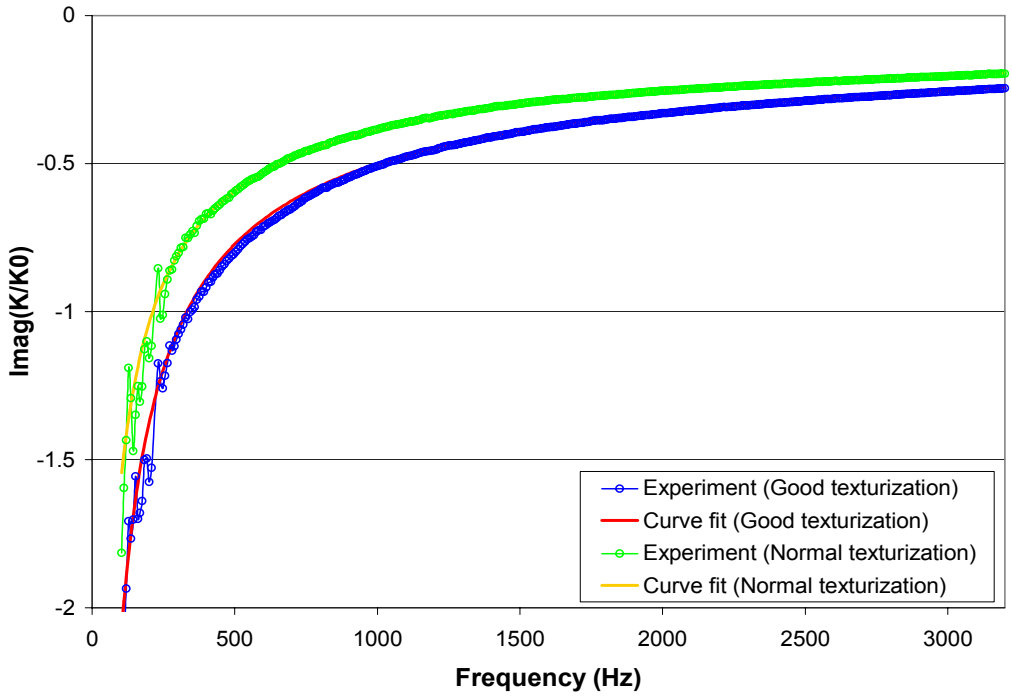

(b)

Figure 5.10: Comparison of wavenumber of fibrous material for both texturization conditions ($\rho_f = 100$ kg/m^3); (a) real part and (b) imaginary part.

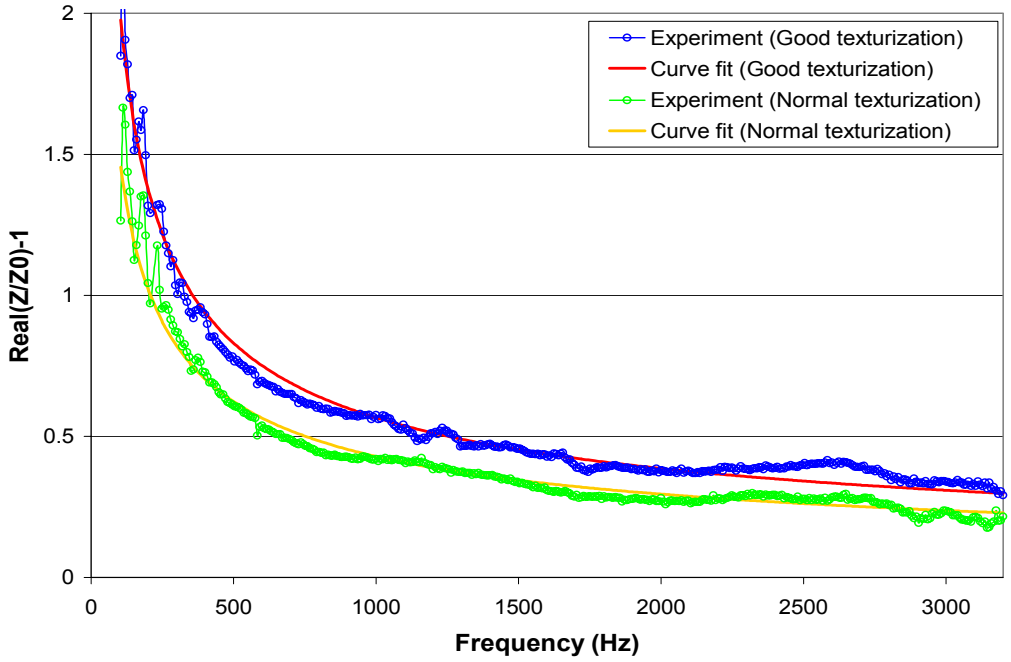

(a)

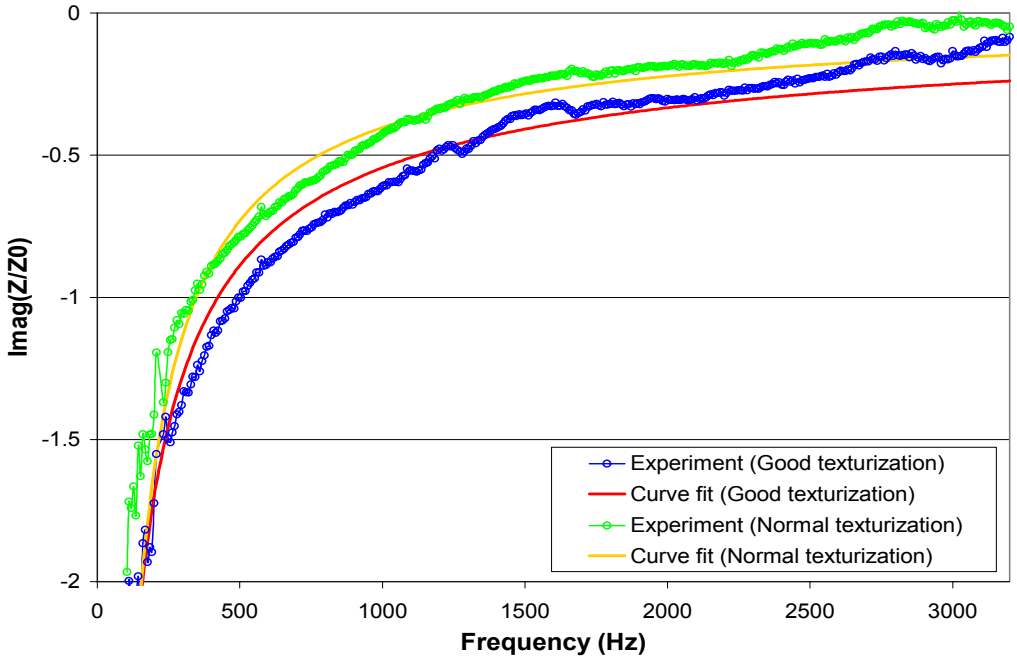

(b)

Figure 5.11: Comparison of characteristic impedance of fibrous material for both texturization conditions ($\rho_f = 200$ kg/m^3); (a) real part and (b) imaginary part.

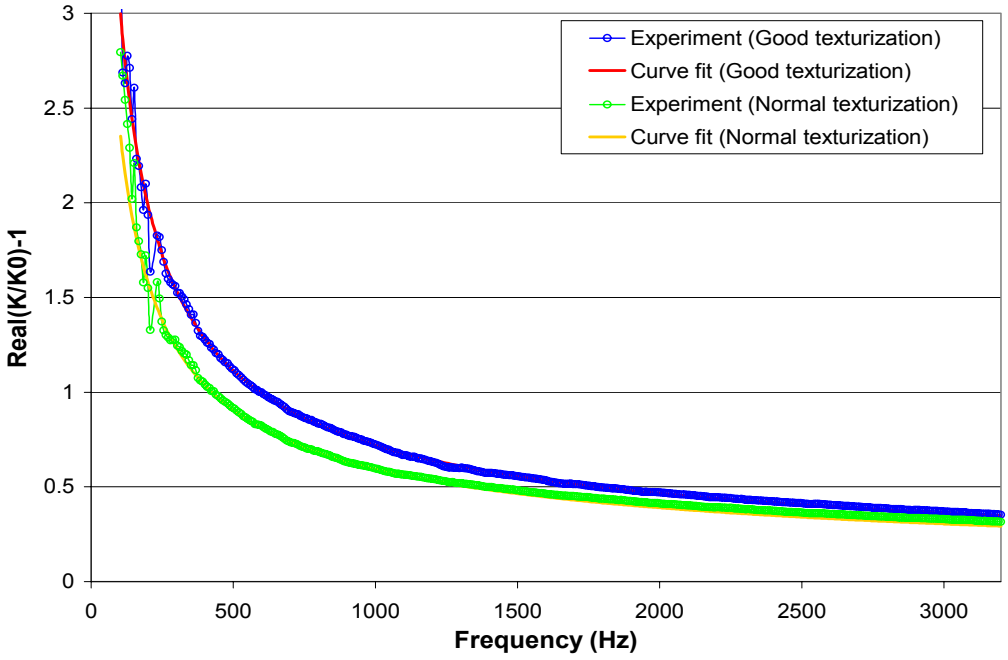

(a)

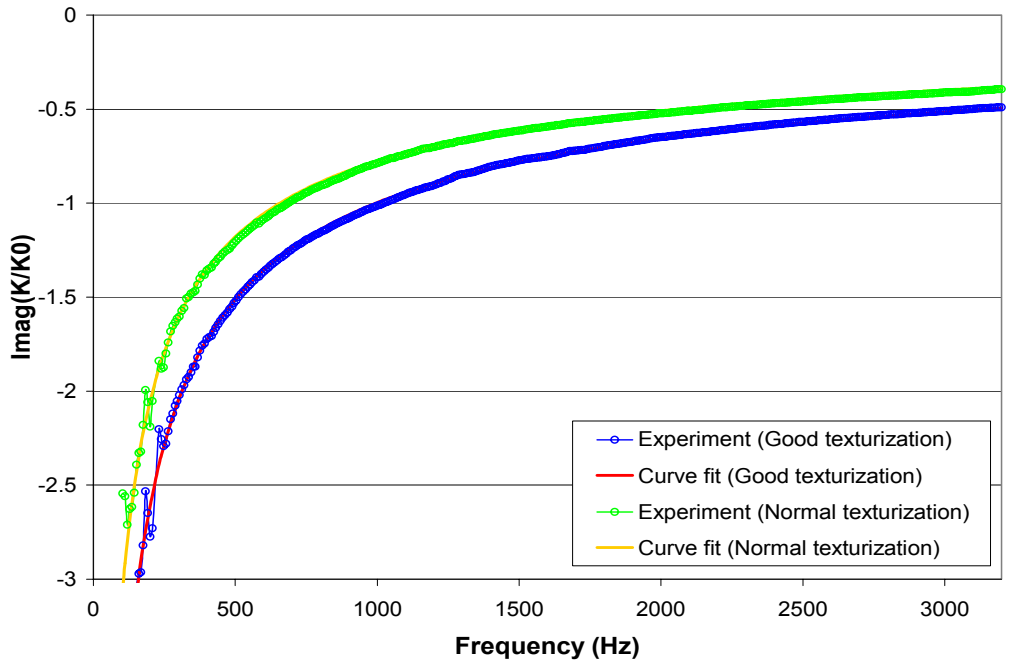

(b)

Figure 5.12: Comparison of wavenumber of fibrous material for both texturization conditions ($\rho_f = 200$ kg/m^3); (a) real part and (b) imaginary part.

5.3.4 Speed of sound in the fibrous material

The knowledge of speed of sound through the absorbing material may be useful, for example, in calculating the cut-off frequencies of higher modes. The phase speed of sound $\tilde{c}_{ph}$ through the absorbing material can be estimated from the measured complex wavenumbers as,

$$\tilde{c}_{ph} = \frac{c_0}{\text{Real}\left(\frac{\tilde{k}}{k_0}\right)}. \tag{5.14}$$

Figure 5.13 shows the frequency-dependent speed of sound estimated in this study using the real part of wavenumbers for both $\rho_f = 100$ and 200 kg/m^3 filling densities. The speed of sound for $\rho_f = 200$ kg/m^3 is lower than that of $\rho_f = 100$ kg/m^3. Scott (1946c) also presented the phase velocity in a Rock-wool in the range of 100 – 300 m/s for 100 – 3200 Hz. Song and Bolton (2000) also illustrated the low phase speed of sound through the absorbing material, 0.5 – 0.8 times the speed of sound in air. The lower phase speed of sound in the fibrous material suggests that that higher order modes can propagate at lower frequency in absorbing material than in air. Therefore, the predictions of acoustic behavior by one-dimensional analysis for dissipative silencers may fail at frequencies lower than for reactive silencers with similar dimensions.

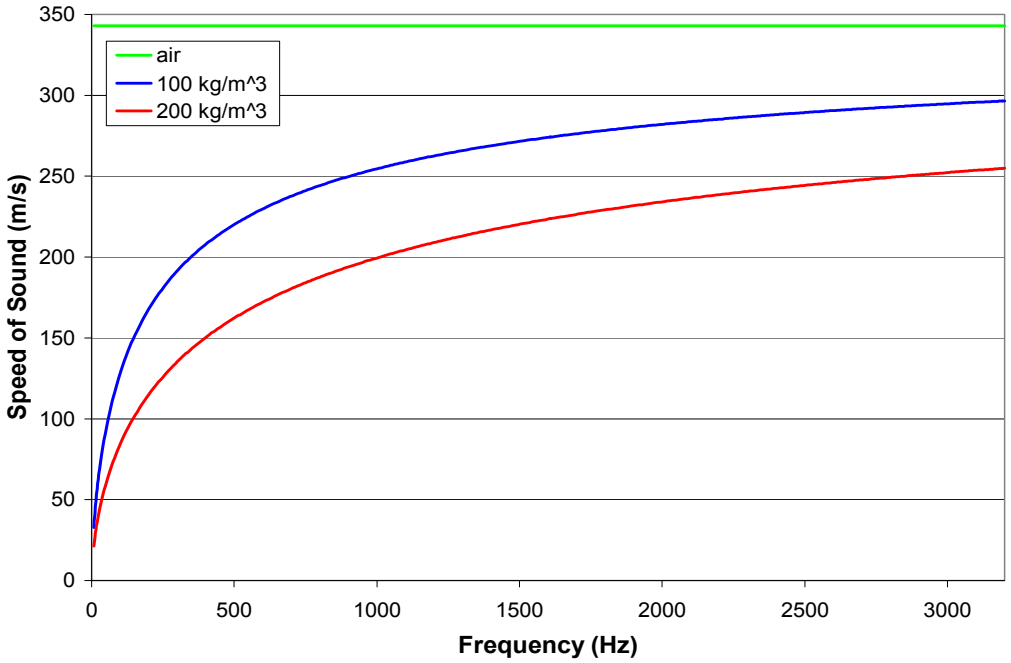

Figure 5.13: Estimated speed of sound through absorbing materials.

CHAPTER 6

ACOUSTIC IMPEDANCE OF PERFORATIONS

Acoustic impedance of perforations is essential for the prediction of both reactive and dissipative silencers, because perforations form an interface, for example, connecting a main duct and an outer chamber. This impedance is dependent on the perforation geometry (porosity, shape and size of holes, wall thickness, and stagger pattern), the flow field (glazing and through flow), sound pressure level, and the medium in contact with the perforation. The complexity of the perforation impedance confines the analytical approaches only to simple perforations. Thus, experimental methods are generally applied to obtain the impedance, such as those by Sullivan and Crocker (1978), Melling (1973), Dickey *et al*. (2000, 2001), and Lee and Ih (2003). However, these results are limited to perforations in contact with air, learning the perforation impedance facing fibrous to be explored.

The present study experimentally determines the acoustic impedance of perforations facing air-air (Fig. 6.1a) and air-fibrous material (Fig. 6.1b) in the absence and presence of mean flow. First, the measurement methodology developed in this study (see Chapter 4) is applied to the perforations facing air-air in the absence of

(a)

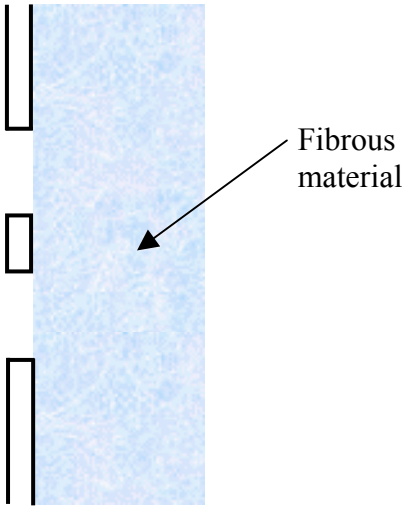

(b)

Figure 6.1: Perforations in contact with air-air and air-fibrous material; (a) air-air and (b) air-fibrous material.

mean flow, and the results are compared with the available literature. Then, perforation impedance in contact with air-fibrous material of $\rho_f = 100$ and 200 kg/m^3 are acquired. Two different texturization conditions, 'normal' and 'good' (See Chapter 5), are considered for each filling density. Finally, the effect of mean flow on the perforation impedance facing air-fibrous material is presented.

6.1 Perforation samples

Table 6.1 presents 11 samples of circular plates with different porosity ϕ, wall thickness t_w, and hole diameter d_h that are considered in this study to investigate the effect of such parameters on the perforation impedance. The dimensions and pictures of the sample plates are shown in Figs. 6.2 and 6.3. Perforation facing air-air with higher than 10 % porosity has not been, in general, considered in the literature since the effect of varying perforations at high porosities on the transmission loss is insignificant. However, with the fibrous material, the transmission loss may be affected by the perforation impedance even at higher porosities. Thus, four duct porosities ($\phi = 2.1$, 8.4, 13.6, and 25.2 %) are considered here, defined by the area ratio of all holes to the plate. The samples are categorized into three groups; (1) group A is the base with $d_h = 0.249$ cm and $t_w = 0.08$ cm; (2) group B has the same hole diameter as group A and doubles the wall thickness $t_w = 0.16$; and (3) group C has the same wall thickness as group A, while doubling the hole diameter $d_h = 0.498$ cm. The numbers (1 – 4) after the group identification by (A – C) in Table 6.1 indicate different duct porosities. The holes on the plates are distributed to achieve similar distances between the holes in the vertical

Sample No.	Hole diameter, d_h (cm)	Wall thickness, t_w (cm)	Porosity, ϕ (%)
A1	0.249	0.08	2.1
A2			8.4
A3			13.6
A4			25.2
B1		0.16	2.1
B2			8.4
B3			13.6
B4			25.2
C2	0.498	0.08	8.4
C3			13.6
C4			25.2

Table 6.1 Perforation samples.

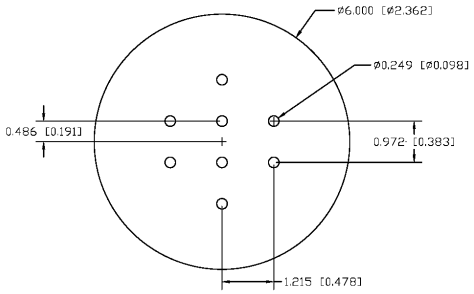

(a) A1 and B1

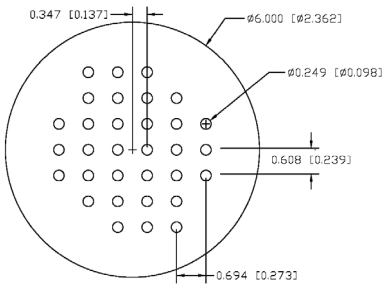

(b) A2 and B2

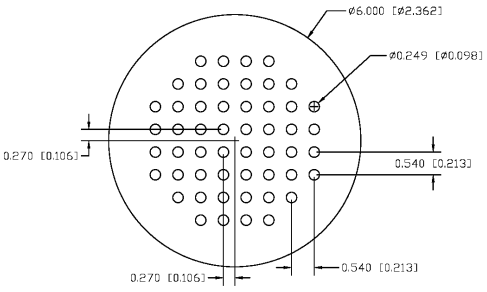

(c) A3 and B3

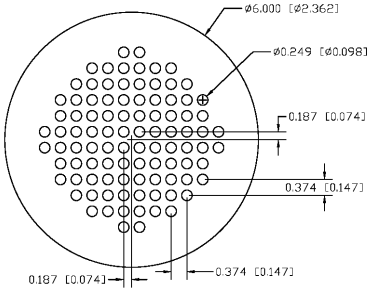

(d) A4 and B4

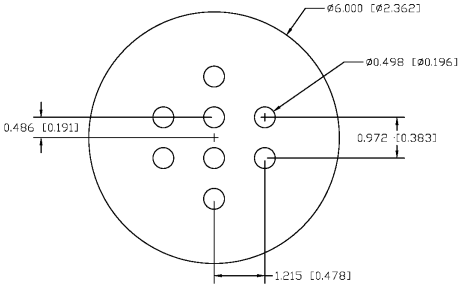

(e) C2

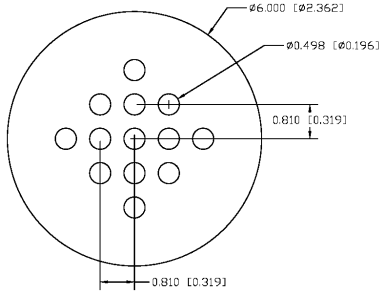

(f) C3

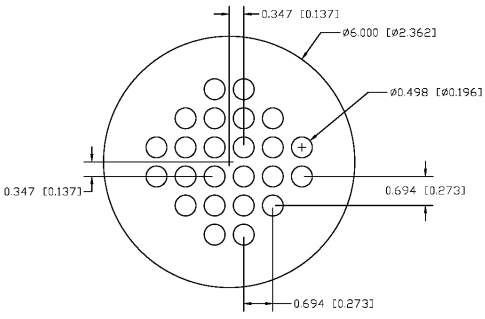

(g) C4

Figure 6.2: Dimensions of perforated plate samples (unit: cm [inch]).

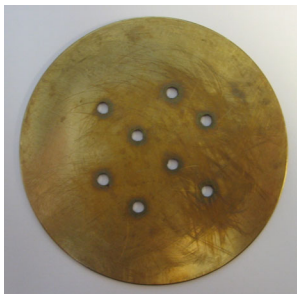

(a) A1 and B1

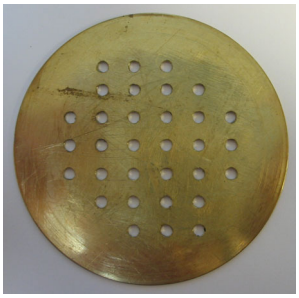

(b) A2 and B2

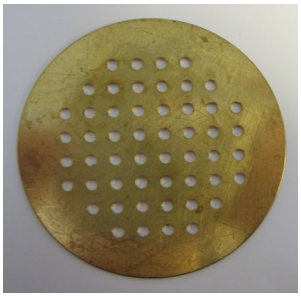

(c) A3 and B3

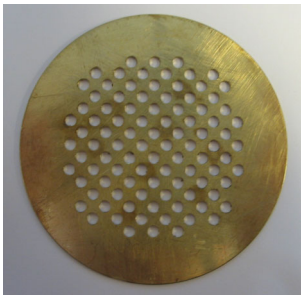

(d) A4 and B4

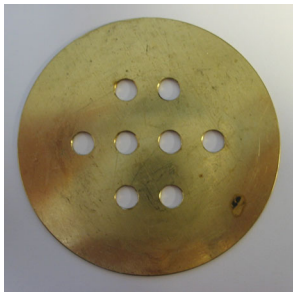

(e) C2

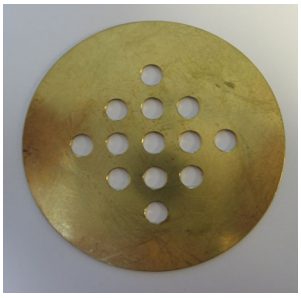

(f) C3

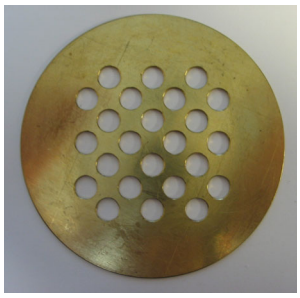

(g) C4

Figure 6.3: Pictures of perforated plate samples.

and horizontal directions, as shown in Fig. 6.2. For impedance measurements, the circular sample plates are installed in the impedance tube of 4.9 cm inner diameter, as shown in Fig. 4.3. The distance from the tube wall to the nearest hole is chosen to be longer than the distance between holes in order to minimize the effect of the interaction between holes and wall.

6.2 Perforation impedance in the absence of mean flow

Acoustic impedance of a perforate plate can be expressed, using Eq. (3.116), as

$$\zeta_p = \frac{R + ik_0\left(t_w + \alpha d_h\right)}{\phi}, \tag{6.1}$$

where R is the resistance, k_0 the wavenumber in air, and α an end correction coefficient of reactance which is associated with the interaction among holes. The present study experimentally determines R and α for the perforations facing air-air and air-fibrous material. Although the resistance has been considered as frequency-dependent by some researchers, such as Dickey *et al.* (2001) and Melling (1973), the present study assumes frequency-independent resistance consistent with Sullivan and Crocker (1978) and Rao and Munjal (1986). The resulting single value of resistance provides an effective comparison of perforations without and with the fibrous material. Furthermore, the effect of variation of resistance on transmission loss will be shown later in Chapter 7 not to be significant.

6.2.1 Acoustic impedance of perforations in contact with air-air

Available formulations

The empirical relationship of Sullivan and Crocker (1978) given by

$$\zeta_p = \frac{0.006 + ik_0\left(t_w + 0.75d_h\right)}{\phi} \tag{6.2}$$

has been widely used for the perforation impedance with air-air contact. This expression was obtained using a perforation with $\phi = 4.2$ %. In Eq (6.2), the coefficient 0.75 is associated with the end correction of the perforation. While the theoretical maximum value is 0.85 for a single hole, the coefficient may be smaller for multi-holes due to the interaction among holes. Melling (1973) graphically illustrated the interaction between two holes as shown in Fig. 6.4. He also introduced the Fok function ψ' (See also Rschevkin, 1963), which analytically considers the effect of interaction among holes on the end correction as

$$\begin{aligned}\psi'(\xi) = 1 - 1.40925\xi + 0.33818\xi^3 + 0.06793\xi^5 - 0.02287\xi^6 + 0.03015\xi^7 \\ -0.01641\xi^8 + 0.01729\xi^9 - 0.01248\xi^{10} + 0.01205\xi^{11} - 0.00985\xi^{12}\end{aligned} \tag{6.3}$$

and

$$\xi = \frac{d_h}{2\sqrt{S/\pi}}, \tag{6.4}$$

where S is the zone area of each hole and d_h is the hole diameter as shown in Fig. 6.5. The end correction coefficient for multi-holes can be expressed in term of the end correction for single hole and the Fok function as $0.85/\psi'(\xi)$. As the porosity increases, the Fok function shown in Fig. 6.6 increases, hence the end correction coefficient α decreases.

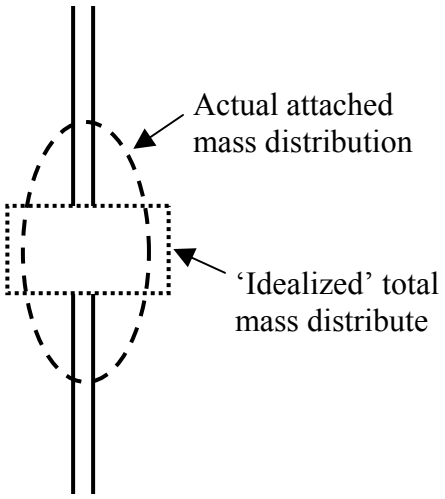

(a)

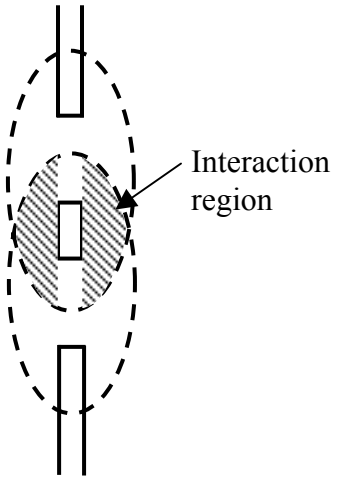

(b)

Figure 6.4: End correction of the perforations in contact with air-air (Melling, 1973); (a) single hole and (b) double holes.

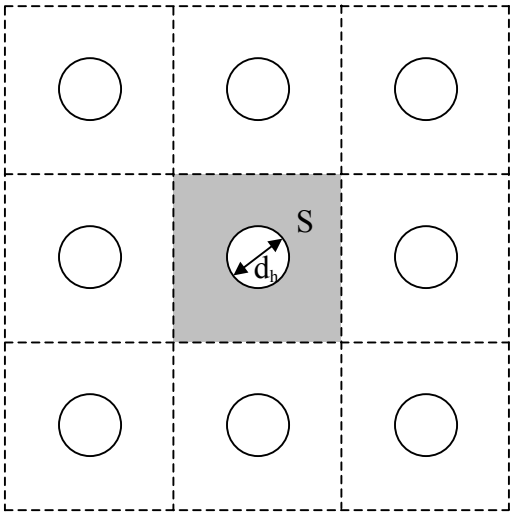

Figure 6.5: Zone area of a hole.

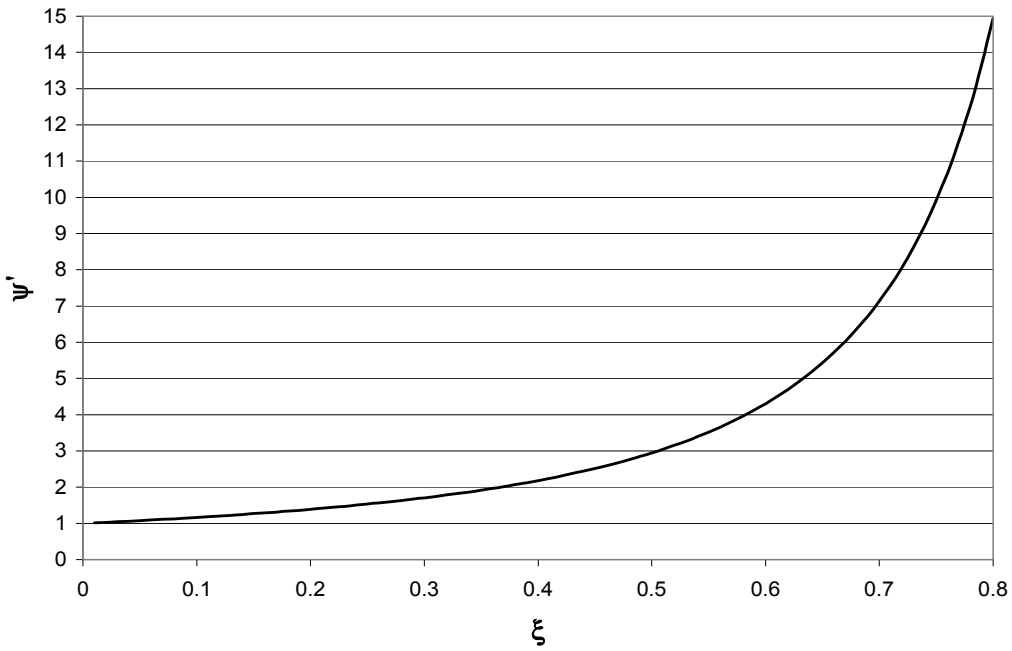

Figure 6.6: Fok function.

New Expressions

The resistance R and the end correction coefficient α of the perforation samples [refer to expression Eq. (6.1)] with air-air contact are experimentally determined using the impedance tube setup depicted in Fig. 4.3. This setup is originally designed to measure the perforation impedance facing fibrous material (to be elaborated in Section 6.2.2), but it can also be utilized for the perforation in contact with air only. Five experiments for each sample are performed and their averaged values are post-processed. The end correction coefficients are calculated from the curve-fitted reactance in the frequency range of 100 – 3200 Hz for the most samples. The only exception is A1 and B1 with $\phi = 2.1$ % which are curve-fitted in the range of 100 – 2600 Hz due to the unstable signals at frequencies higher than 2600 Hz. The mean values of resistance in the same frequency range are also obtained.

Table 6.2 and Fig. 6.7 present the measured R and α for the perforation samples of Table 6.1, facing air-air. Figure 6.7 shows that the resistance R decreases as the porosity increases, especially from $\phi = 2.1$ to 8.4 %. The group B ($t_w = 0.16$ cm) has higher resistance than group A ($t_w = 0.08$ cm), due to the doubled wall thickness. The resistance 0.006 in Eq. (6.2) obtained by Sullivan and Crocker (1978) for $\phi = 4.2$ % is in the range between the resistance of $\phi = 2.1$ and 8.4 % in Fig. 6.7(a).

Figure 6.7(b) illustrates the effect of porosity, wall thickness, and hole diameter on α, thus reactance of the perforation impedance. As the porosity increases, the end correction coefficient α decreases because of the shorter distance between holes, hence

Sample No.	R	α
A1	0.007624	0.5350
A2	0.005101	0.4409
A3	0.004437	0.2506
A4	0.004500	0.1286
B1	0.008429	0.5179
B2	0.006074	0.4224
B3	0.005744	0.2666
B4	0.005539	0.1066
C2	0.005318	0.4707
C3	0.005013	0.4473
C4	0.004395	0.2471

Table 6.2 R and α of the perforation in contact with air-air in the absence of mean flow.

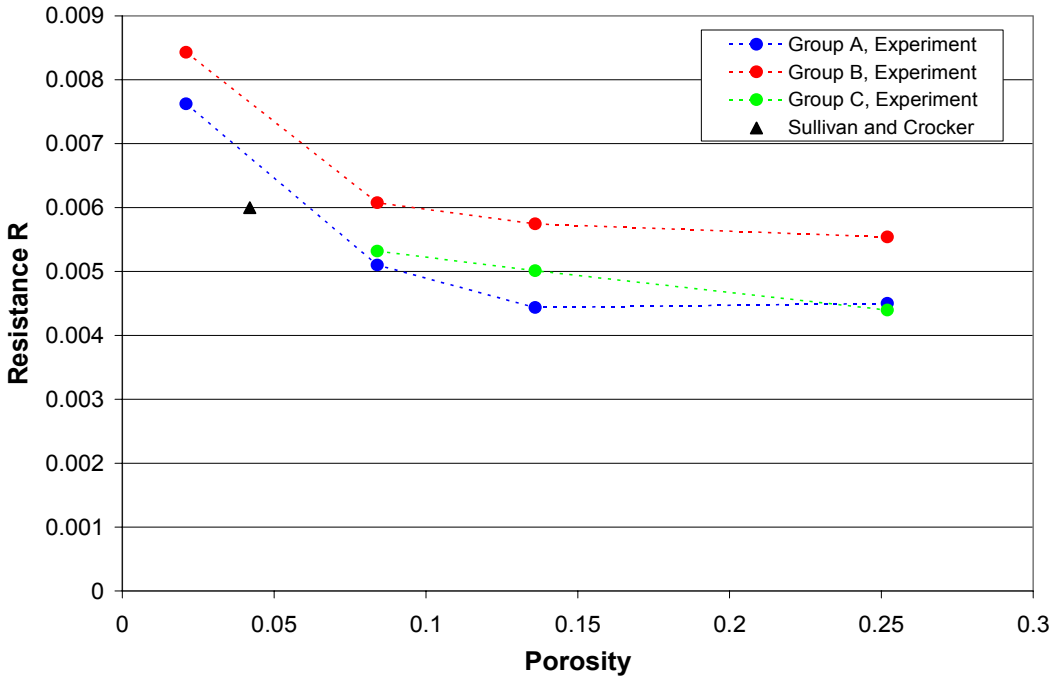

(a)

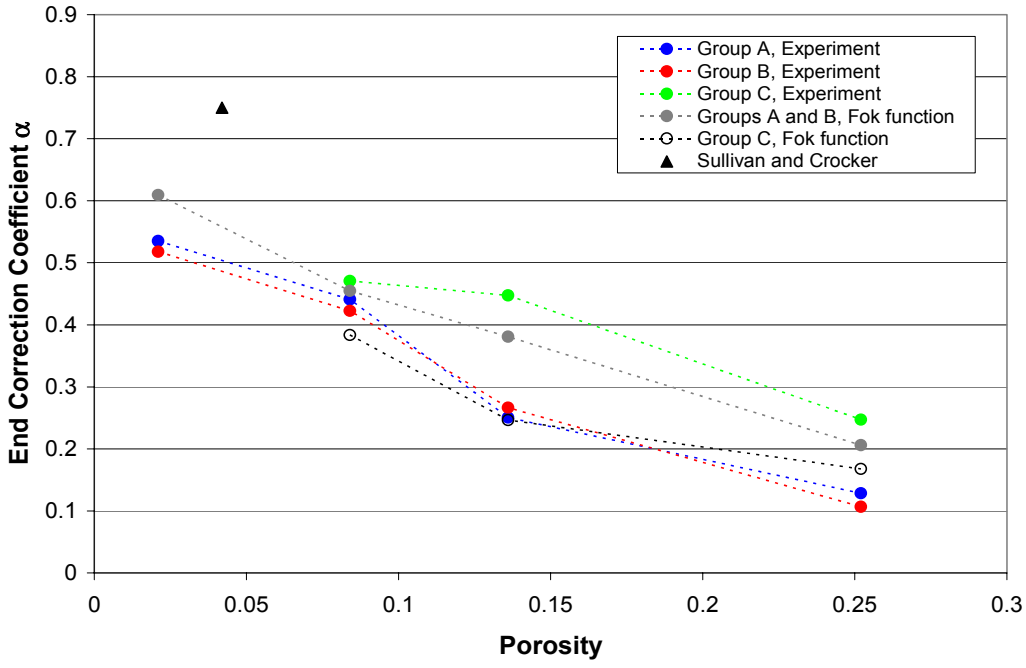

(b)

Figure 6.7: Comparison of measurement and Fok function for the acoustic impedance of a hole in contact with air-air; (a) resistance and (b) end correction coefficient.

the stronger interaction among holes. The groups A and B have similar values of α indicating that the end correction coefficient is independent of wall thickness. The group C has higher values of α than the counterparts of group A since the larger hole diameter results in a longer distance among holes, thus reducing the interactions. The end corrections obtained in the present study are lower than 0.75 of Eq. (6.2) for all porosities. Figure 6.7(b) also shows that the predicted end correction coefficients using Fok function, Eqs. (6.3) and (6.4), have a trend similar to the results of the present study, although some deviations in magnitude are observed.

6.2.2 Acoustic impedance of perforations in contact with air-fibrous material

The acoustic impedance of perforations in contact with air-fibrous material is different than the one facing air-air due to the influence of the material as shown in Fig. 6.8. The fiber filling density and texturization condition in contact with the perforation are particularly important. Ingard (1954a) claims that the fiber properties only within a distance of one hole diameter is significant. Thus the air gap between the perforation and the fibrous material may also alter the perforation impedance. The present study considers only the perforations directly in contact with the fibrous material without the air gap.

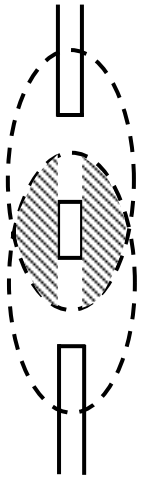

(a)

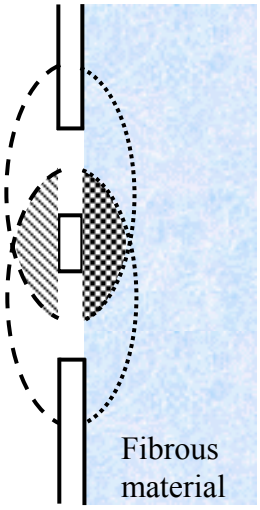

(b)

Figure 6.8: End correction of the perforations facing air-air and air-fibrous material; (a) air-air and (b) air-fibrous material.

Available formulations

Kirby and Cummings (1998) suggested a semi-empirical acoustic impedance $\tilde{\zeta}_p$ for perforated plates facing air-fibrous material by modifying the one that faces air-air ζ_p as

$$\tilde{\zeta}_p = \frac{\left(\zeta_p \phi - i0.425 k_0 d_h + i0.425 \dfrac{\tilde{Z}}{\rho_0 c_0} \tilde{k} d_h \right)}{\phi}. \tag{6.5}$$

In Eq. (6.5), half of the end correction for a perforation facing air-air [the second term in Eq. (6.5)] is replaced by a third term to account for the effect of the fibrous material. However, the use of Eq. (6.5) for dissipative silencers lead to erroneous transmission loss predictions possibly due, according to Kirby (2001), to an overestimated perforation impedance. Such overestimation may be attributed to the ignored interaction among holes. Selamet *et al*. (2001) improved the concept by applying Eq. (6.2) to the perforations facing air-fibrous material, accounting for the effect of interaction among holes, as follows:

$$\tilde{\zeta}_p = \frac{0.006 + ik_0 \left(t_w + \dfrac{0.75}{2} \left(1 + \dfrac{\tilde{Z}}{\rho_0 c_0} \dfrac{\tilde{k}}{k_0} \right) d_h \right)}{\phi}. \tag{6.6}$$

In Eq. (6.6), the effect of absorbent is considered with the complex characteristic impedance $\tilde{Z}$ and wavenumber $\tilde{k}$ of the material, thus both real and imaginary parts of the impedance can be modified in Eq. (6.2). Figure 6.9 shows the comparison of real and imaginary parts of $\tilde{\zeta}_p$ between Eqs. (6.2) and (6.6) for the perforation with $\phi = 8.4$ %, $d_h = 0.249$ cm, and $t_w = 0.09$ cm. The acoustic properties of the fibrous material given

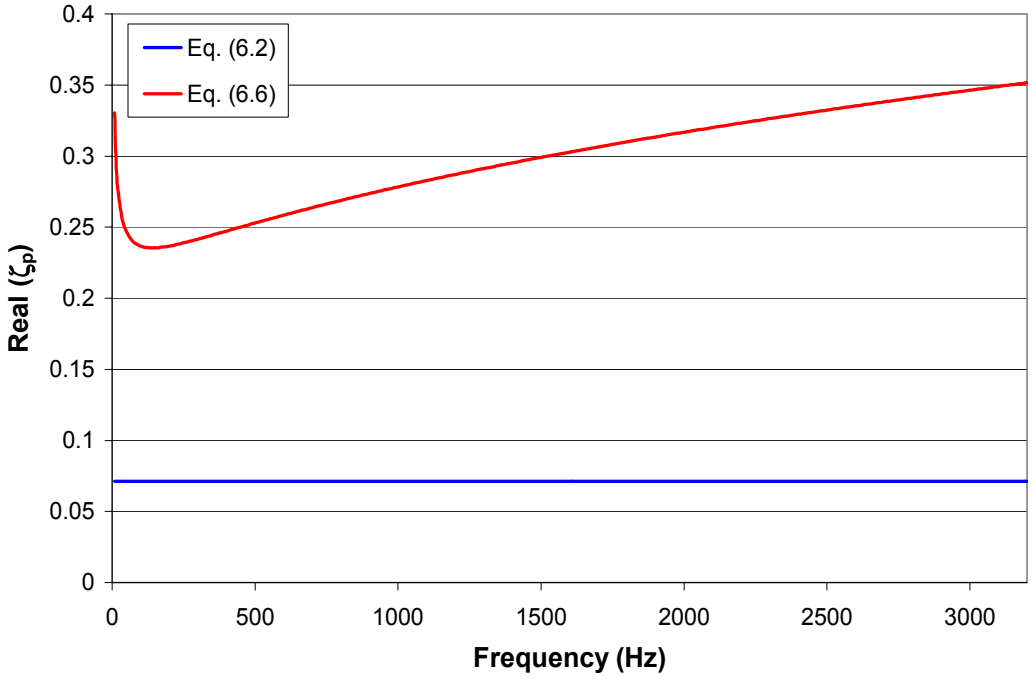

(a)

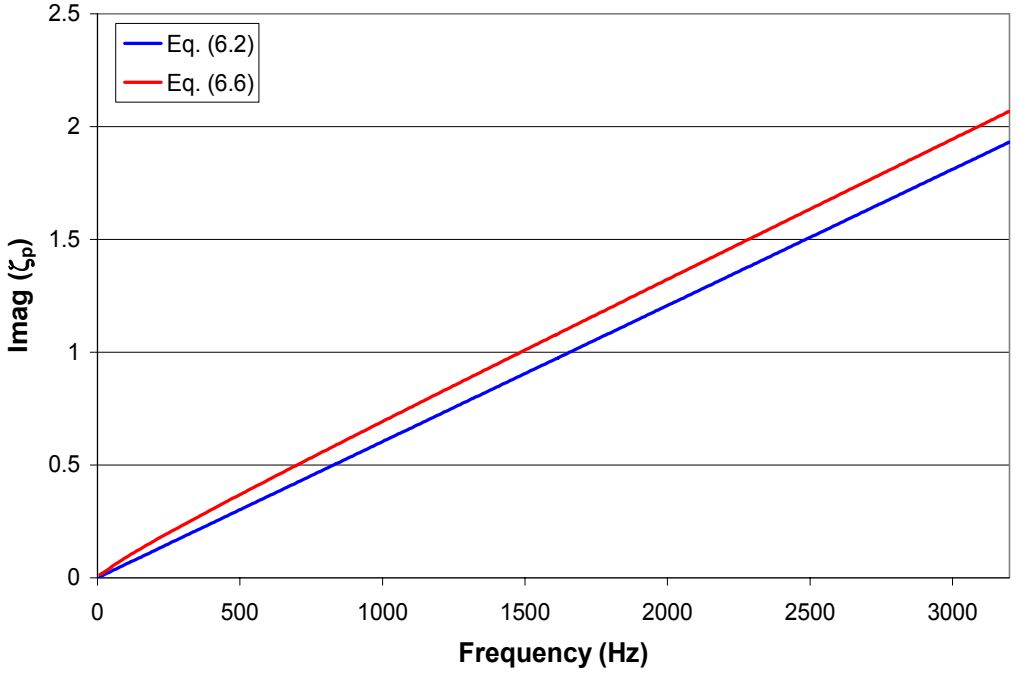

(b)

Figure 6.9: Comparison of Eqs. (6.2) and (6.6) for the acoustic impedance of the perforated plate with $\phi = 8.4$ % and $d_h = 0.249$ cm; (a) real part and (b) imaginary part.

by Eqs. (5.6) and (5.7) are used in this calculation. Figure 6.9 shows increased resistance and reactance due to Eq. (6.6) relative to Eq. (6.2). Equation (6.6) may be valid only near $\phi = 4.2$ %, since it is obtained by modifying Eq. (6.2) which is based on this particular porosity.

New expressions

Acoustic impedance of perforations facing air-fibrous material is measured in the present study using the impedance tube presented in Fig. 4.3. The averaged results from five experiments with different fibrous material samples are utilized in the post-process. For example, the averaged values of the resistance and reactance for the sample plate A2 with and without fibrous material, along with their constant and curve fits, are shown in Fig. 6.10. The relative range of variation in individual experiments for the resistance is broader than that for the end correction coefficient, particularly at high filling densities.

Since the resistance and reactance form the impedance of a plate given by Eq. (3.114), the resistance R and end correction coefficient α for a hole are obtained by using the relations given in Eqs. (3.113) and (3.116). The experimental results of R and α of the perforations (groups A, B, and C) facing an absorbent with $\rho_f = 100$ and 200 kg/m^3 as well as air only are shown in Figs. 6.11 – 6.13, and Tables 6.3 and 6.4. In order to investigate the effect of texturization conditions on the perforation impedance, two texturization conditions, 'good' and 'normal', are also applied in the experiments. Figures 6.11 – 6.13 show that fibrous material substantially increases both resistance and end correction coefficients for all three groups. The resistance R of $\rho_f = 200$ kg/m^3 are

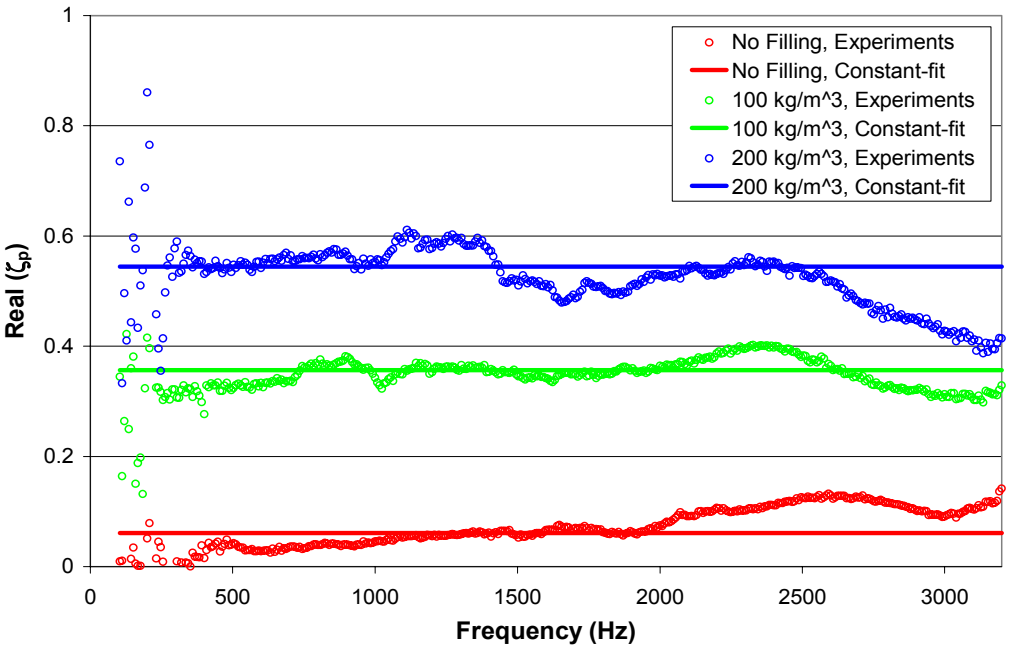

(a)

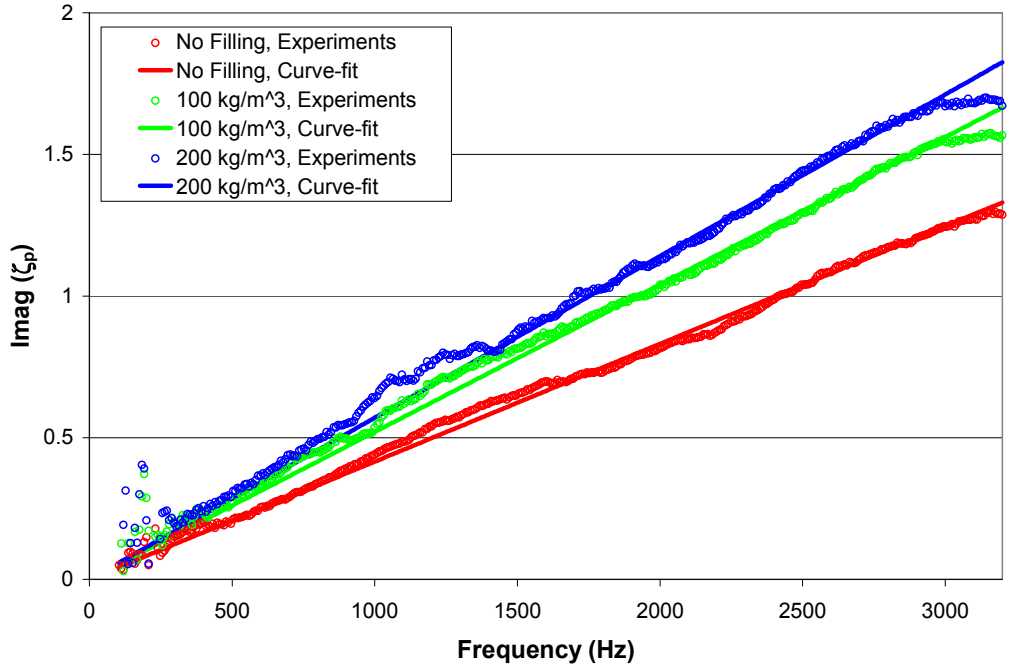

(b)

Figure 6.10: Acoustic impedance of the perforated plate A2; (a) real part and (b) imaginary part.

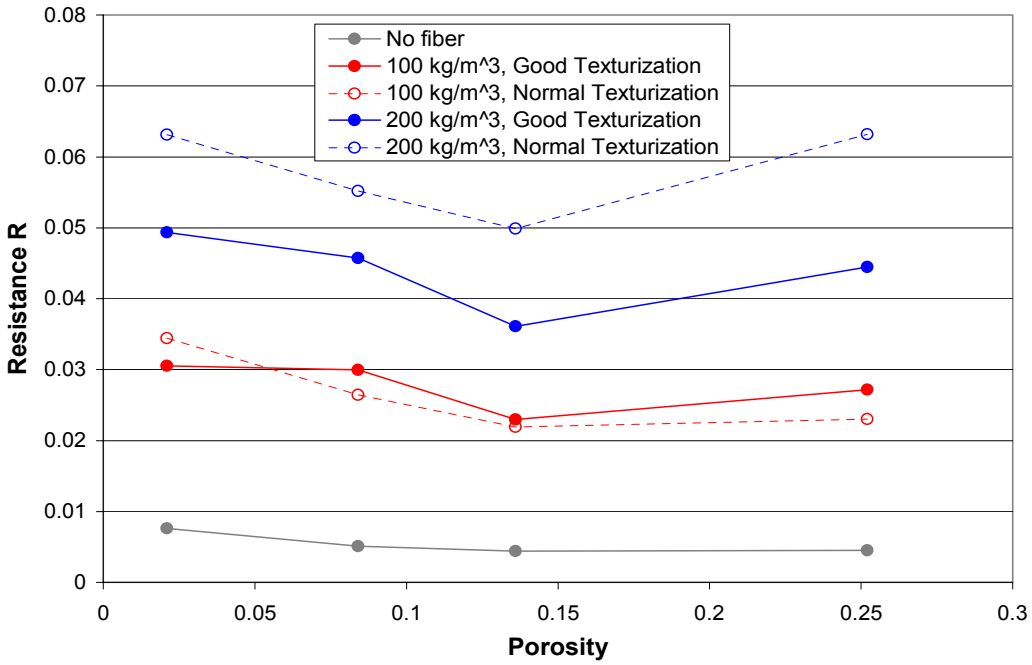

(a)

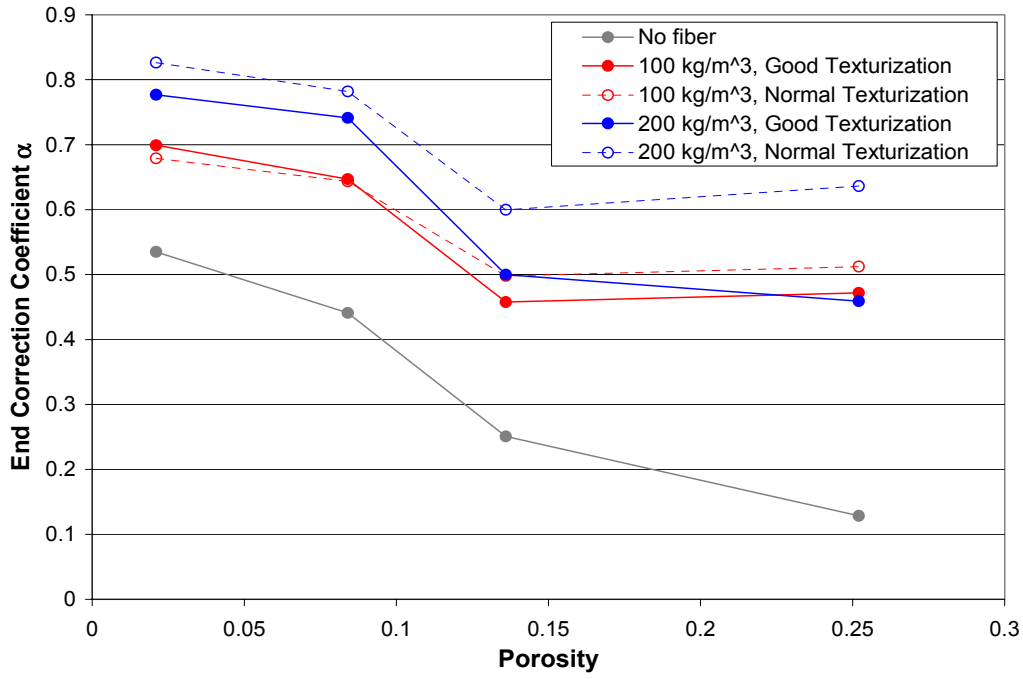

(b)

Figure 6.11: Acoustic impedance of a hole, Group A; (a) resistance and (b) end correction coefficient.

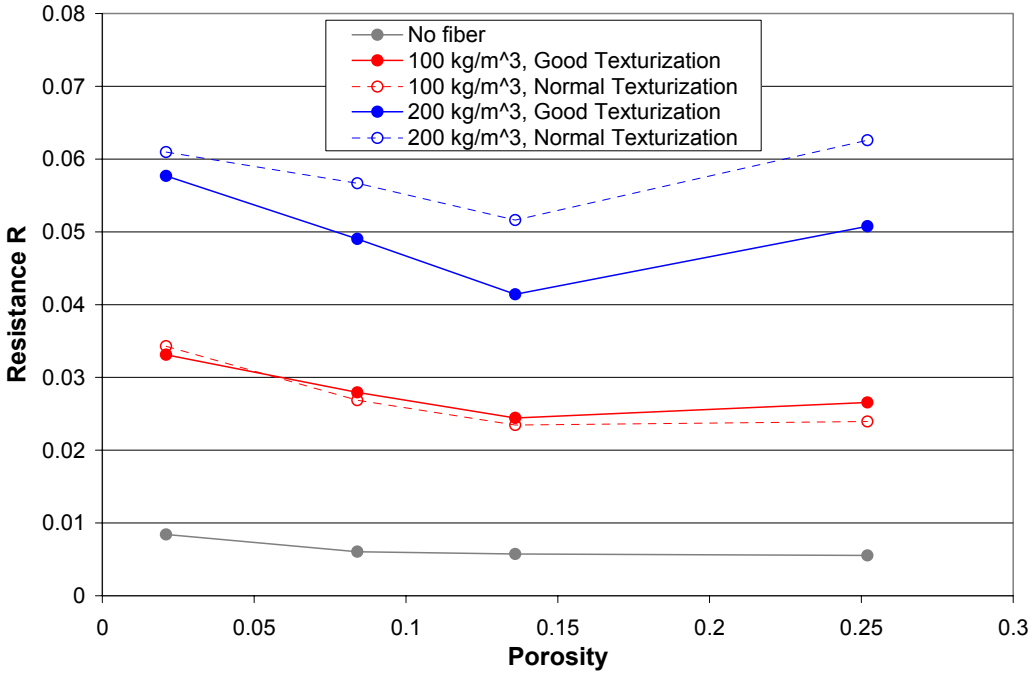

(a)

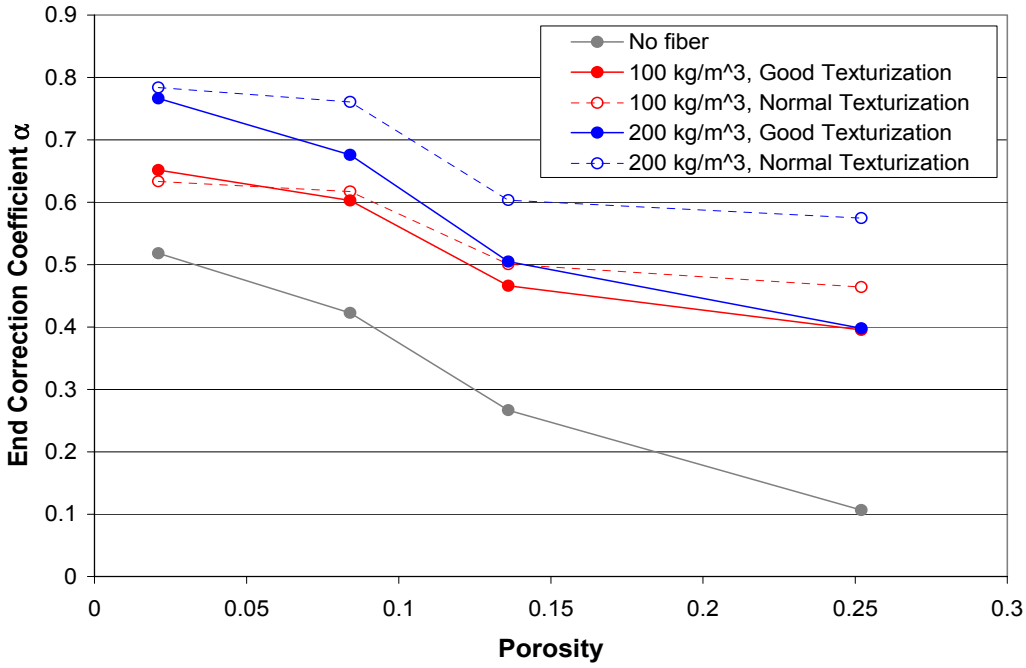

(b)

Figure 6.12: Acoustic impedance of a hole, Group B; (a) resistance and (b) end correction coefficient.

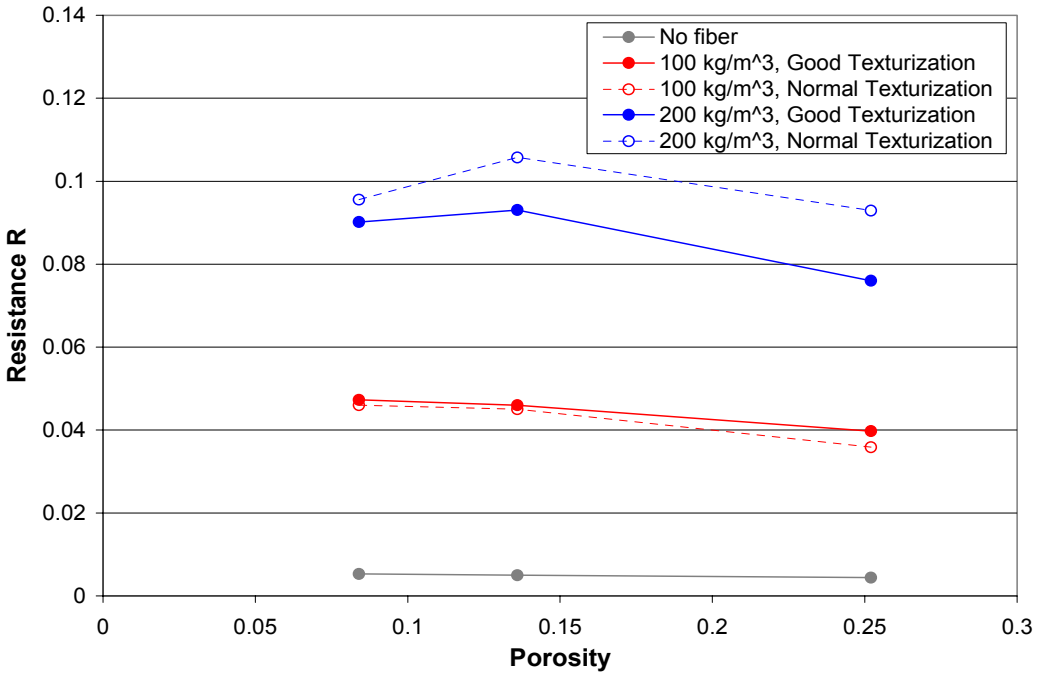

(a)

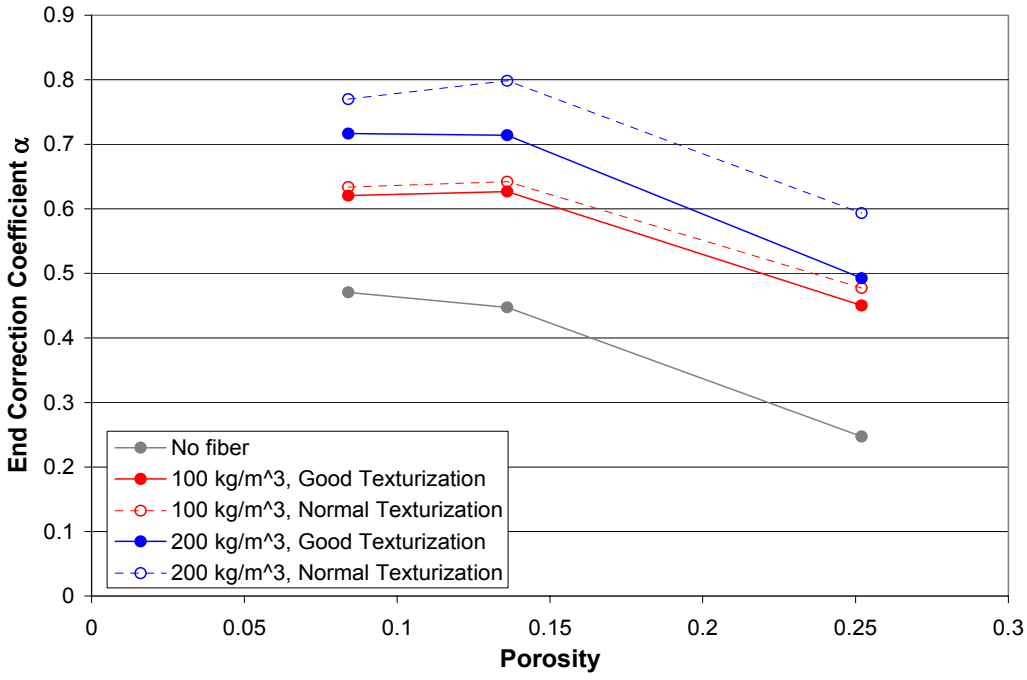

(b)

Figure 6.13: Acoustic impedance of a hole, Group C; (a) resistance and (b) end correction coefficient.

Sample No.	$\rho_f = 100$ kg/m^3		$\rho_f = 200$ kg/m^3	
	R	α	R	α
A1	0.03054	0.6989	0.04935	0.7769
A2	0.02996	0.6471	0.04575	0.7412
A3	0.02298	0.4576	0.03610	0.4999
A4	0.02716	0.4717	0.04447	0.4590
B1	0.03313	0.6514	0.05770	0.7663
B2	0.02793	0.6026	0.04900	0.6758
B3	0.02444	0.4661	0.04142	0.5048
B4	0.02657	0.3951	0.05076	0.3980
C2	0.04728	0.6206	0.09015	0.7167
C3	0.04598	0.6269	0.09308	0.7142
C4	0.03973	0.4504	0.07604	0.4926

Table 6.3 R and α of the perforation in contact with air-fibrous material in the absence of mean flow ('Good' texturization).

Sample No.	$\rho_f = 100$ kg/m^3		$\rho_f = 200$ kg/m^3	
	R	α	R	α
A1	0.03441	0.6789	0.06315	0.8265
A2	0.02645	0.6436	0.05521	0.7821
A3	0.02190	0.4977	0.04990	0.5997
A4	0.02302	0.5121	0.06317	0.6363
B1	0.03428	0.6333	0.06094	0.7839
B2	0.02687	0.6170	0.05668	0.7608
B3	0.02345	0.5005	0.05161	0.6033
B4	0.02393	0.4639	0.06259	0.5744
C2	0.04600	0.6337	0.09558	0.7700
C3	0.04501	0.6423	0.10570	0.7985
C4	0.03586	0.4774	0.09292	0.5934

Table 6.4 R and α of the perforation in contact with air-fibrous material in the absence of mean flow ('Normal' texturization).

higher than those of lower filling density $\rho_f = 100$ kg/m^3 for all samples. However, the effect of different filling density on α diminishes for the samples A4 and B4 with 'good' texturization conditions. For groups A and B, as the porosity increases, both R and α decrease for both filling densities except for the samples A4 and B4. Particularly, the R of $\phi = 25.2$ % is higher than that of $\phi = 13.6$ % for the samples A4 and B4. The relative increase of resistance by the filling material in group C ($d_h = 0.498$ cm) is considerably higher than in groups A and B ($d_h = 0.249$ cm). Unlike the resistance, the α of group C does not increase more rapidly by the filling material than groups A and B. Figures 6.11 – 6.13 also show that while the impact of texturization condition of the fibrous material on R and α is insignificant for $\rho_f = 100$ kg/m^3, the 'normal' texturization for $\rho_f = 200$ kg/m^3 exhibits higher R and α for all samples particularly at high porosities, possibly due to the presence of more fiber locally in contact with the perforations. Such trends with normal texturization should be treated, however, with caution, since there is a substantial experimental spread among the results from corresponding samples.

6.3 Perforation impedance in the presence of grazing mean flow

The present study explores the effect of the grazing mean flow on the perforation impedance in contact with the air-fibrous material using the setup described in Section 4.2.1 and depicted in Fig. 4.5. Two flow speeds of Ma = 0.05 and 0.1 at room temperature (19±1 °C) and 1 atm are applied in the main duct. The flow is fully developed at the perforate samples which are installed flush with the main duct. Two

different densities of $\rho_f = 100$ and 200 kg/m^3 with 'good' texturization condition are filled in the side branch as shown in Fig. 4.5. Three fiber samples are used for each perforation plate and their averaged values are presented here.

The plane wave is assumed in the main duct and the cut-on frequency of the first higher order mode is calculated as 2250 Hz based on the dimensions of the rectangular duct (5.08×7.62 cm). Thus, the frequency range of the experiment is limited up to 2000 Hz. The resistance and end correction coefficient in the presence of mean flow are presented next as normalized relative to their no-mean-flow values.

6.3.1 Resistance of perforation impedance with mean flow

Figure 6.14 shows the measured resistance of perforation impedance in contact with air-fibrous material with $\rho_f = 100$ and 200 kg/m^3 for Ma = 0.05 and 0.1. The resistance with mean flow is normalized relative to that without mean flow, $R_{Ma=0.0}$, thus lower than unity, for example, indicates a decrease in resistance due to mean flow. The resistance obtained in the experiments with $\phi = 25.2$ % (samples A4, B4, and C4) exhibit negative values in the presence of mean flow, thus those results are excluded from the present study. Such negative values of resistance have also been measured by Cummings (1986) especially for the perforation with a large hole diameter, for example, of 1.38 cm. Cummings attributes the negative resistance to flow-interactions, which was discussed by Howe (1979). Figure 6.14 shows that the normalized resistance for Ma = 0.05 is lower than unity, suggesting that the resistance decreases due to the mean flow. Such decrease of resistance at low flow rate has also been observed by Dickey *et al*. (2001).

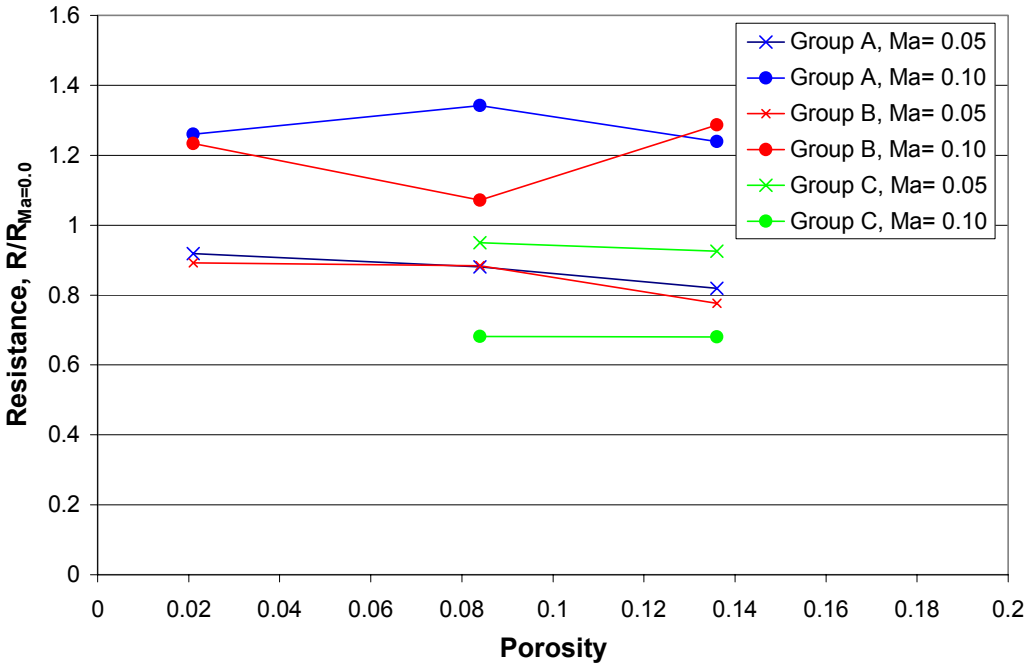

(a)

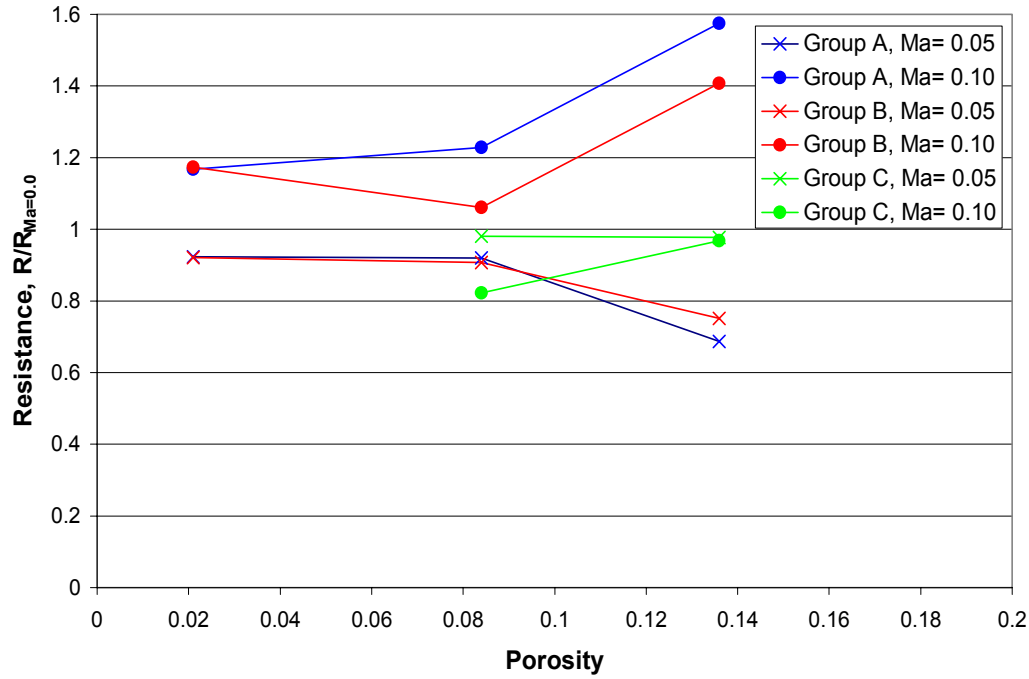

(b)

Figure 6.14: The measured resistance of a hole in contact with air-fibrous material in the presence of mean flow; (a) $\rho_f = 100$ kg/m^3 and (b) $\rho_f = 200$ kg/m^3.

For Ma = 0.1, groups A and B have higher resistance than those without flow, due possibly to the shedding and diffusion of acoustically induced vorticity (Cummings, 1986; Dickey *et al*., 2001). Noting that the present study has used a representative single value over the entire frequency range of interest, the reduced resistance for group C may be attributed to the dominating contribution of lower values at high frequencies. It is conceivable that such an averaging approach may not be suitable for a strong frequency-dependent behavior.

6.3.2 Reactance of perforation impedance with mean flow

Figure 6.15 shows the measured end correction coefficient for perforations in contact with air-fibrous material of $\rho_f = 100$ and 200 kg/m^3 for Ma = 0.05 and 0.1. The end correction coefficient with mean flow is normalized relative to that without mean flow, $\alpha_{Ma=0.0}$, thus lower than unity indicates a decrease in the end correction due to mean flow.

The end correction coefficient for two filling densities show trends similar to each other in Fig. 6.15, even though the magnitude is different. Mean flow is generally observed to reduce α, since the flow tends to "blow away" the end correction, consistent with earlier studies (Dickey *et al.*, 2001). While the effect of mean flow with Ma = 0.05 is not drastic (within 10 % variation from $\alpha_{Ma=0.0}$) for both $\rho_f = 100$ and 200 kg/m^3, the flow with Ma = 0.1 shows a substantial effect for groups A and B, especially for a low porosity. For group C, the flow influence is not as substantial. Thus, the effect of mean

flow needs to be considered particularly for a small hole diameter and with a high flow speed. On the contrary, the perforation high porosity or large hole diameter may not be significantly influenced by the mean flow.

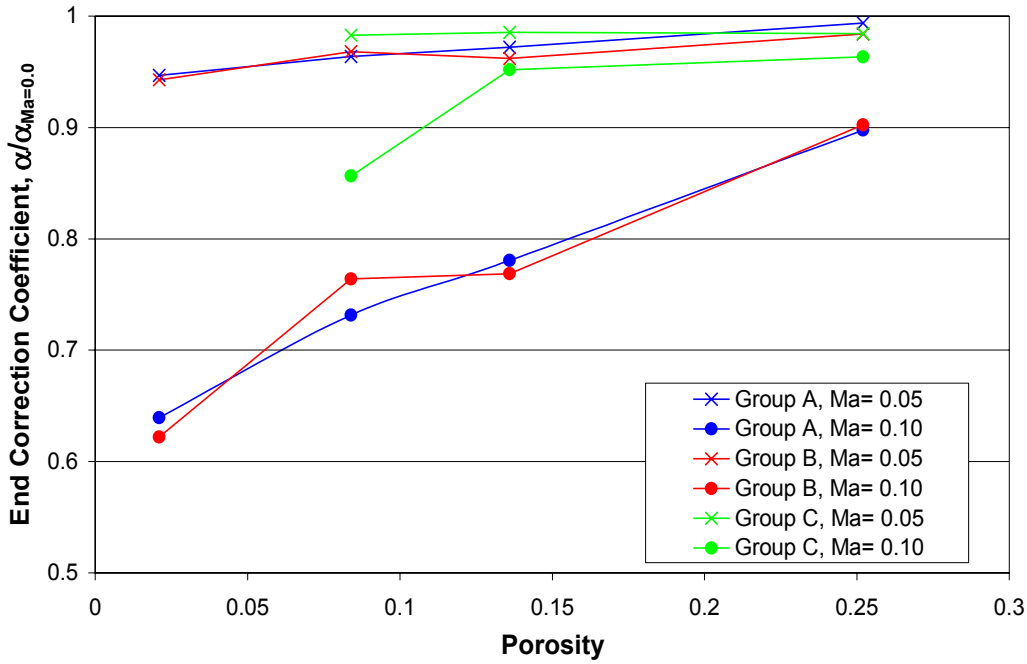

(a)

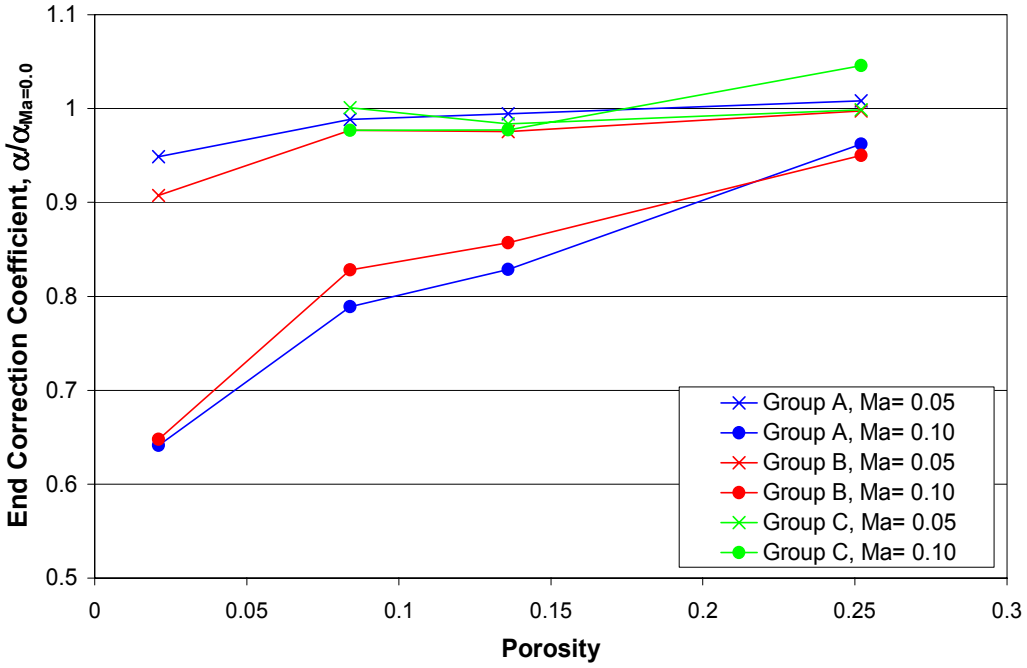

(b)

Figure 6.15: The measured end correction coefficients of a hole in contact with air-fibrous material in the presence of mean flow; (a) $\rho_f = 100$ kg/m^3 and (b) $\rho_f = 200$ kg/m^3.

CHAPTER 7

TRANSMISSION LOSS OF SILENCERS

The acoustic properties of fibrous material and the perforation impedance developed in the study are integrated into the predictions of silencers in the present chapter. Transmission loss is used to assess the acoustic performance since it is independent of the input and termination impedances, therefore representative of the silencer itself. The predictions are compared with the experimental results of reactive and dissipative silencers with various porosities and different hole diameters. For the dissipative silencers, different filling densities and texturization conditions are also applied for both experiments and predictions. The influence of variation in each property of the fibrous material and the perforation impedance is illustrated using the BEM predictions. The effects of grazing mean flow and the variation of internal geometry, such as baffles and extended inlet/outlet, are also examined. Finally, the transmission loss of multi-chamber silencers are examined to illustrate the effect of connecting tube length between the two chambers.

7.1 Simple expansion chamber

Before the investigation of perforated silencers, the measured and predicted transmission loss of a simple concentric expansion chamber depicted in Fig. 7.1 are presented. The diameters of the chamber and the inlet/outlet ducts are 16.44, and 4.9 cm, respectively, and the length of the chamber is 25.72 cm. These dimensions are adopted for all reactive and dissipative silencers investigated in the present study. The predicted transmission loss from the BEM and 1D analytical approach are compared with the experiments in Fig. 7.2. The BEM predictions show good agreement with the experimental results, while the 1D analytical method deviates at frequencies above 2100 Hz due to its inability to account for the higher order modes of wave propagation. Thus, the 1D approach would not be appropriate at high frequencies, even for a simple expansion chamber. A sample mesh of the expansion chamber used for the BEM predictions is displayed in Fig. 7.3. This mesh is generated by IDEAS® and has 8 nodes on each element of 2×2 cm. This mesh type and size are applied for all BEM predictions of silencers hereafter.

7.2 Perforated reactive silencers

The acoustic characteristics of perforated reactive silencers are investigated next experimentally and numerically. These reactive silencers are then used in the following section as baselines for the dissipative silencers. By comparing the transmission loss from experiments and predictions, this investigation also provides an assessment of the acoustic impedance of perforations measured in the present study in contact with air only.

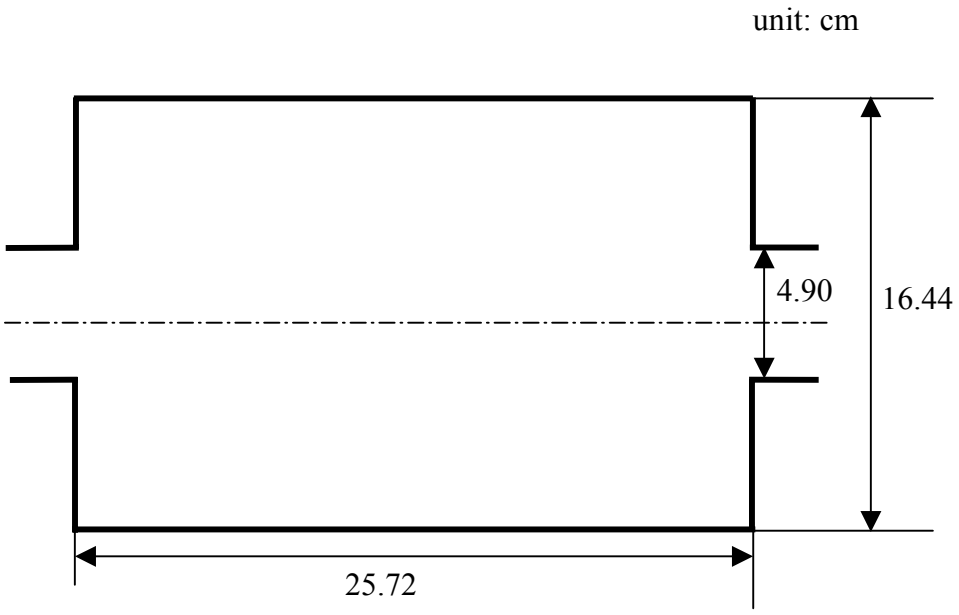

Figure 7.1: The schematic of a reactive expansion chamber.

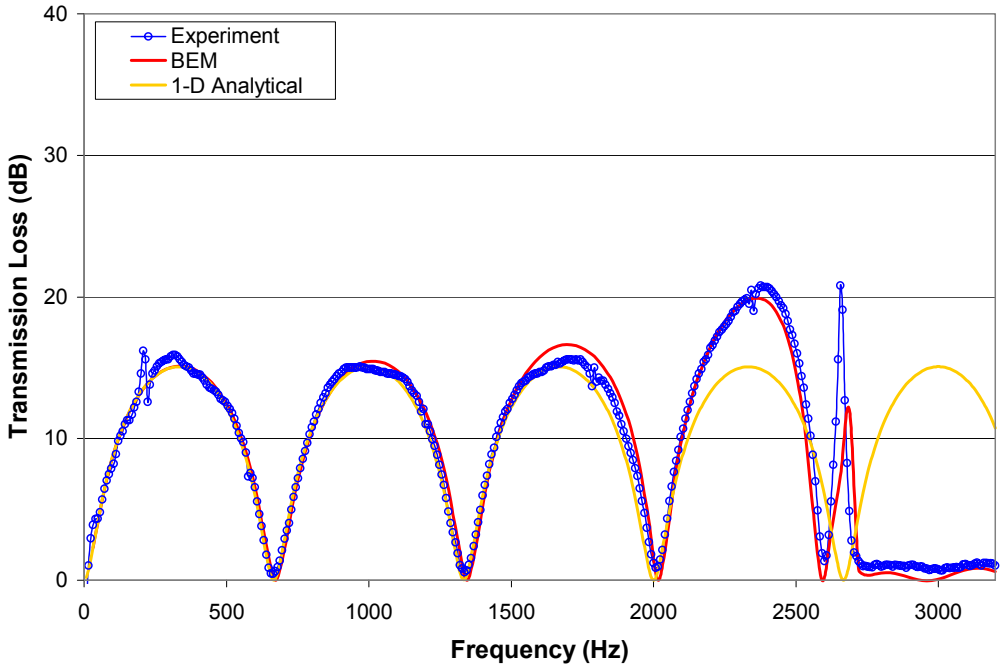

Figure 7.2: The transmission loss of the reactive expansion chamber without perforations; experiments vs. predictions.

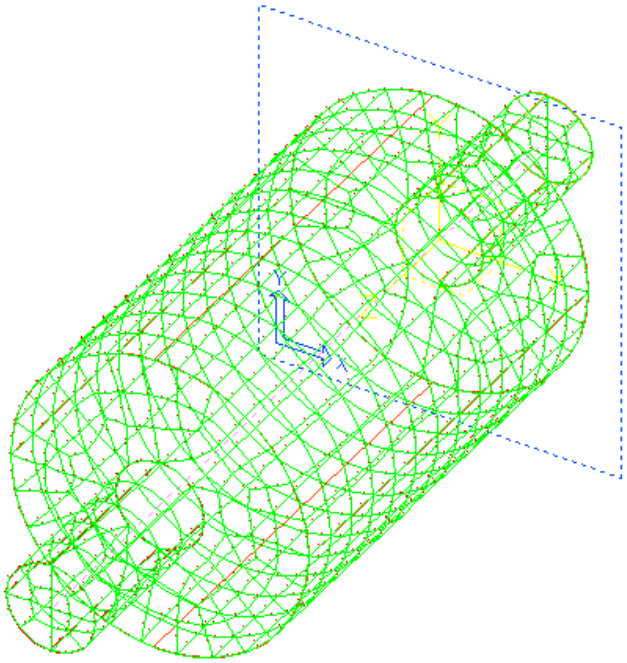

Figure 7.3: Sample mesh of the expansion chamber using IDEAS; 2×2 cm mesh size.

Four perforated brass tubes with different porosities ($\phi = 8.4$ and 25.7 %) and hole diameters ($d_h = 0.249$ and 0.498 cm) are fabricated and applied to the expansion chamber of Fig. 7.1. Such porosities and hole diameters are the same or close to those of the flat circular perforation samples used for the measurement of perforation impedance (see Table 6.1). The inner diameter of the tube is 4.9 cm and the wall thickness is 0.09 cm. The schematics and pictures of the fabricated perforated tubes are shown in Figs. 7.4 and 7.5. The tubes are designed to have comparable distance between holes in axial and circumferential directions. For example, the perforated duct of Fig. 7.4(a) has 0.76 and 0.79 cm between the holes in two directions. The fabricated reactive silencer with the perforated tube on the impedance tube setup is shown in Fig. 7.6. The transmission loss measured using the impedance tube setup are compared next with the predictions using the perforation impedance of available literature vs. the present study. Using the BEM predictions, the effect of real and imaginary parts of perforation impedance on the transmission loss is evaluated and presented in this section.

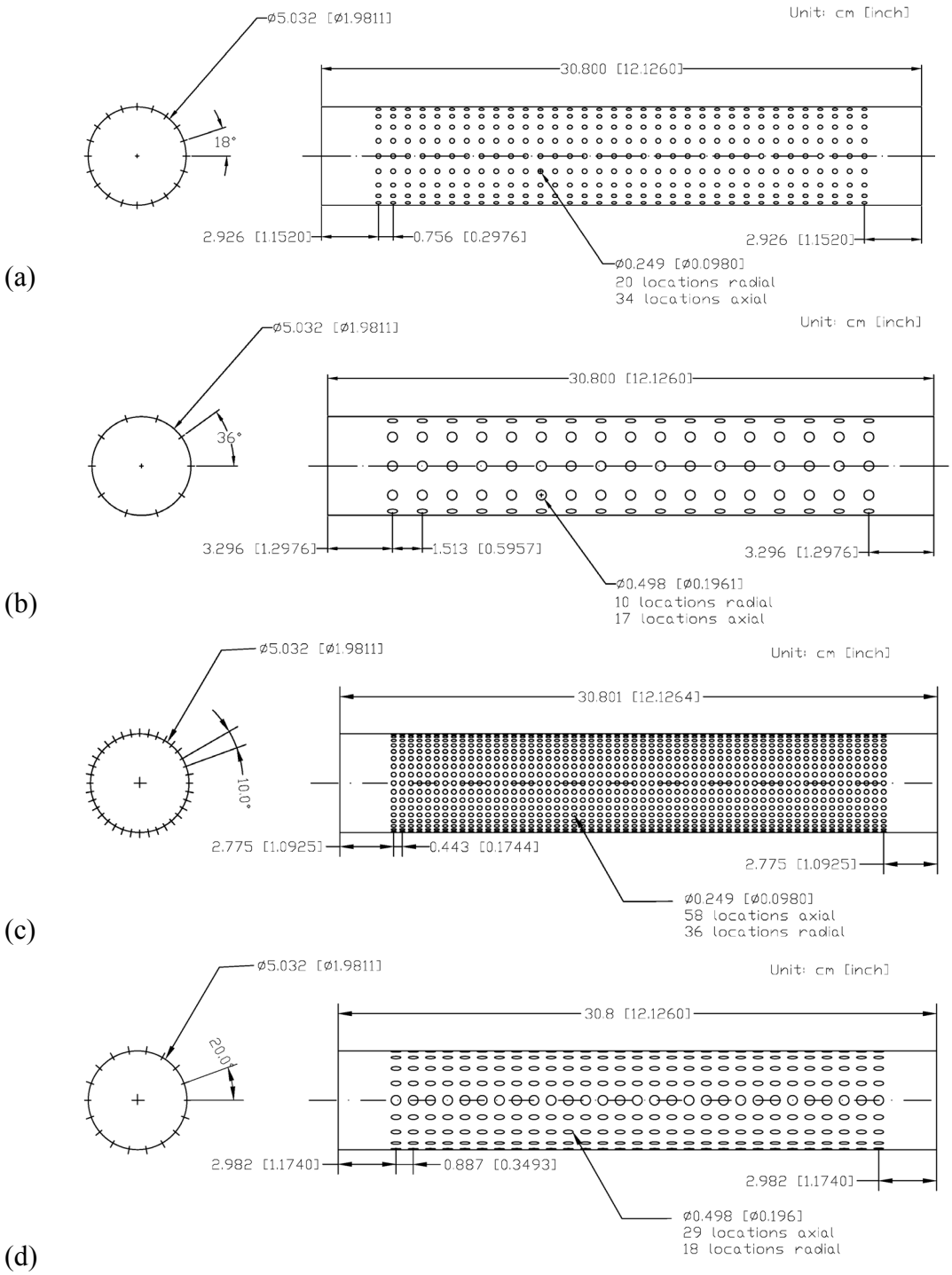

Figure 7.4: The schematics of perforated ducts; (a) $\phi = 8.4$ %, $d_h = 0.249$ cm, (b) $\phi = 8.4$ %, $d_h = 0.498$ cm, (c) $\phi = 25.7$ %, $d_h = 0.249$ cm, and (d) $\phi = 25.7$ %, $d_h = 0.498$ cm.

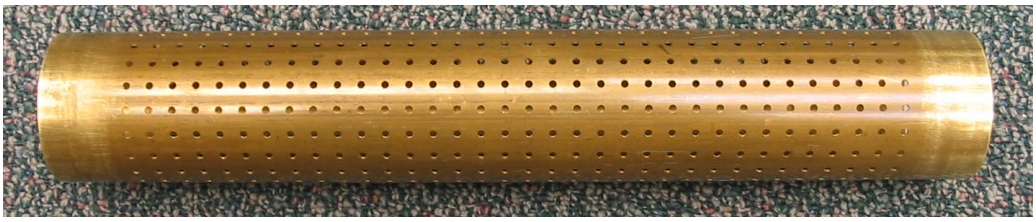

(a)

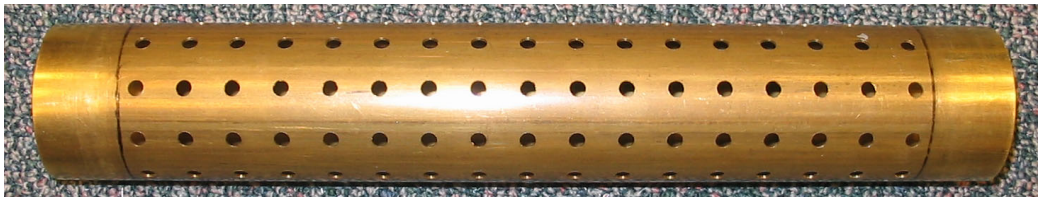

(b)

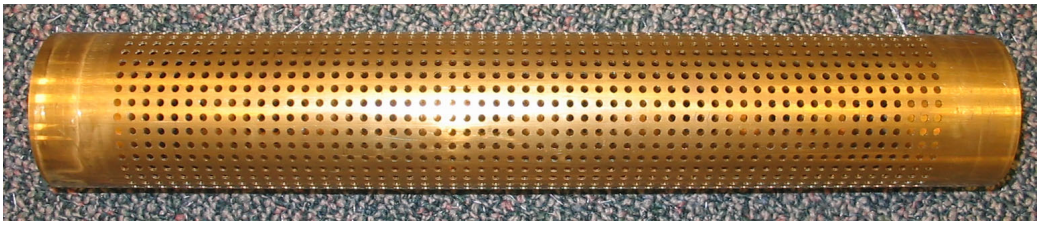

(c)

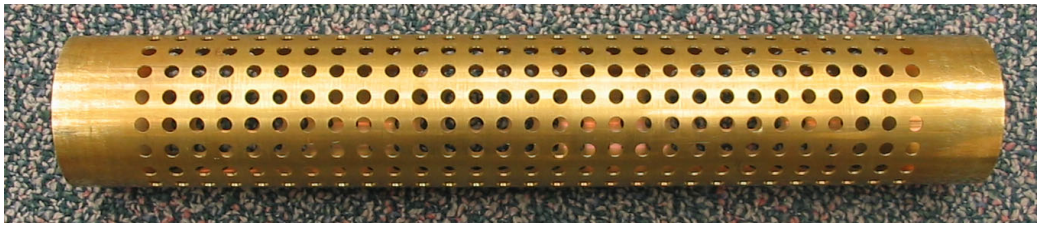

(d)

Figure 7.5: The pictures of perforated ducts; (a) $\phi = 8.4$ %, $d_h = 0.249$ cm, (b) $\phi = 8.4$ %, $d_h = 0.498$ cm, (c) $\phi = 25.7$ %, $d_h = 0.249$ cm, and (d) $\phi = 25.7$ %, $d_h = 0.498$ cm.

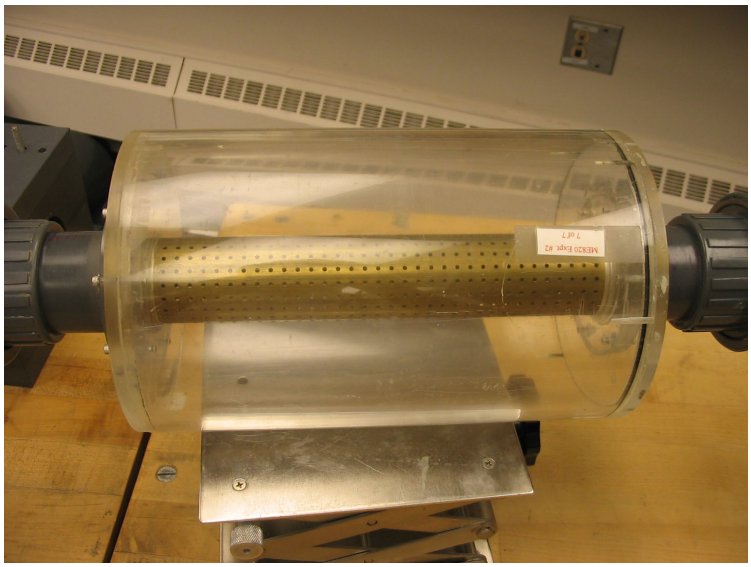

(a)

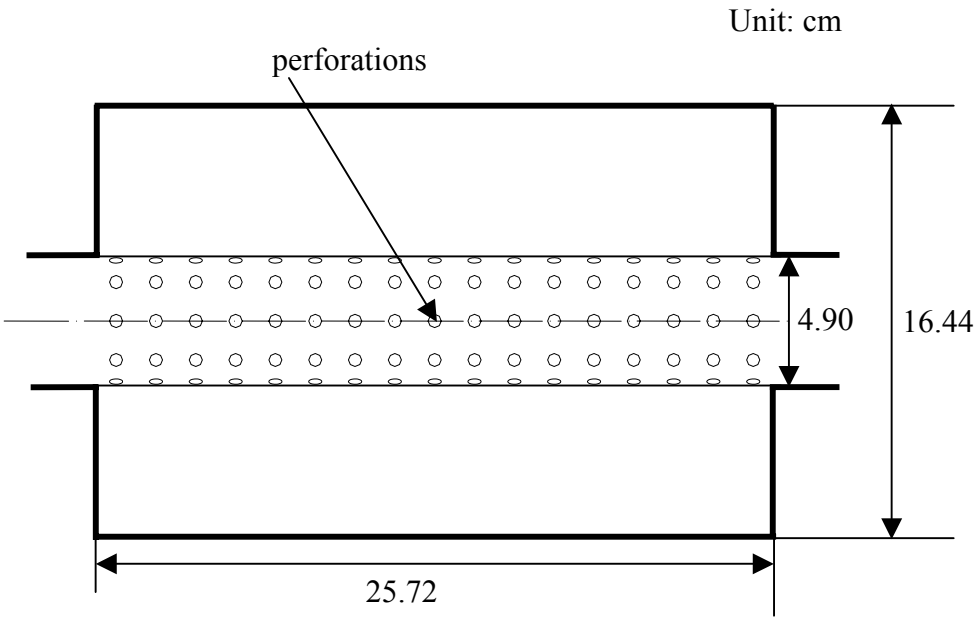

(b)

Figure 7.6: A perforated reactive silencer; (a) picture and (b) schematic.

7.2.1 Comparisons of predictions and experiments

The measured and predicted transmission loss of perforated reactive silencers with hole diameters ($d_h = 0.249$ and 0.498 cm) and $\phi = 8.4$ % are presented in Figs. 7.7 and 7.8. The perforation impedance developed in the present study [Table 6.2 or Fig. 6.7] and Sullivan and Crocker's expression [Eq. (6.2)] are used for the predictions. The BEM predictions using the new expression of the present study show better agreement with experiments compared to those using Eq. (6.2). The results suggest that Sullivan and Crocker's expression (based on $\phi = 4.2$ %) would not be appropriate for high porosities. Thus, Figs. 7.9 and 7.10 present the comparison of experiments with the predictions for two different hole diameters ($d_h = 0.249$ and 0.498 cm) and $\phi = 25.7$ % using only the new expression of the present study. The BEM predictions show good agreement with the experiments for both hole diameters.

7.2.2 Effect of perforation geometry on the transmission loss

Figure 7.11 shows the measured transmission loss for the simple expansion chamber, and the perforated reactive silencer with different porosities and hole diameters. The presence of perforated ducts of $\phi = 8.4$ % substantially increases the transmission loss at the third attenuation dome, and reduces the width of the fourth dome along with a shift to lower frequencies. The perforated duct with $\phi = 25.7$ % also changes the transmission loss to some degree, but not as significantly as the one with $\phi = 8.4$ %.

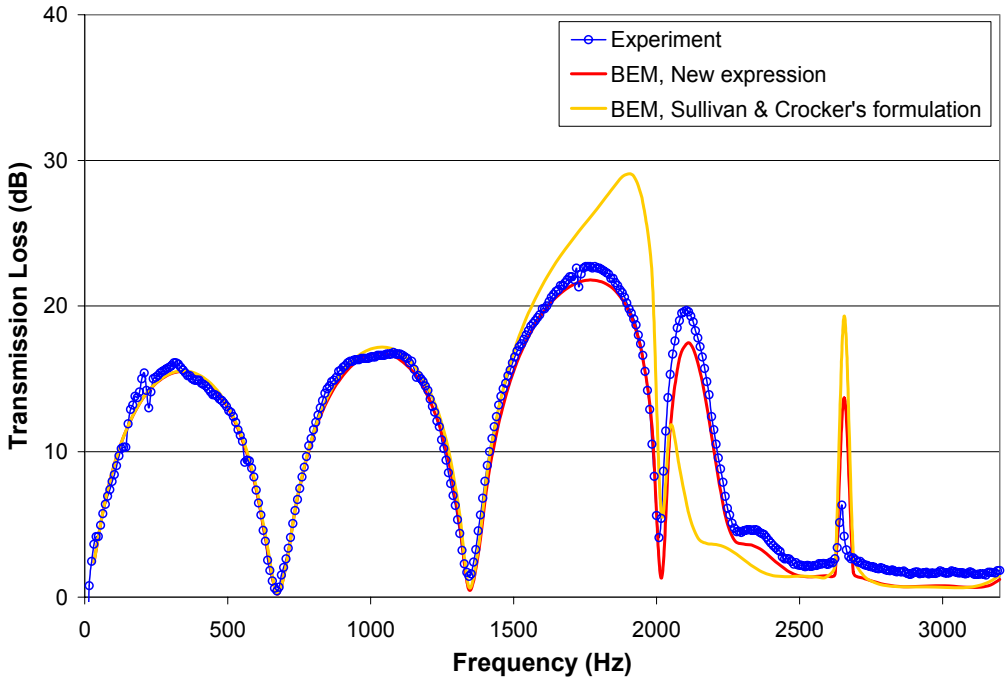

Figure 7.7: The transmission loss of the perforated reactive silencer ($\phi = 8.4$ %, $d_h = 0.249$ cm).

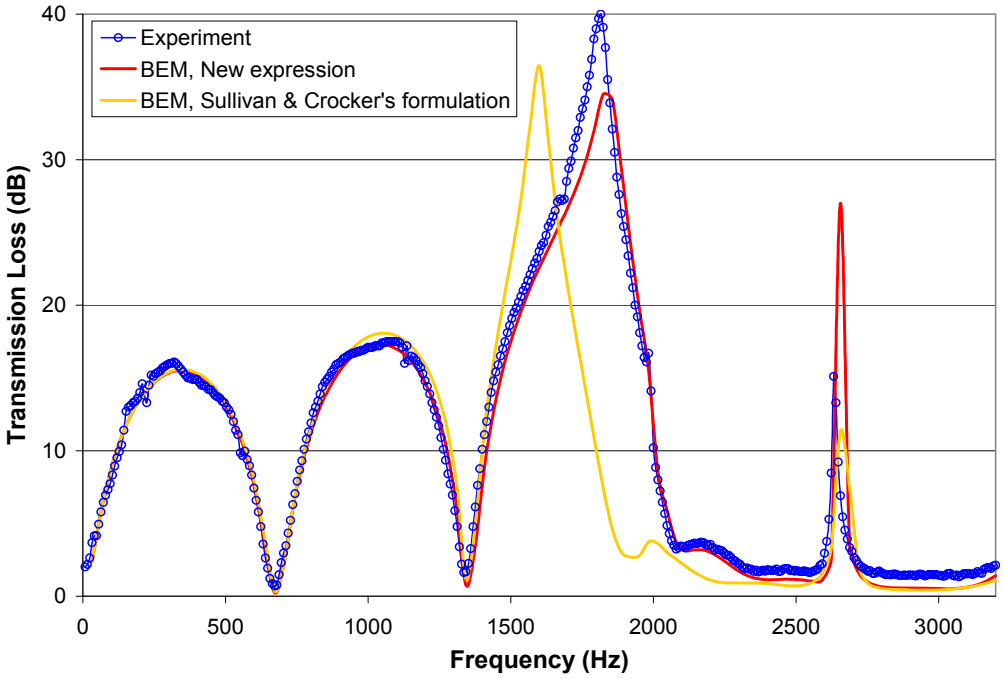

Figure 7.8: The transmission loss of the perforated reactive silencer ($\phi = 8.4$ %, $d_h = 0.498$ cm).

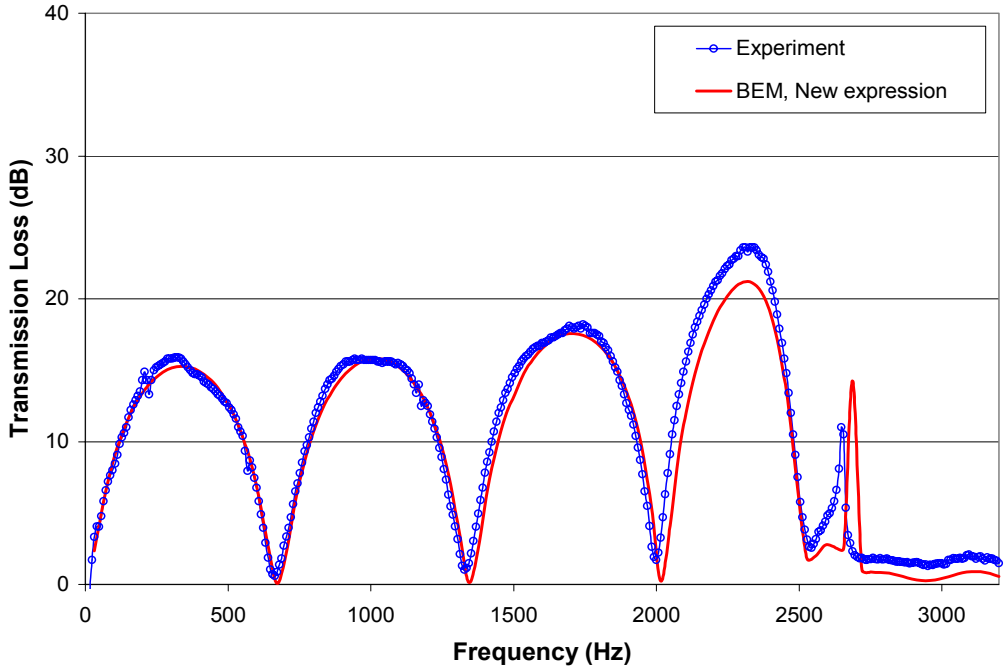

Figure 7.9: The transmission loss of the perforated reactive silencer ($\phi = 25.7$ %, $d_h = 0.249$ cm).

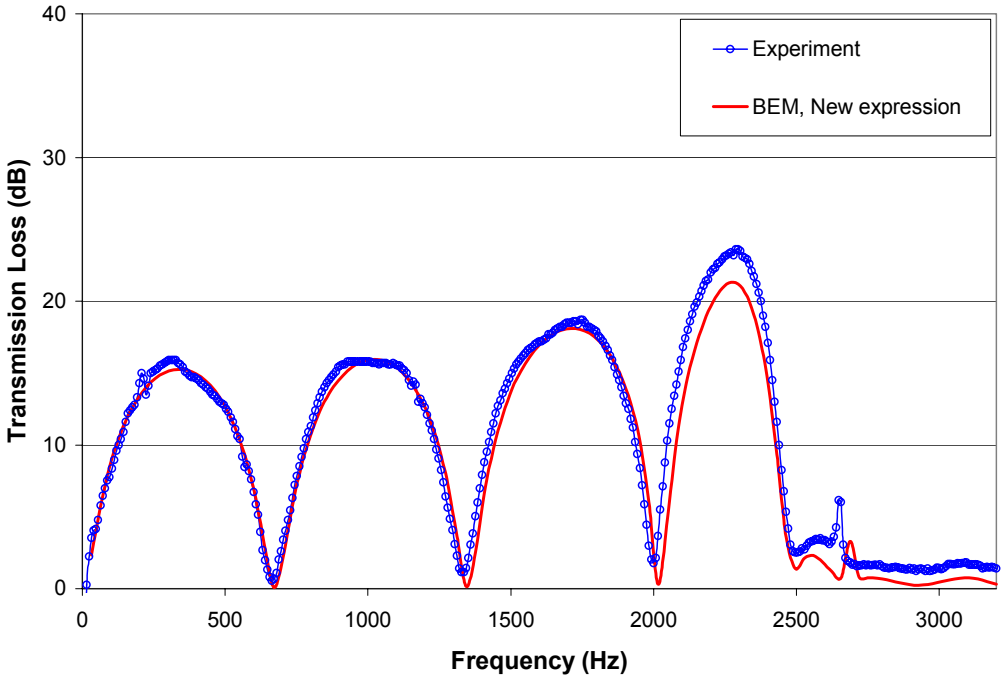

Figure 7.10: The transmission loss of the perforated reactive silencer ($\phi = 25.7$ %, $d_h = 0.498$ cm).

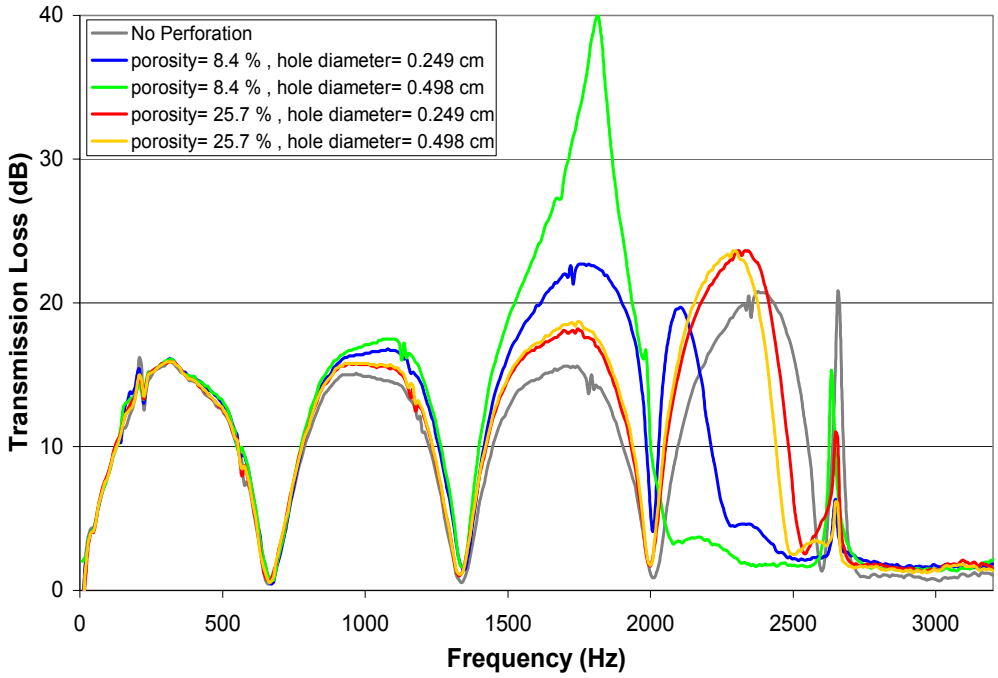

Figure 7.11: The effect of perforation impedance on the transmission loss of the perforated reactive silencers; experiments.

The variation of hole diameters ($d_h = 0.249$ and 0.498 cm) exhibits a substantial effect on the transmission loss for $\phi = 8.4$ %, whereas this effect diminishes for $\phi = 25.7$ %.

Figures 7.7 – 7.11 illustrate the importance of perforation impedance on the transmission loss predictions. Thus, the effect of resistance and end correction coefficient on the predicted transmission loss is shown in Fig. 7.12 for the silencer with $\phi = 8.4$ % and $d_h = 0.249$ cm. While the variation in the end correction substantially influences the transmission loss at mid frequencies, 1500 – 2500 Hz, the effect of resistance is negligible except for high frequencies. Therefore, accurate measurements of end correction are critical for improved transmission loss predictions.

Unlike the similar hole spacing of Figs. 7.7 – 7.11, Fig. 7.13 shows the experimental results of transmission loss with different hole spacing, as depicted in Fig. 7.14, while retaining the same porosity ($\phi = 8.4$ %) and the hole diameter ($d_h = 0.249$ cm). The unequal spacing between holes [Fig. 7.14 (a)] tends to increase the peak attenuation compared to the one with nearly equal spacing [Fig. 7.14(b)] since the former may increase the end correction by reducing the interaction among holes. The considerable effect of the spacing illustrates the difficulty in obtaining a generalized perforation impedance for various porosity, and hole size and shape.

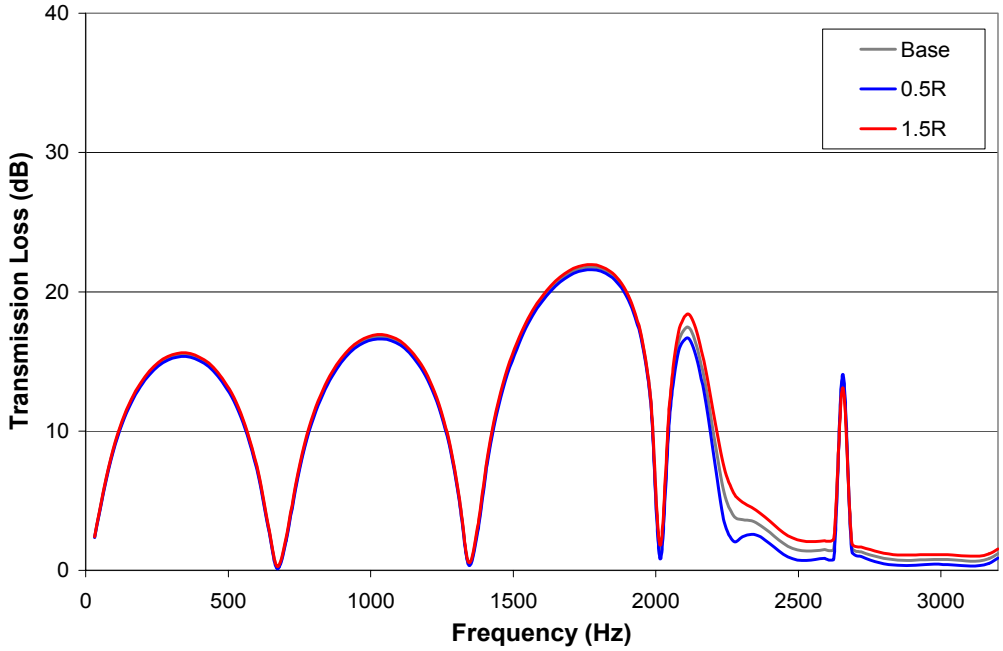

(a)

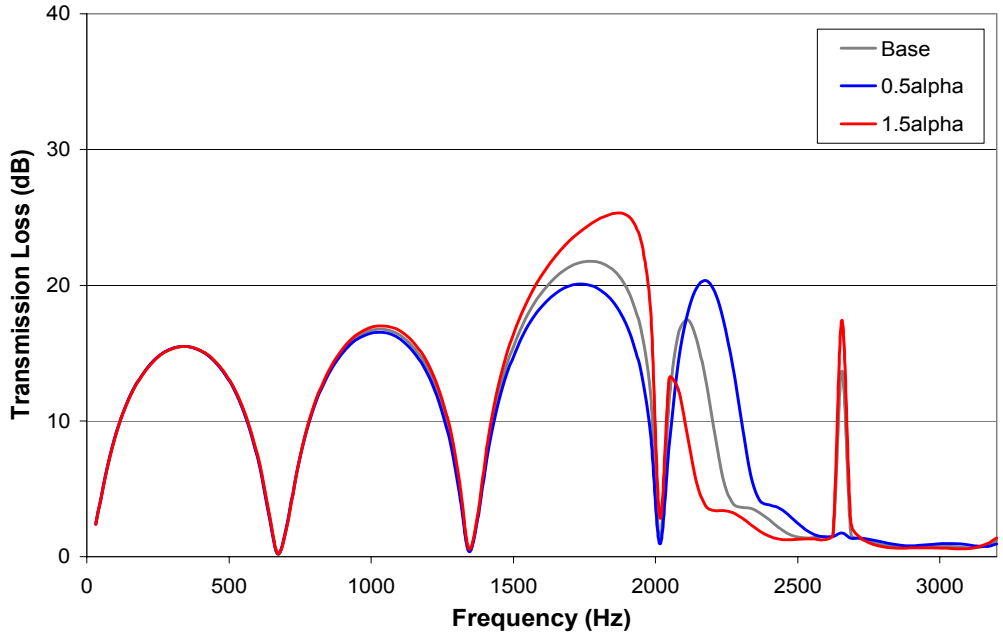

(b)

Figure 7.12: The effect of perforation impedance on the transmission loss of the perforated reactive silencer ($\phi = 8.4$ %, $d_h = 0.249$ cm), BEM predictions; (a) resistance and (b) end correction coefficient.

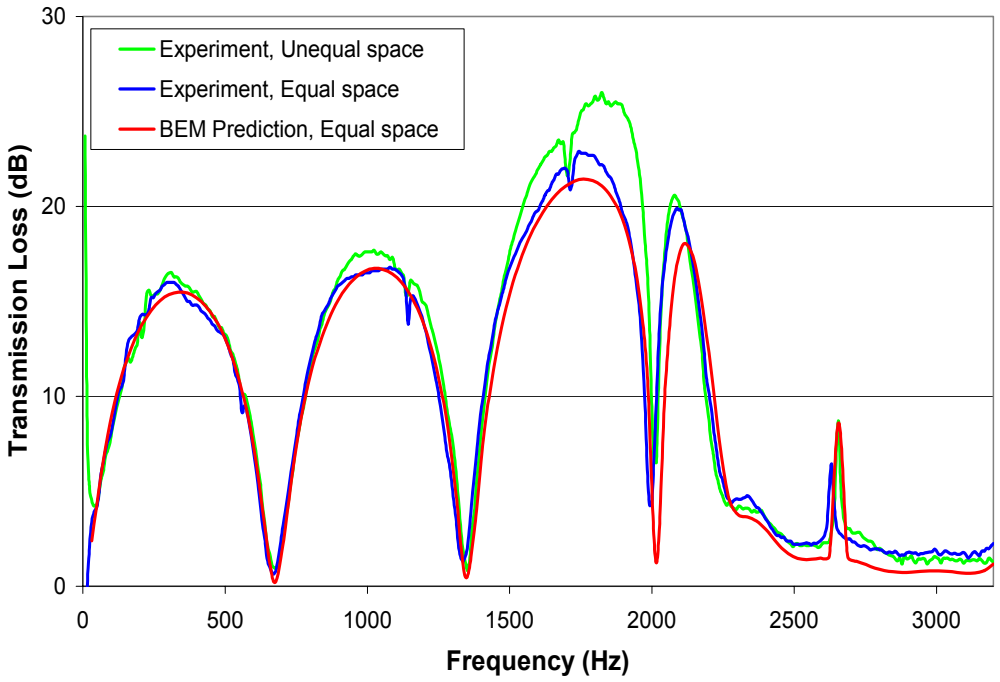

Figure 7.13: The effect of hole spacing on the transmission loss of a perforated reactive silencer ($\phi = 8.4$ %, $d_h = 0.249$ cm); experiments.

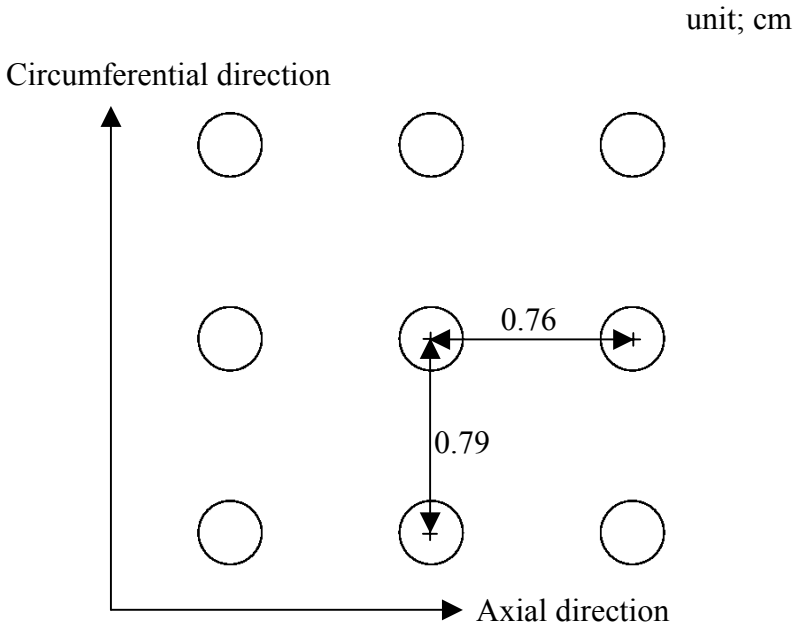

(a)

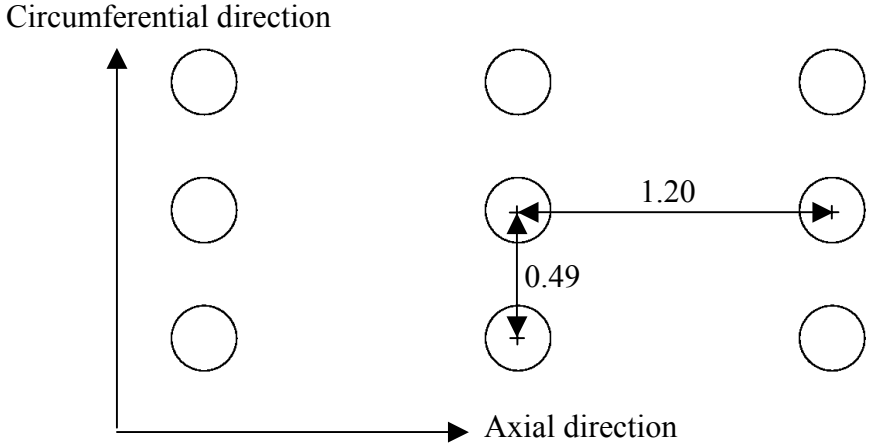

(b)

Figure 7.14: The distances between holes for two different perforated ducts ($\phi = 8.4$ %, $d_h = 0.249$ cm); (a) equal spacing and (b) unequal spacing.

7.3 Single pass dissipative silencers

The perforated reactive chambers of the preceding sections are now filled with fibrous material (Fig. 7.15) and the transmission loss is investigated experimentally and numerically. The measured transmission loss with different porosities, hole diameters, and filling densities are shown in Fig. 7.16. Filling the chamber with fibrous material dramatically changes the transmission loss from a multi-dome behavior to a single peak with substantially higher attenuation, illustrating the effectiveness of fiber. Figure 7.16 also demonstrates the dependence of the transmission loss of dissipative silencers on the porosity (ϕ), fiber filling density (ρ_f), and hole diameter (d_h). Thus the understanding of the effect of such parameters on the transmission loss is important for the predictions of dissipative silencers.

This section first compares the experiments and the predictions using the complex characteristic impedance and wavenumber of fibrous material, and the perforation impedance presented in Chapters 5 and 6, respectively. Then the effect of variations in such parameters on the transmission loss is explored using the BEM predictions. The influence of mean flow and variation of internal geometry of dissipative silencers is also illustrated.

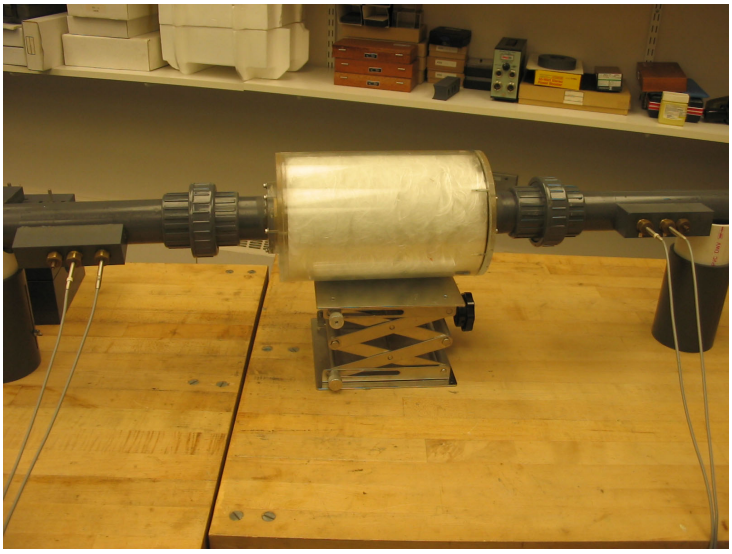

(a)

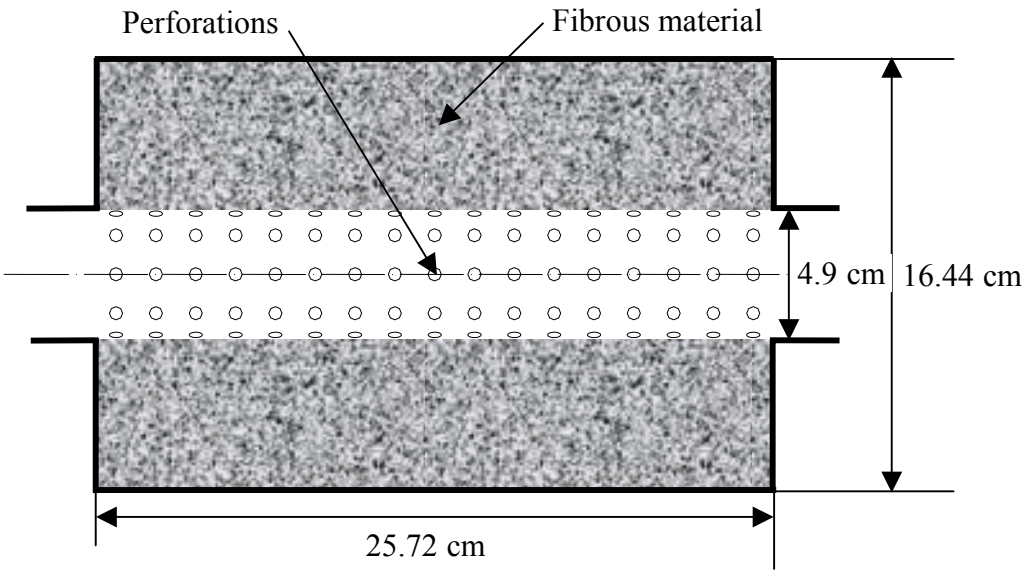

(b)

Figure 7.15: The pictures and schematics of a dissipative perforated reactive silencer; (a) picture and (b) schematic.

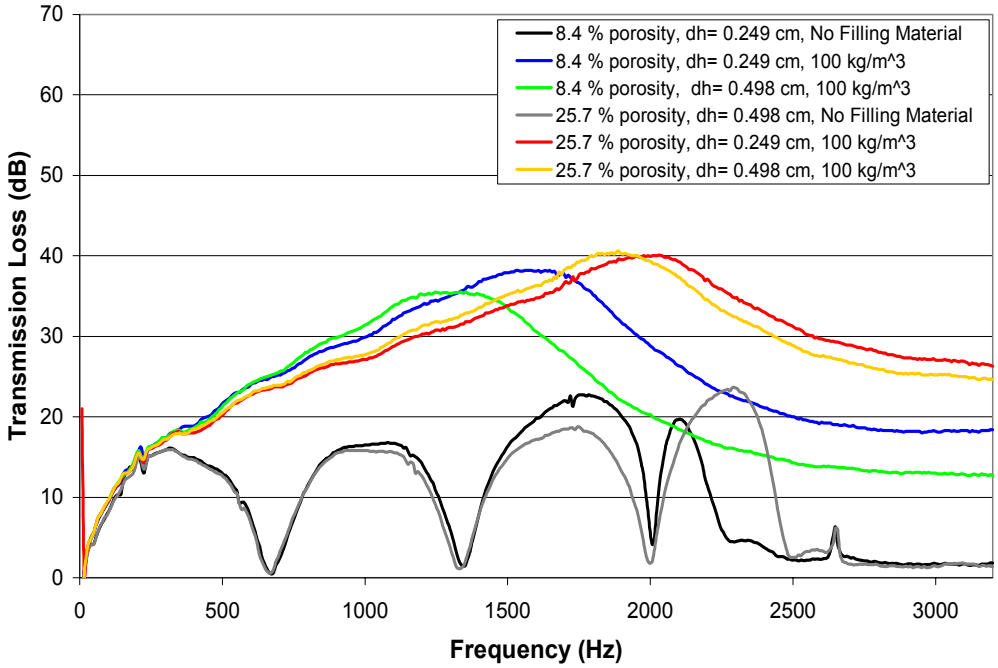

(a)

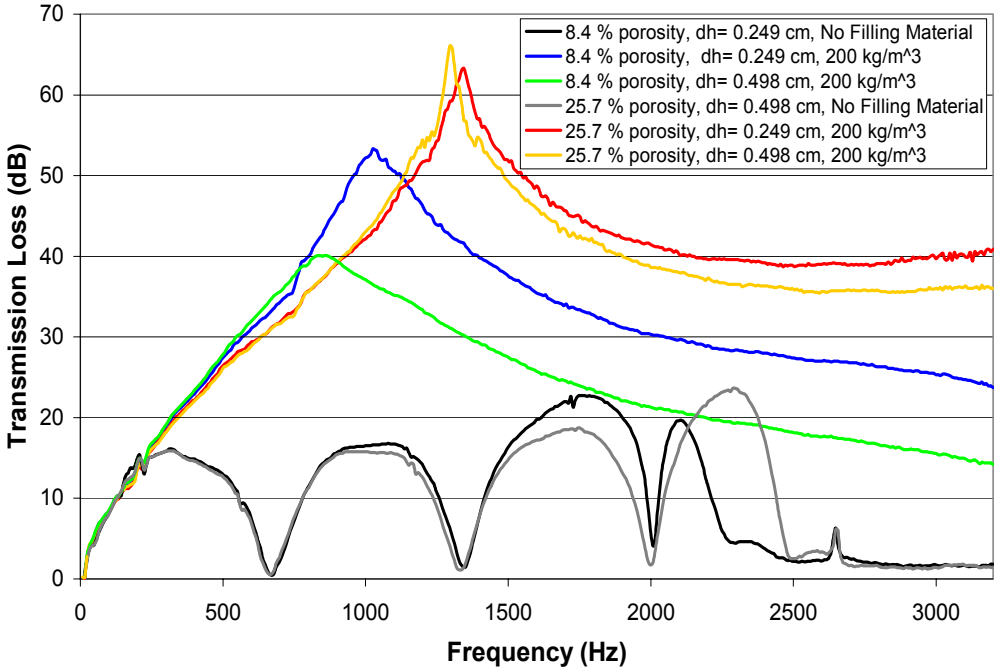

(b)

Figure 7.16: The transmission loss of the perforated dissipative silencer; Experiments; (a) $\rho_f = 100$ kg/m^3 and (b) $\rho_f = 200$ kg/m^3.

7.3.1 Comparisons of predictions and experiments

Figures 7.17 and 7.18 compare the transmission loss from predictions and experiments for silencers with $d_h = 0.249$ cm, different duct porosities ($\phi = 8.4$ and 25.7 %), and filling densities ($\rho_f = 100$ and 200 kg/m^3). 1D and 2D analytical approaches and 3D BEM developed in the present study are used for the predictions, along with the complex characteristic impedance and wavenumber [Eqs. (5.6) − (5.13)] and perforation impedance [Tables 6.3 and 6.4]. The texturization conditions of the fibrous material in the silencers can be assumed 'good', although the condition may be locally less texturized due to the hand filling of a large amount of fibrous material in the chamber. While the BEM predictions for both texturization conditions are provided, only 'good' texturization is applied for the 1D analytical approach. The BEM predictions with 'good' texturization in Fig. 7.17 ($\phi = 8.4$ %) show reasonable agreement with the experiments for both filling densities, while the 1D analytical predictions deviate at frequencies above 700 Hz, limiting the use of 1D approach to low frequencies. The BEM predictions in Fig. 7.18 ($\phi = 25.7$ %) show some deviations from the experiments, possibly due to the discrepancy of perforation impedance from the sample plates and susceptibility of the high porosity to the variation of fiber filling conditions.

Figures 7.17 and 7.18 exhibit higher transmission loss predictions with 'good' texturization compared to the ones with 'normal' conditions, except for the Fig. 7.17(b). The 2D analytical predictions are essentially identical to the 3D BEM predictions, thus the results from 2D analytical approach are not shown here. The 2D analytical approach

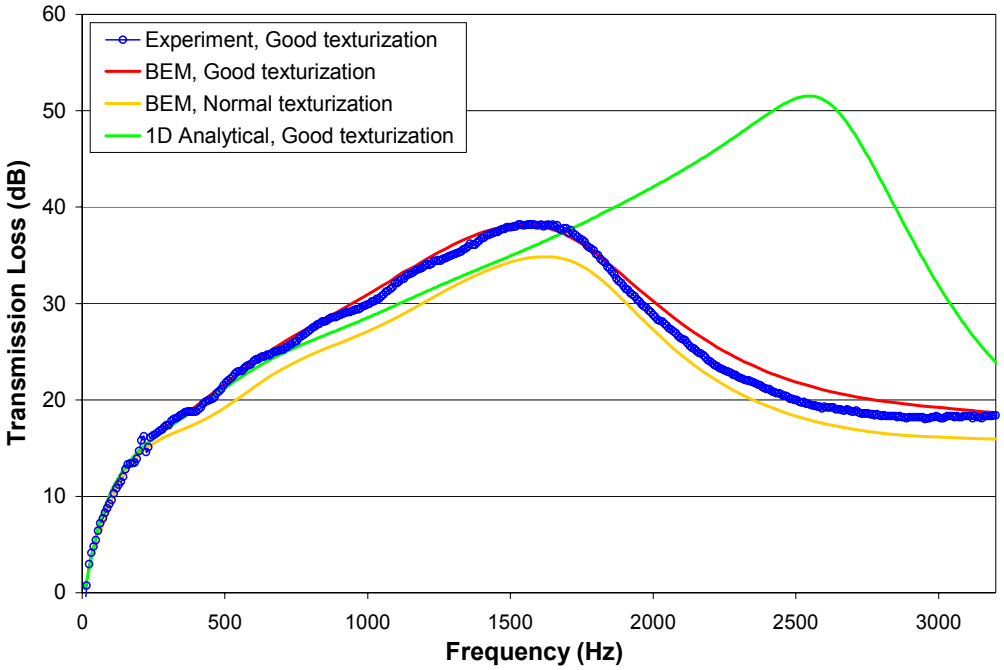

(a)

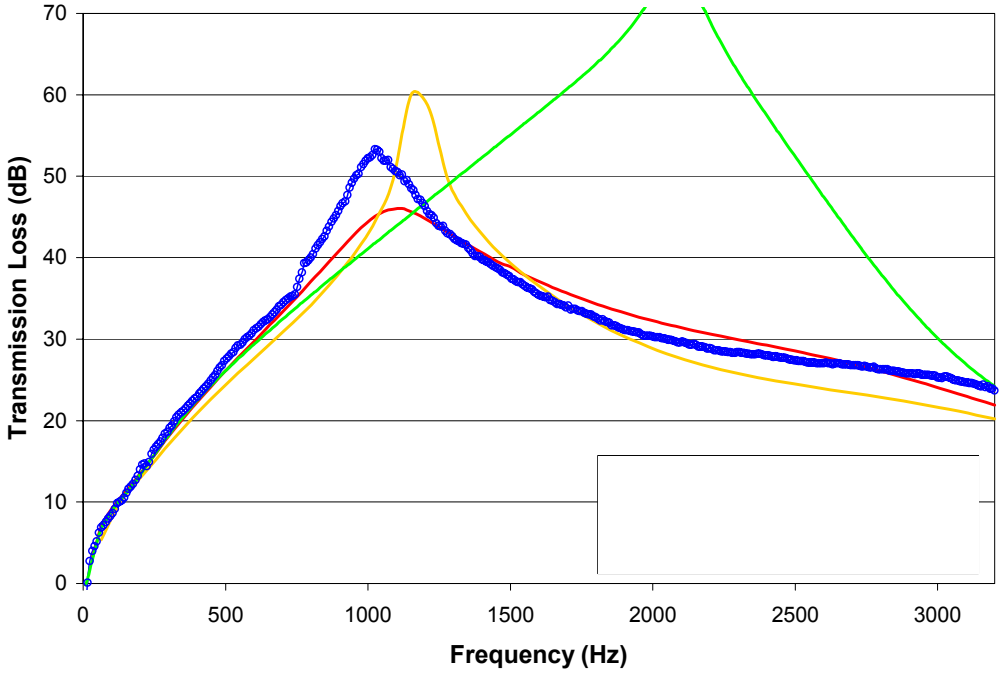

(b)

Figure 7.17: The transmission loss of the perforated dissipative silencer ($\phi = 8.4$ %, $d_h = 0.249$ cm); (a) $\rho_f = 100$ kg/m^3 and (b) $\rho_f = 200$ kg/m^3.

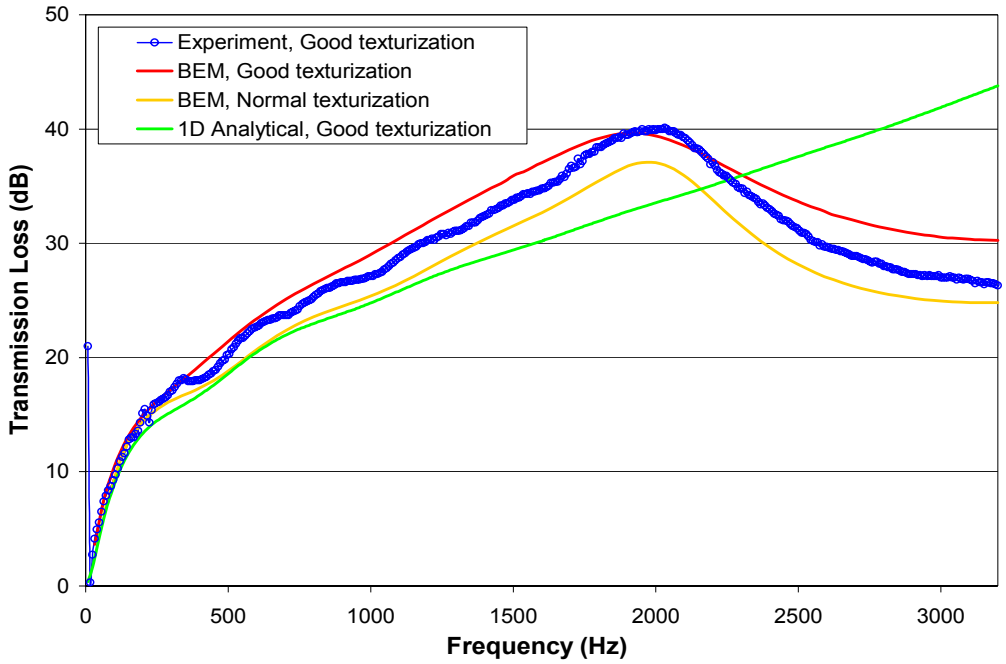

(a)

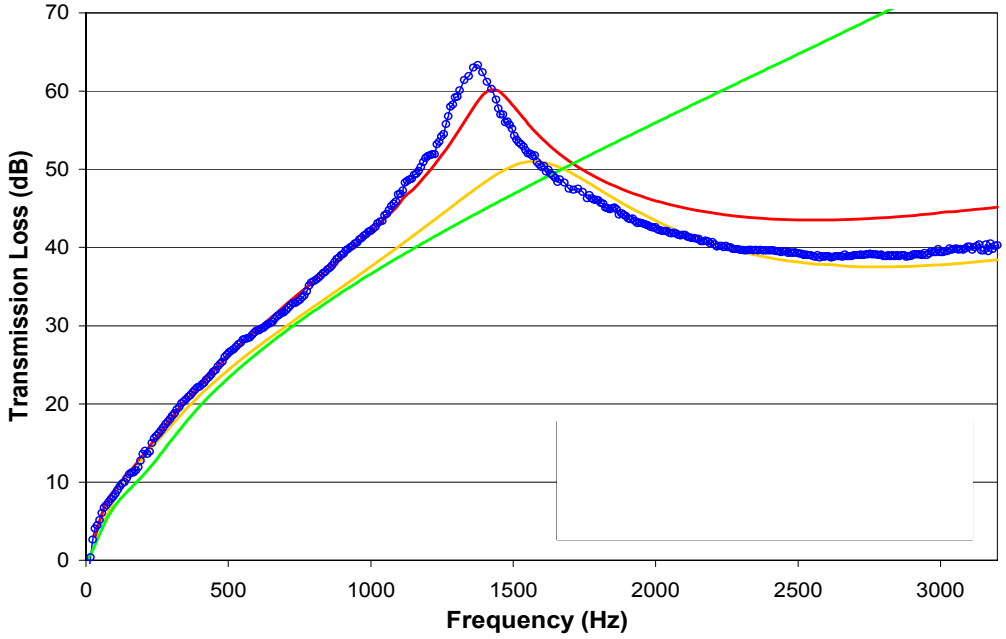

(b)

Figure 7.18: Transmission loss of the perforated dissipative silencer ($\phi = 25.7$ %, $d_h = 0.249$ cm); (a) $\rho_f = 100$ kg/m^3 and (b) $\rho_f = 200$ kg/m^3.

applied for dissipative silencers may be found in the literature (Selamet *et al*., 2004, 2005a, 2005b).

7.3.2 Effect of acoustic properties of fibrous material on the transmission loss

The effect of variation in both real and imaginary parts of the characteristic impedance and wavenumber on the transmission loss is presented for the silencers with $\phi = 25.7$ % and $d_h = 0.249$ cm in Fig. 7.19 (for $\rho_f = 100$ kg/m^3) and Fig. 7.20 (for $\rho_f = 200$ kg/m^3). Each parameter is allowed to vary below and above the base value by 20 %. Figure 7.19 shows that the decrease of the imaginary part of the wavenumber reduces the transmission loss for $\rho_f = 100$ kg/m^3, while the influence of other parameters are almost negligible. Figure 7.20(b) shows that both real and imaginary parts of the wavenumbers influence the transmission loss for $\rho_f = 200$ kg/m^3. Particularly, the variation of the real part of the wavenumber shifts the peak frequency and changes the magnitude. Unlike $\rho_f = 100$ kg/m^3, the increase of the imaginary part of the wavenumber by 20 % from the base does not substantially affect the transmission loss for $\rho_f = 200$ kg/m^3. Figures 7.19 and 7.20 show that the effect of variation in the characteristic impedance is less significant compared to the wavenumber for both ρ_f. Thus, the accurate knowledge of wavenumber for the fibrous material is important for reliable transmission loss predictions.

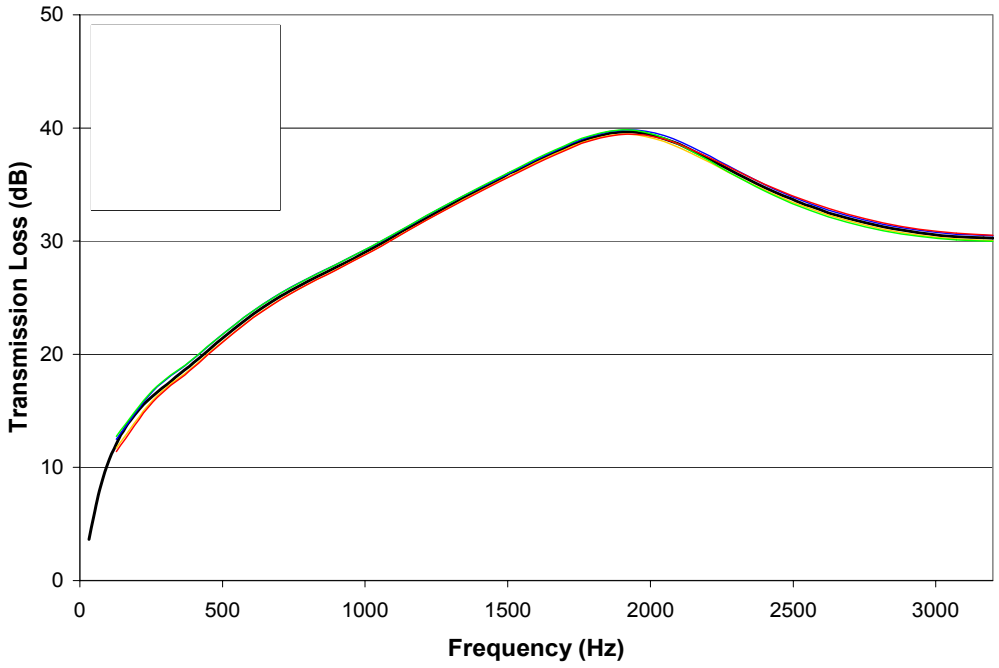

(a)

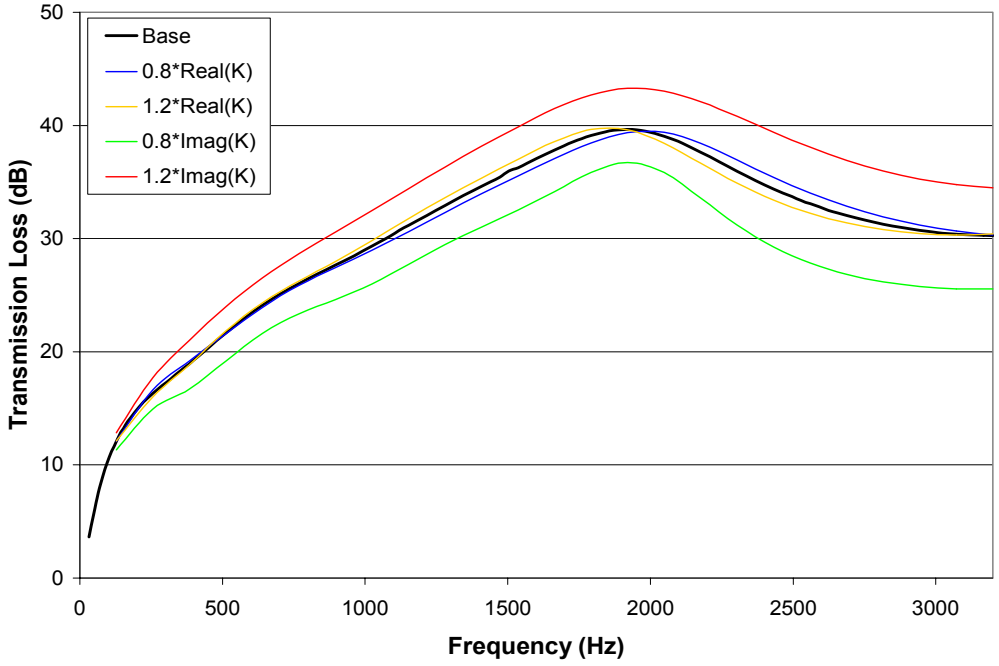

(b)

Figure 7.19: The effect of acoustic properties of fibrous material on the transmission loss of the perforated dissipative silencer ($\phi = 25.7$ %, $d_h = 0.249$ cm, $\rho_f = 100$ kg/m^3), BEM predictions; (a) characteristic impedance and (b) wavenumber.

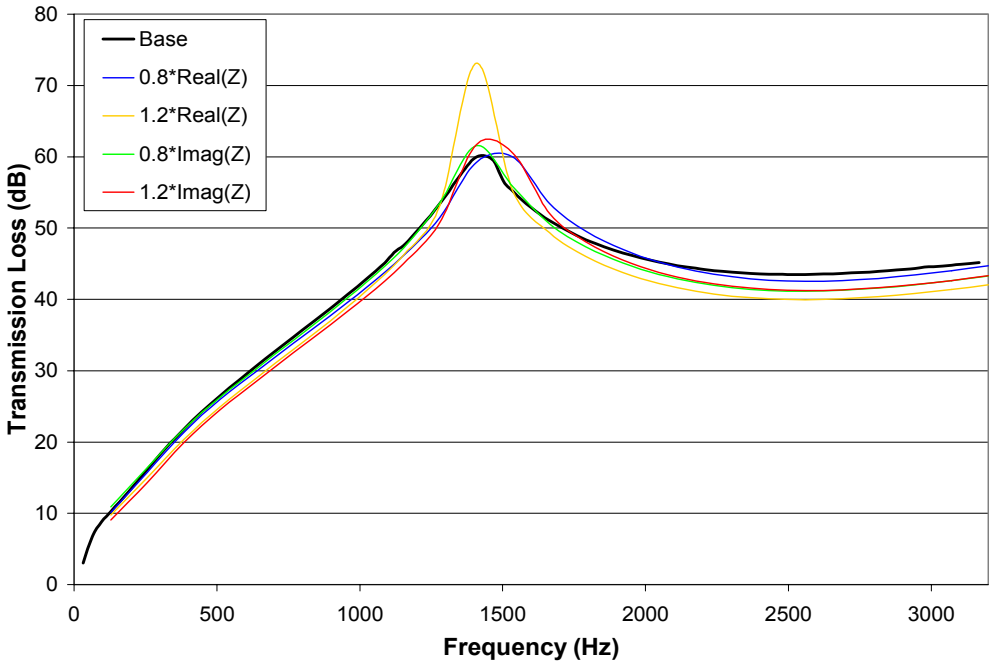

(a)

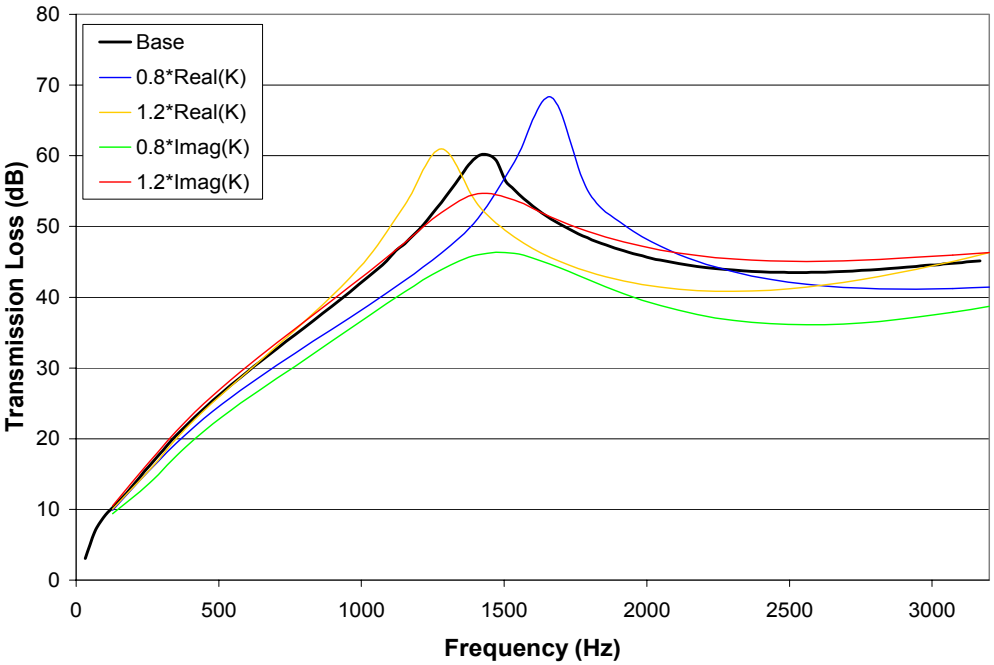

(b)

Figure 7.20: The effect of acoustic properties of fibrous material on the transmission loss of the perforated dissipative silencer ($\phi = 25.7$ %, $d_h = 0.249$ cm, $\rho_f = 200$ kg/m^3), BEM predictions; (a) characteristic impedance and (b) wavenumber.

The effect of texturization condition on the acoustic properties has been demonstrated in Chapter 5, thus the texturization condition is now expected to affect the transmission loss. Figure 7.21 depicts the experimental results and predictions with different texturization conditions for a silencer with $\phi = 25.7$ %, $d_h = 0.498$ cm, and $\rho_f = 100$ kg/m^3. High porosity of $\phi = 25.7$ % is used to identify the effect of texturization conditions on the transmission loss with the minimum effect from the perforation impedance variation. As the texturization condition is improved, the magnitude of transmission loss increases. Thus, better texturization with the same amount of fiber can lead to higher acoustic attenuation for dissipative silencers. The texturization conditions can change the perforation impedance as well as the wave propagation through the fibrous material, particularly for the silencers with low perforate porosities and high filling densities. Thus, the trend shown in Fig. 7.21 may be different for such dissipative silencers.

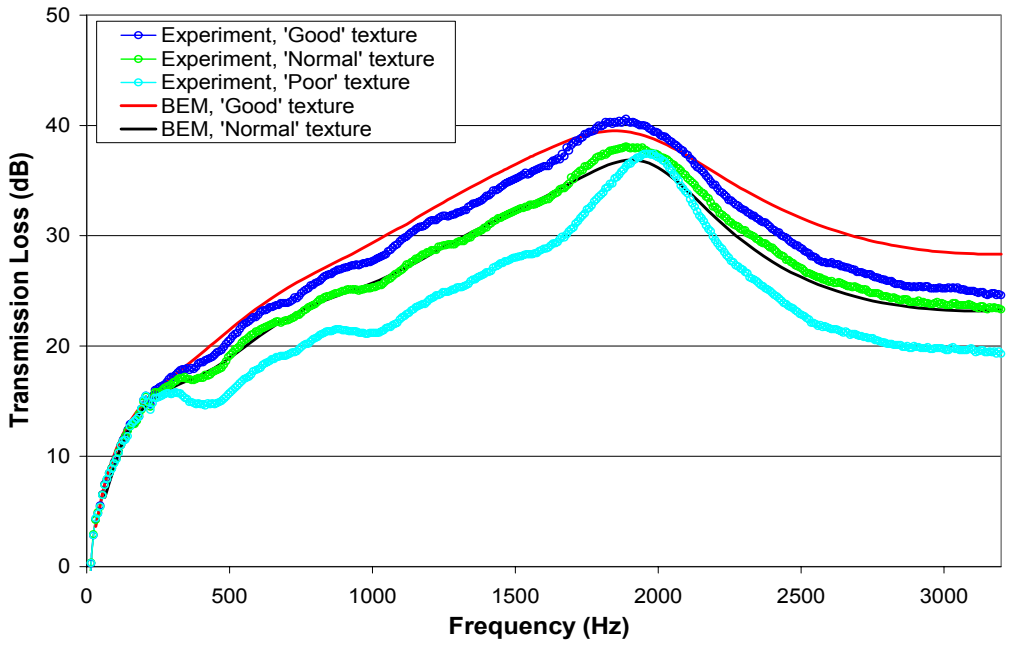

Figure 7.21: The effect of fiber texturization condition on transmission loss of the perforated dissipative silencer ($\phi = 25.7$ %, $d_h = 0.498$ cm, $\rho_f = 100$ kg/m^3).

7.3.3 Effect of acoustic impedance of perforations on the transmission loss

The acoustic impedance of perforation in contact with air-air have been frequently used for predictions of dissipative silencers due to lack of information on perforations in contact with fibrous material. A modified expression for the impedance of dissipative silencers is suggested by Selamet *et al*. (2001). They demonstrated the effectiveness of the semi-empirical expression for the silencer with $\phi = 2$ % and $\rho_f = 200$ kg/m^3. The impact of perforation impedance on the transmission loss of dissipative silencers is further illustrated next. Figure 7.22 shows the comparisons of experiments with the predictions using the perforation impedance with air-air (Table 6.2) and air-absorbent (Table 6.3). While the predictions using the impedance of perforations facing air-fibrous material show good agreement with experiments, the ones facing air-air exhibit a substantial discrepancy from the experiments particularly at high porosity and frequencies.

Figures 7.23 and 7.24 illustrate the influence of the variation of resistance R and end correction coefficient α of perforation impedance on the transmission loss for a silencer with $\phi = 8.4$ %, $d_h = 0.249$ cm. Figure 7.23 shows that the lower α shifts the peak to higher frequencies, therefore broadens the transmission loss, whereas the effect of R is nearly insignificant for $\rho_f = 100$ kg/m^3. Unlike Fig. 7.23(a), Fig. 7.24(a) exhibits substantial effect from the variation in R for $\rho_f = 200$ kg/m^3. The effect of α shown in Fig. 7.24(b) is similar to that of Fig. 7.23(b).

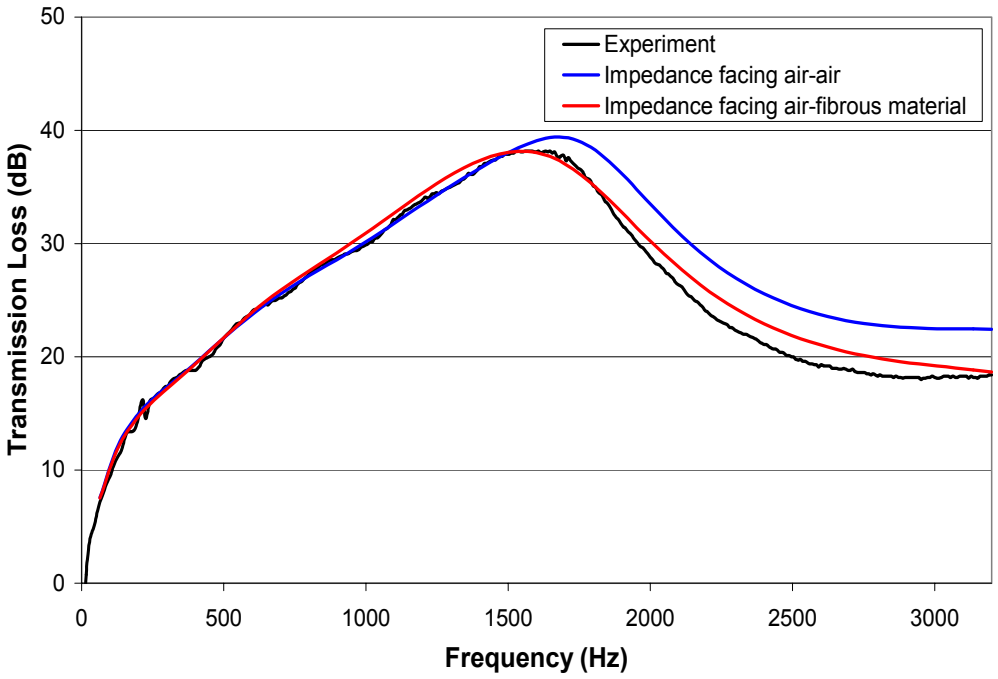

(a)

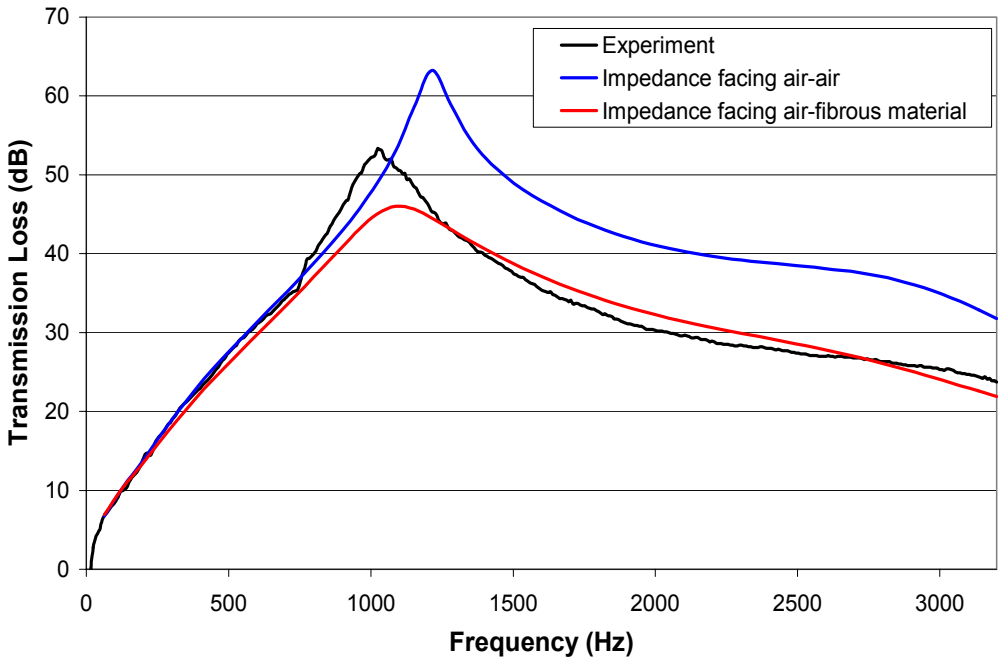

(b)

Figure 7.22: The effect of perforation impedance on the transmission loss of the perforated dissipative silencer ($\phi = 8.4$ %, $d_h = 0.249$ cm); (a) $\rho_f = 100$ kg/m^3 and (b) $\rho_f = 200$ kg/m^3.

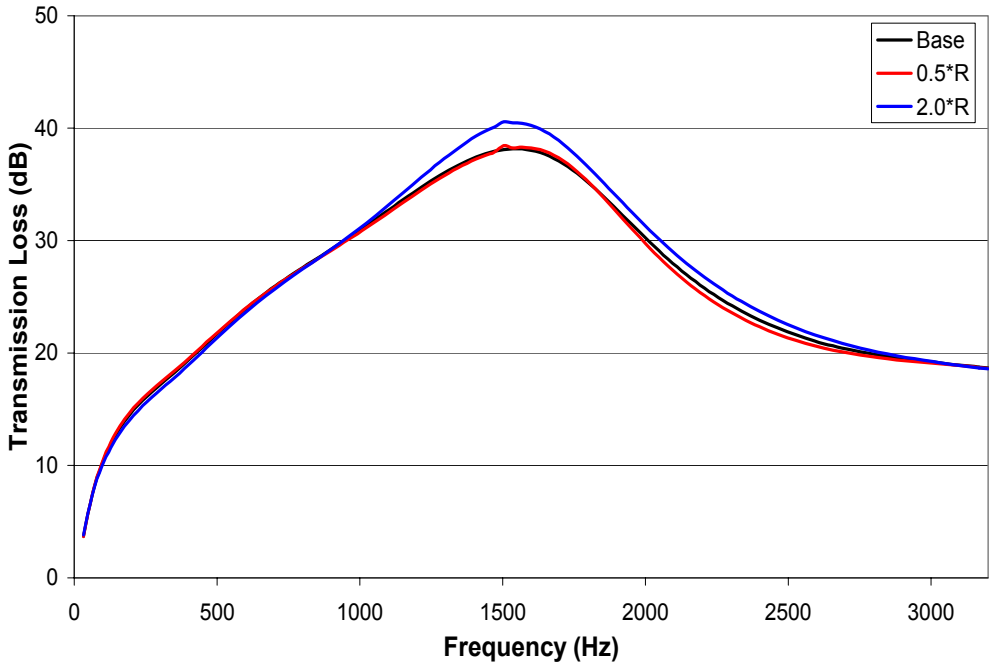

(a)

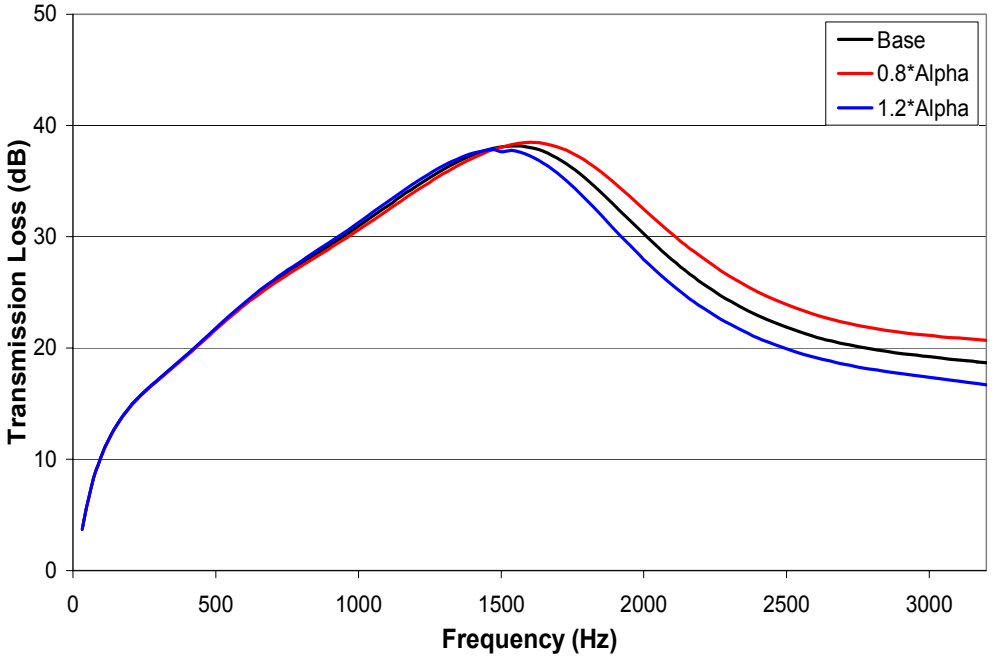

(b)

Figure 7.23: The effect of perforation impedance on the transmission loss of the perforated dissipative silencer ($\phi = 8.4$ %, $d_h = 0.249$ cm, $\rho_f = 100$ kg/m^3); BEM predictions; (a) real part and (b) imaginary part.

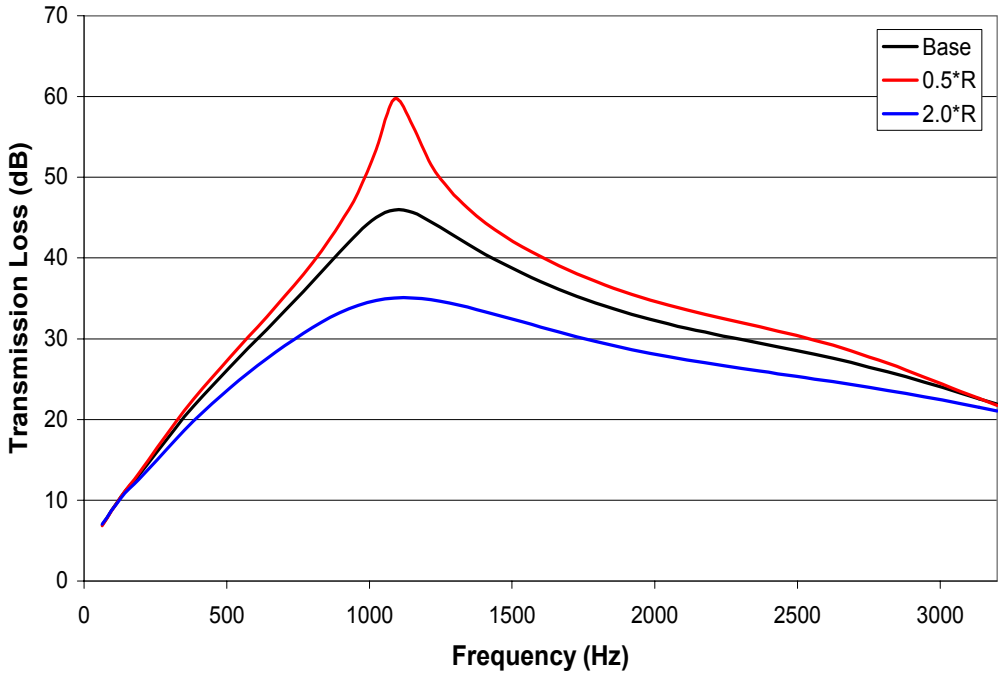

(a)

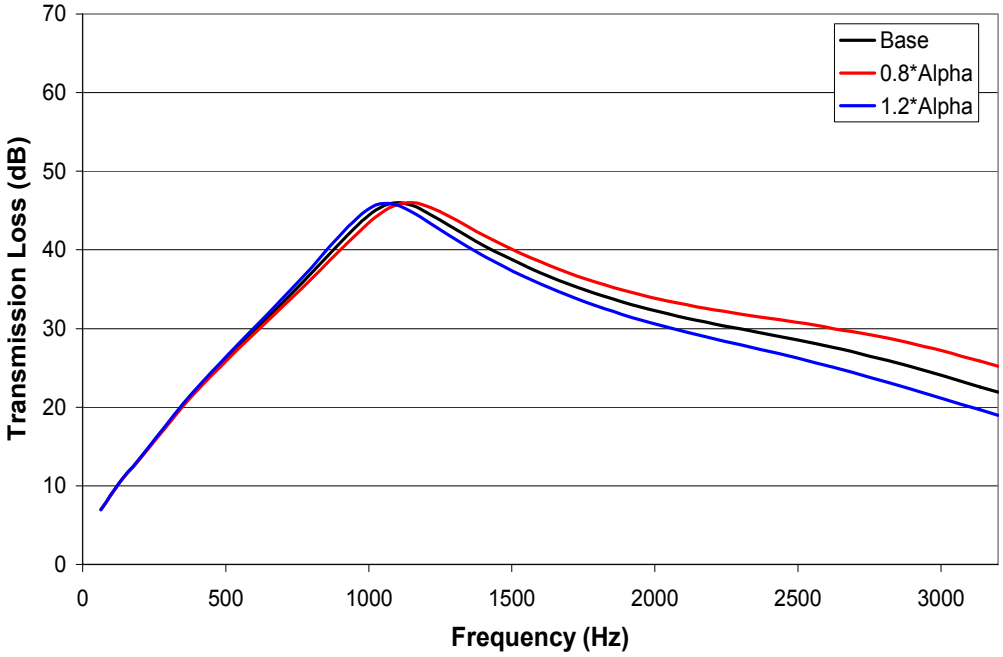

(b)

Figure 7.24: The effect of perforation impedance on the transmission loss of the perforated dissipative silencer ($\phi = 8.4$ %, $d_h = 0.249$ cm, $\rho_f = 200$ kg/m^3), BEM predictions; (a) real part and (b) imaginary part.

7.3.4 Effect of mean flow on the transmission loss

The effect of mean flow of Ma= 0.1 (at room temperature and 1 atm pressure) on the transmission loss of dissipative silencers with $d_h = 0.249$ cm and $\rho_f = 100$ kg/m^3 for two different porosities ($\phi = 8.4$ and 25.7 %) is shown in Fig. 7.25. The experimental setup for the measurements of transmission loss in the presence of mean flow has been described earlier (Fig. 4.4). A single sine wave is applied at 80 Hz intervals as the sound source to generate higher sound power than the background flow noise. While the effect of mean flow is not noticeable for $\phi = 25.7$ %, its influence is substantial for $\phi = 8.4$ % at high frequency, due to the lowered end correction coefficient. Experimental results given in Fig. 6.15 show the reduction of end correction coefficient, due to the mean flow, to 90 and 73 % of the one without mean flow. Using these values, the BEM predictions illustrate similar trends to the experiments in Fig. 7.25. The convective effect in the BEM predictions is ignored to illustrate the influence of perforation impedance in the presence of mean flow. Figure 7.23 also shows that the reduced end correction coefficient increases the transmission loss at higher frequencies.

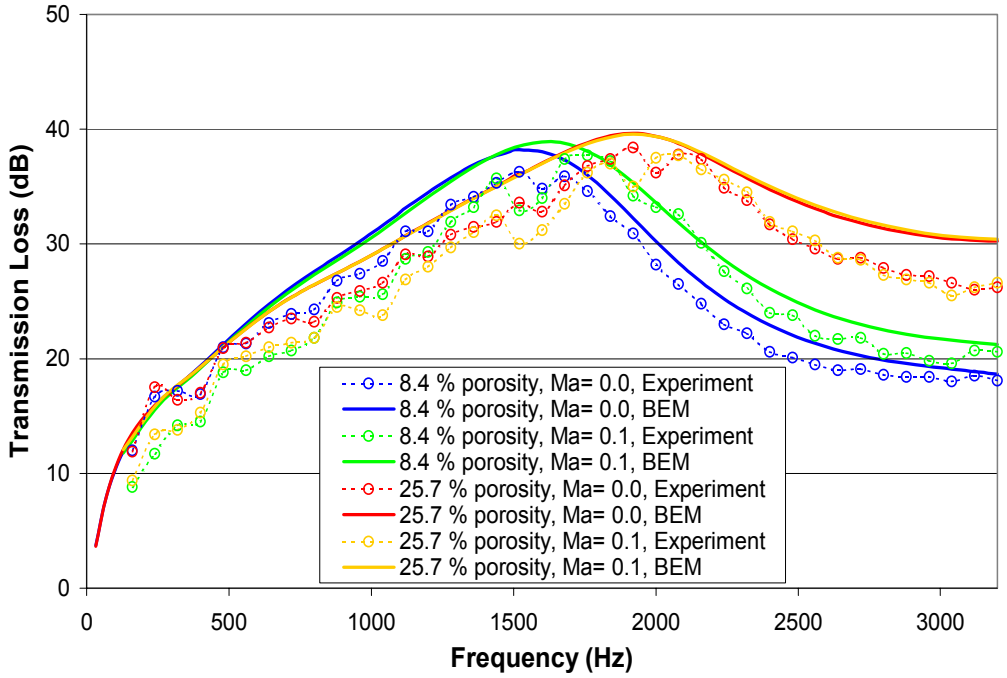

Figure 7.25: The effect of mean flow on the transmission loss of the dissipative silencer ($d_h = 0.249$ cm, $\rho_f = 100$ kg/m^3).

7.3.5 Effect of baffles and extended inlet/outlet on the transmission loss

Modifications in internal geometry of a single dissipative silencer can change the overall transmission loss. The effect of a baffle and the extended inlet/outlet ducts in the chamber of a silencer with $\phi = 8.4$ %, $d_h = 0.249$ cm, and $\rho_f = 100$ kg/m^3 is investigated using the BEM predictions. Figure 7.26 is the schematic of the dissipative silencer with a baffle, and the corresponding BEM results are given Fig. 7.27, as contrasted to the silencer without baffle (base). The baffle increases the magnitude of the transmission loss while shifting the resonance to lower frequencies. However, the use of baffle reduces the transmission loss at frequencies lower than 250 Hz.

The other modification is the extension of inlet and outlet ducts into the chamber. The schematic of the dissipative silencer with the extensions is given in Fig. 7.28 and the corresponding BEM results are presented in Fig. 7.29 along with the predictions for the silencer without extensions (base). The silencer with $\phi = 8.4$ %, $d_h = 0.249$ cm, and $\rho_f = 100$ kg/m^3 has 3.5 cm long extensions into the chamber. The extensions shift the resonance to a lower frequency and increase the magnitude at mid frequency at the cost of lower noise reduction at higher frequencies. Thus, appropriate modifications can improve the acoustic performance of dissipative silencers depending on the frequency range of interest. In addition to the baffle and extended inlet/outlet, layered or uneven fillings, partial fillings with void volume, and change of perforation impedance by the placement of another material or air are possible modifications depending on the application of the silencers.

unit: cm

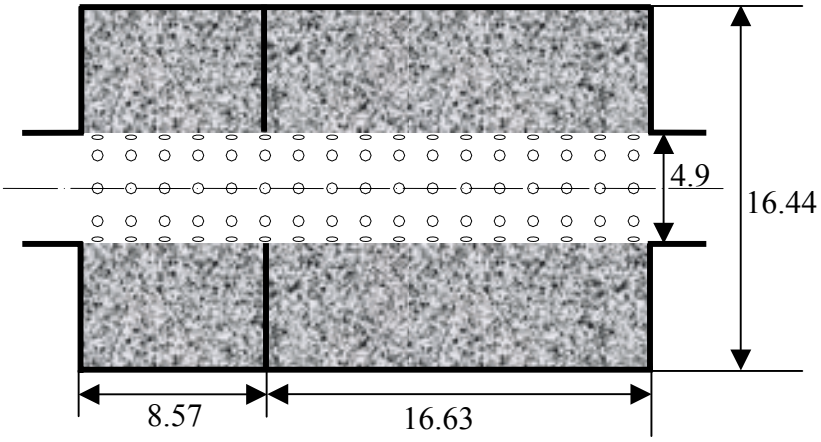

Figure 7.26: The schematic of the dissipative silencer with a baffle ($\phi = 8.4$ %, $d_h = 0.249$, and $\rho_f = 100$ kg/m^3).

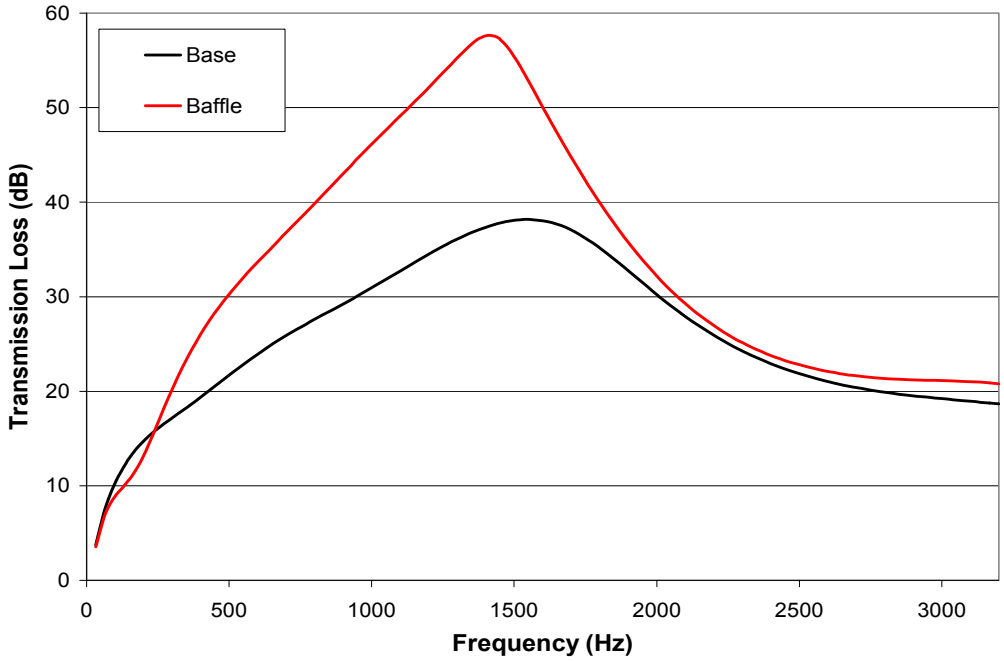

Figure 7.27: The effect of a baffle on the transmission loss of the dissipative silencer, BEM predictions.

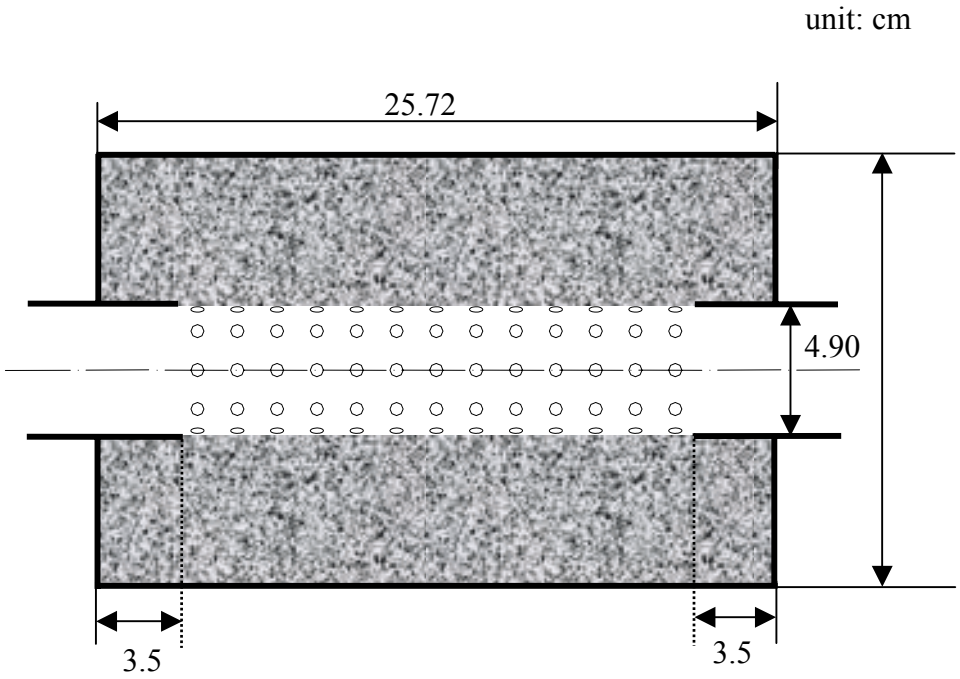

Figure 7.28: The schematic of the dissipative silencer with extended inlet and outlet ($\phi = 8.4$ %, $d_h = 0.249$, and $\rho_f = 100$ kg/m^3).

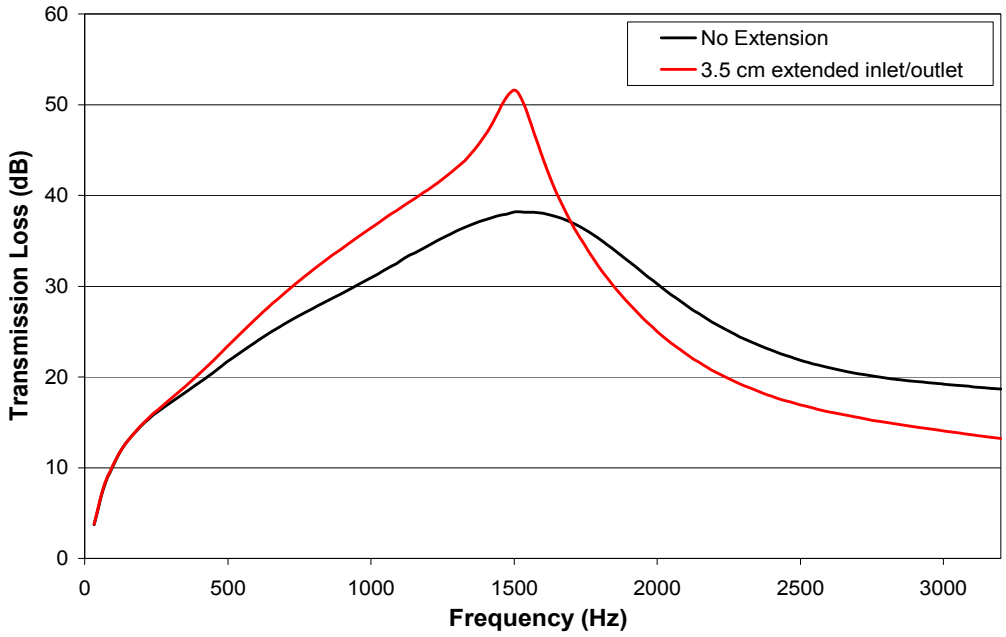

Figure 7.29: The effects of extended inlet and outlet on the transmission loss of the dissipative silencer, BEM predictions.

7.4 Hybrid silencers

In many applications of dissipative silencers, they are combined with reactive components to enhance the acoustic performance at low frequencies. In such cases, the effect of the connection between the silencers needs to be considered in addition to the analysis of individual silencers. Thus, a hybrid silencer, consisting of a dissipative silencer and a Helmholtz resonator as depicted in Fig. 7.30, is examined with varying connecting tube lengths (L_C) using 1D and BEM predictions. 1D analytical method can be applied to the connecting tube because of its small diameter (4.9 cm). The transfer matrix of the tube is then combined with the matrices of the dissipative silencer and the Helmholtz resonator calculated from BEM. The dissipative silencer is filled with $\rho_f = 100$ kg/m^3 and has $\phi = 8.4$ % and $d_h = 0.249$ cm. Figure 7.31(a) shows that the transmission loss of the hybrid silencer is similar to the sum of reactive and dissipative silencers, except near the resonance frequencies of the Helmholtz resonator. For some applications of hybrid silencers, such as the vehicle exhaust systems, acoustic performance at low frequency is important. Figure 7.31 (b) shows the transmission loss of the hybrid silencer at low frequencies. Though the resonance frequency does not move, the magnitude varies drastically near the resonance frequency as a function of the connecting tube length. Thus, the connecting tube effect needs to be accounted in such designs of hybrid silencers.

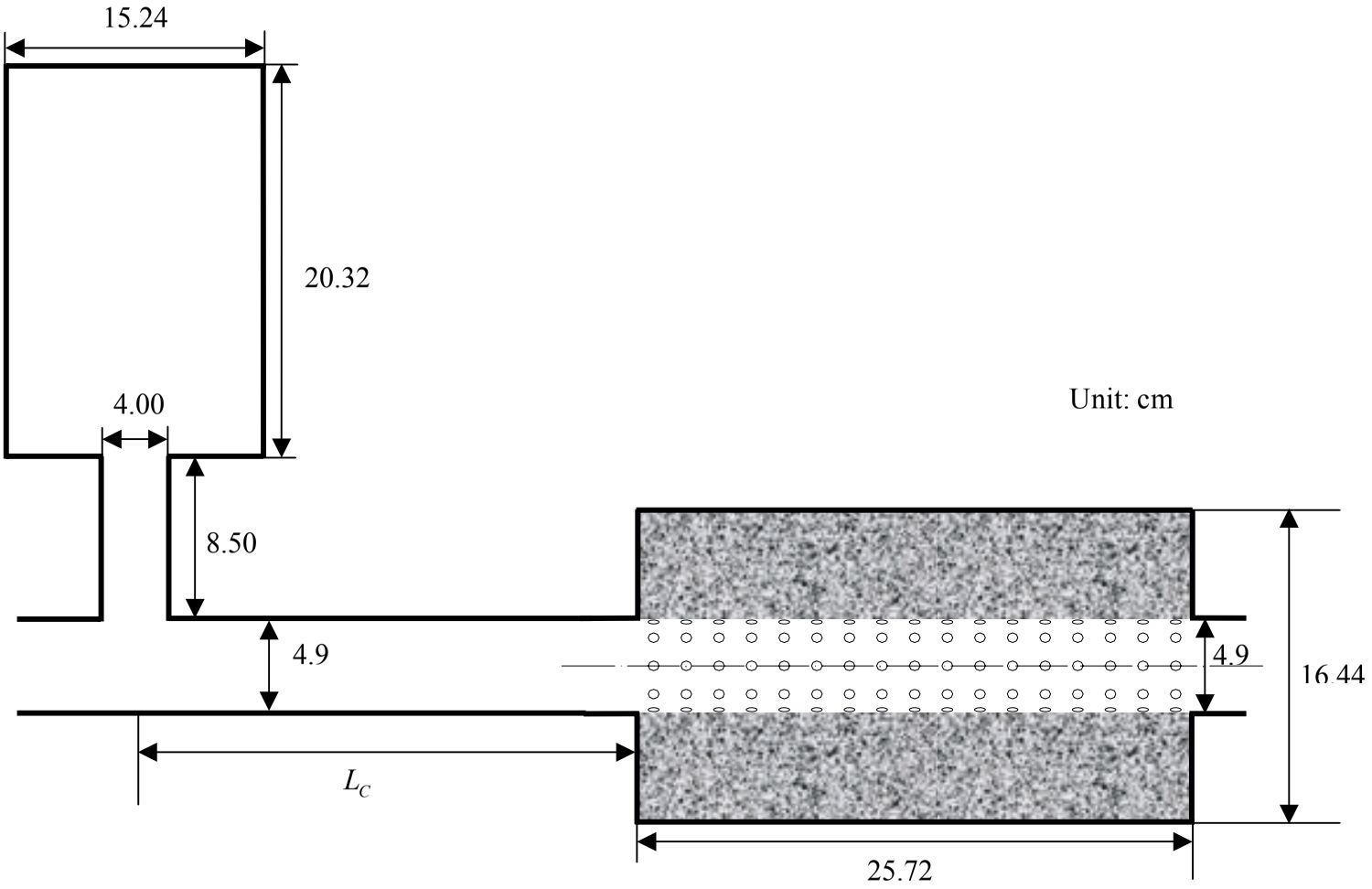

Figure 7.30: Schematic of a hybrid silencer.

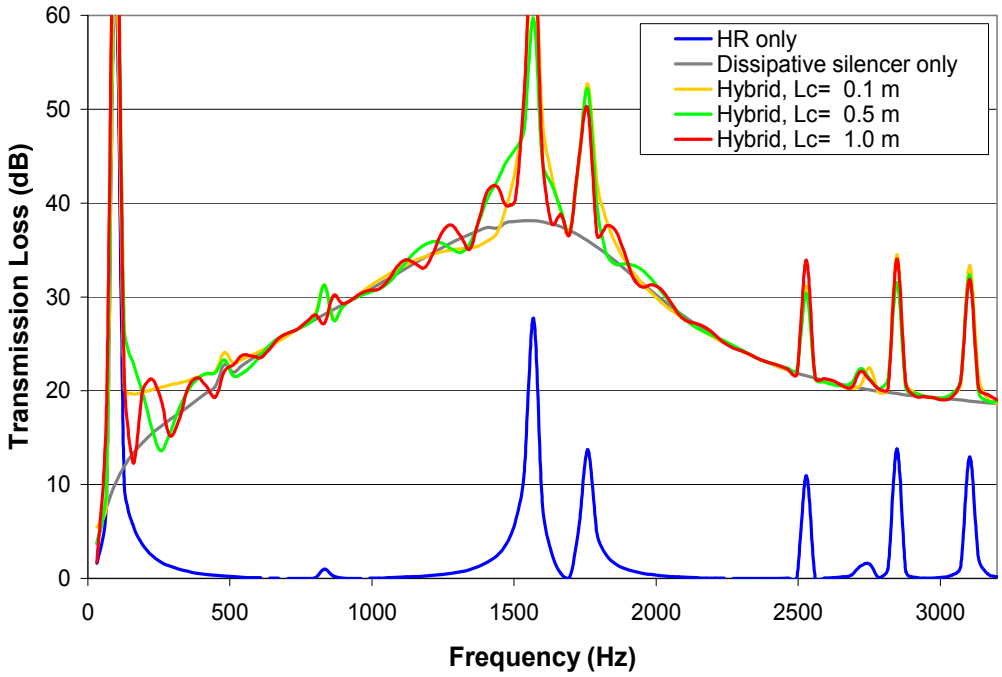

(a)

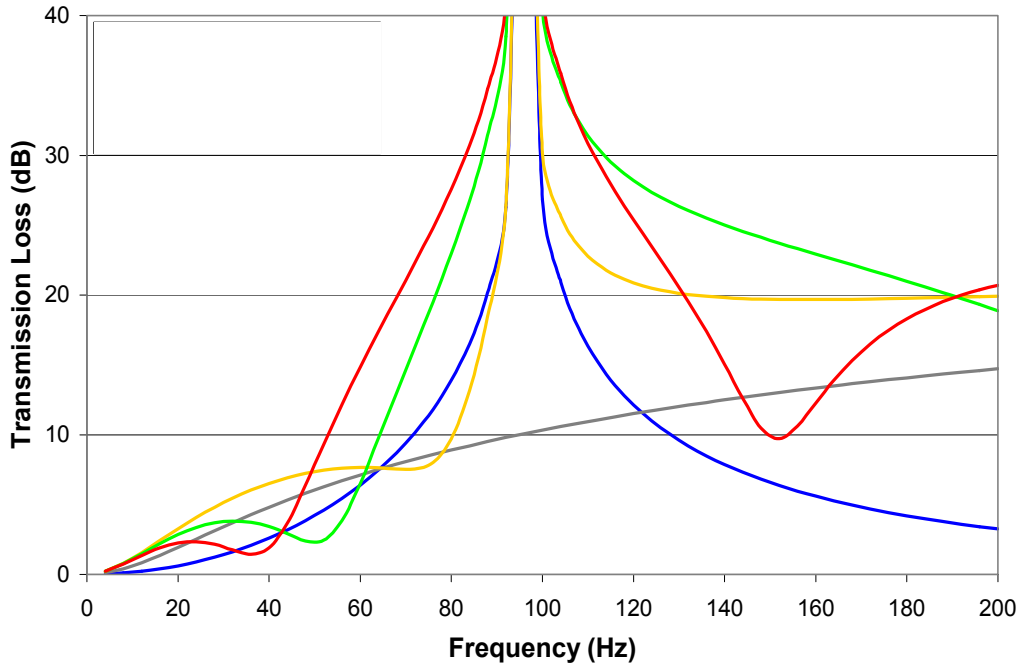

(b)

Figure 7.31: Transmission loss hybrid silencers, BEM predictions; (a) overall frequency range and (b) low frequency range.

CHAPTER 8

CONCLUSIONS

The acoustic characteristics of perforated dissipative silencers filled with fibrous material are investigated experimentally, analytically, and computationally. The understanding of the acoustic behavior of the fibrous material and perforations is critical for such dissipative silencers. Therefore, the present study has developed experimental setups to measure: (a) the complex characteristic impedance and the complex wavenumber of the fibrous material, and (b) the acoustic impedance of perforations. These properties are then integrated into the predictions of transmission loss, which are compared with the experimental results. The effect of each acoustic property of the fibrous material and the perforation impedance on the transmission loss is established using the predictions from BEM developed in the present study. Furthermore, the influence of internal geometrical variation of the dissipative silencers and the effect of the connecting tube length between two silencers are investigated using the BEM predictions. The conclusions are briefly described next.

Acoustic properties of fibrous material

The characteristic impedance and wavenumber of the fibrous material with two filling densities ($\rho_f = 100$ and 200 kg/m^3) and two different texturization conditions ('good' and 'normal') are obtained using an impedance tube setup (Fig. 4.2) with four microphones and two different termination conditions. The averaged values from five samples are curve-fitted as a function of frequency. These curve-fits represent most of the data points well, particularly for the wavenumber at both filling densities. The 'good' texturization leads to higher magnitudes for each parameter compared to that of 'normal' conditions. The characteristic impedance and wavenumber inferred from the experiments are then used for the measurement of acoustic impedance of perforations in contact with the fibrous material, and for the predictions of transmission loss of dissipative silencers.

Perforation impedance

A new experimental setup (Fig. 4.3) is developed in the present study for the measurement of acoustic impedance of perforations in contact with the fibrous material as well as with air alone in the absence of mean flow using the transfer matrix of the sample. The resistance R and the end correction coefficient α of 11 perforation samples with different porosities ($\phi = 2.1$, 8.4, 13.6, and 25.2 %), hole diameters ($d_h = 0.249$ and 0.498 cm), and wall thickness ($t_w = 0.08$ and 0.16 cm) are measured. The fibrous material of $\rho_f = 100$ and 200 kg/m^3 with both texturization conditions are employed in the experiments. The same samples in contact with the fibrous material are then used in another setup (Fig. 4.5), also developed in the present study, for the measurements of

perforation impedance in the presence of mean flow of Ma = 0.05 and 0.1. The empirical expressions of the perforation impedance obtained from the experiments are then utilized in the transmission loss predictions. The following conclusions are reached from the study of perforation impedance:

- The resistance R and the end correction coefficient α of the perforations in contact with air decrease as the porosity increases.
- The fibrous material significantly increases both R and α compared to the perforation in contact with air only.
- For both filling densities, both R and α decrease as the porosity increases, except for the highest porosity ($\phi = 25.2$ %) considered.
- The effect of texturization conditions on the perforation impedance is significant for $\rho_f = 200$ kg/m^3, but not for $\rho_f = 100$ kg/m^3.
- The mean flow of Ma = 0.1 increases R and decreases α, while the effect of mean flow of Ma = 0.05 is insignificant. The decrease of end correction coefficient due to the mean flow is more significant at low porosities.

Transmission Loss

The acoustic properties of fibrous material and perforation impedance measured in the experiments are integrated into the predictions of transmission loss for silencers. Three-dimensional BEM developed in the present study is used primarily to predict the transmission loss because of its ability to treat complex configurations. First, the measured transmission loss of reactive perforated silencers with different porosities

($\phi = 8.4$ and 25.7 %) and hole diameters ($d_h = 0.249$ and 0.498 cm) are compared with the predictions using the empirical perforation impedance obtained in the present study. Then, the reactive silencers are filled with fibrous material with different filling densities ($\rho_f = 100$ and 200 kg/m^3) and texturization conditions. The measured transmission loss of such dissipative silencers are also compared with the BEM predictions. The influence of variation in each parameter of fiber properties and perforation impedance is then illustrated using the BEM predictions.

An experimental setup (Fig. 4.4) for the measurement of transmission loss with mean flow is also designed and fabricated in the present study. The impact of mean flow on the transmission loss is then established by experiments on this setup and the BEM predictions. The variation of internal geometry such as baffles and extended inlet/outlet ducts is also examined using the BEM predictions. Finally, an example of a combination of the dissipative silencer and a reactive Helmholtz resonator is considered. The overall transmission loss of this hybrid silencer is predicted by BEM for various connecting tube lengths between the two components. The following conclusions are drawn from the study of acoustic attenuation in reactive, dissipative, and hybrid silencers:

- The use of fibrous material significantly increases the transmission loss, changing its shape in the frequency domain from multi-dome to a single resonance type.
- The predictions using the complex characteristic impedance and complex wavenumber of the fibrous material combined with the perforation impedance obtained in the present study show a good agreement with the experiments.

- The accuracy of one-dimensional analytical predictions for dissipative silencers is limited to low frequencies.
- The transmission loss of dissipative silencers is dependent on the texturization conditions. Better texturization shows higher transmission loss.
- The transmission loss of dissipative silencers is more sensitive to the variation of wavenumber than the characteristic impedance.
- The perforation effect is more significant for the silencers with higher filling densities and/or lower porosities.
- The transmission loss of dissipative silencers is more sensitive to the variation of reactance, hence the end correction coefficient, than the resistance.
- The mean flow effect on the transmission loss is more substantial for the silencers with lower porosities and smaller hole diameters.
- The use of baffle or extended inlet/outlet increases the noise attenuation depending on the frequencies of interest.
- For the hybrid silencers, the overall transmission loss is similar to the summation of the transmission loss of dissipative and reactive components, except for near the resonance frequencies of a reactive component, where the attenuation is strongly affected by the connecting tube length.

In addition to providing a detailed analysis of dissipative silencers, the present study has also developed experimental methodologies and setups for the measurement of properties that are essential for the prediction of acoustic performance of these silencers. Particularly, the acoustic impedance of perforation in contact with fibrous material

obtained in the present study will contribute towards the accurate predictions of acoustic behavior of dissipative silencers. Such a perforation impedance can be directly utilized for the predictions of dissipative silencers with fibrous material and perforation geometries similar to those of the current study. For the dissipative silencers with the material and/or perforations substantially different than those of the present study, the experimental method suggested here can be employed to obtain the necessary properties. The conclusions of the present study also serve as a design guide for the dissipative or hybrid silencers. For example, an alternative exhaust system for a production engine has been designed based on the findings of the present study, and the assessment of its acoustic performance is presented by Lee *et al.* (2005), as measured in an engine dynamometer laboratory.

The suggestions for future work include: (a) obtaining generalized expressions for the characteristic impedance and wavenumber for different filling densities of fibrous material, and the acoustic impedance of perforations in contact with the fibrous material for various perforation geometry and material; (b) improving the flow impedance tube setup for the higher flow rates by reducing background noise and reflection coefficient from the termination; and (c) investigating further the mean flow effect on the reactive and hybrid silencers using the experimental setup developed in the present study.

APPENDIX A

NOMENCLATURE

A_{in}	magnitudes of incident wave
A_{tr}	magnitudes of transmitted wave
A_n^+	modal amplitude traveling in the positive direction in domain I
A_n^-	modal amplitude traveling in the negative direction in domain I
$B_{1,n},\ B_{2,n},\ B_{3,n},\ B_{4,n}$	coefficients of the eigenfunctions in domain II
B_n^+	modal amplitude traveling in the positive direction in domain II
B_n^-	modal amplitude traveling in the negative direction in domain II
$\tilde{c}$	complex speed of sound in the absorbing material
c_0	speed of sound in air
$\tilde{c}_{ph}$	phase speed of sound in the absorbing material
C_i	edge point coefficient
C_{ac}	acoustic compliance
$C_{ac,D}$	acoustic compliance of the dissipative silencer
C_n^+	modal amplitude traveling in the positive direction in domain III
C_n^-	modal amplitude traveling in the negative direction in domain III
d_1	duct diameter of domain 1
d_2	duct diameter of domain 2
d_h	perforate hole diameter
f	frequency
f_r	resonance frequency of the Helmholtz resonator
$f_{r,P}$	resonance frequency of the perforated silencer
G_{ii}	auto-spectrum of microphones
G_{ij}	cross-spectrum between i and j
H_{ij}	transfer function between microphones i and j
$[I]$	the identity matrix
i	imaginary unit ($=\sqrt{-1}$)
J_0	Bessel function of the first kind of order zero
J_1	Bessel function of the first kind of order one
k	wavenumber
$\tilde{k}$	complex wavenumber in the absorbing material
k_0	wavenumber in air
$k_{A,r,n}$	radial wavenumber in domain I
$k_{A,x,n}$	axial wavenumber in domain I

$k_{B,r,n}$	radial wavenumber in domain IIa
$\tilde{k}_{B,r,n}$	radial wavenumber in domain IIb
$k_{B,x,n}$	axial wavenumber in domain II
$k_{C,r,n}$	radial wavenumber in domain III
$k_{C,x,n}$	axial wavenumber in domain III
ℓ	characteristic dimension
ℓ_1	the length between microphones #1 and #2
ℓ_2	the length between microphones #1 and upstream sample surface
ℓ_3	the length between microphones #3 and upstream sample surface
ℓ_4	the length between microphones #3 and #4
ℓ_5	the length between microphones #2 at the sidebranch and sample surface
ℓ_{eff}	the effective length of a hole
ℓ_f	the length of a fiber sample at the main duct
ℓ'_f	the length of a fiber sample at the sidebranch
ℓ_k	neck length of the Helmholtz resonator
L	silencer length
L_{ac}	acoustic inertance
$L_{ac,D}$	acoustic inertance of the dissipative silencer
L_S	specific inertance of perforation impedance
L_{wi}	incident acoustic power
L_{wt}	transmitted acoustic power
Ma	Mach number of the mean flow
$\vec{n}$	normal vector to the acoustic domain surface
$\vec{n}_x$	x-component of normal vector to the acoustic domain surface
p	acoustic pressure
p_1	acoustic pressure in domain 1
p_2	acoustic pressure in domain 2
p_A	acoustic pressure in domain I
p_B	acoustic pressure in domain II
p_{Ba}	acoustic pressure in domain IIa
p_{Bb}	acoustic pressure in domain IIb
p_C	acoustic pressure in domain III
p_a	acoustic pressure at the upstream of the fiber sample with the first termination condition

p_a'	acoustic pressure at the upstream of the fiber sample with the second termination condition
p_b	acoustic pressure at the downstream of the fiber sample with the first termination condition
p_b'	acoustic pressure at the downstream of the fiber sample with the second termination condition
p_c	acoustic pressure at the perforations contacting air
p_d	acoustic pressure at the perforations contacting fiber
p_f	flow pressure
p_{in}	acoustic pressure at the inlet
p_{out}	acoustic pressure at the outlet
p_H	acoustic pressure at the neck of the Helmholtz resonator
p_{m1}	acoustic pressure at the microphone #1
p_{m2}	acoustic pressure at the microphone #2
p_{m3}	acoustic pressure at the microphone #3
p_{m4}	acoustic pressure at the microphone #4
r_1	duct radius of domains I and III
r_2	duct radius of domain II
r_f	fiber filament radius
R	resistance of perforation impedance
R_1	flow resistance of absorbing material
R_{ac}	acoustic resistance
R_a	reflection coefficient at the upstream sample surface
R_b	reflection coefficient at the downstream sample surface
R_f	flow resistivity of the absorbing material
R_S	Specific resistance of perforation impedance
S	zone area
S_d	main duct area
S_{in}	cross-sectional area of the inlet duct
S_k	cross-sectional area of the Helmholtz resonator neck
S_{out}	cross-sectional area of the outlet duct
t_s	sample thickness of absorbing material
t_w	wall thickness of perforated duct
T_C	room temperature
T_{ij}	transfer matrix elements

TL	transmission loss
u	particle velocity
u_1	particle velocity in domain 1
u_2	particle velocity in domain 2
u_A	particle velocity in domain I
$u_{A,x}$	particle velocity in the axial direction in domain I
u_B	particle velocity in domain II
$u_{Ba,r}$	particle velocity in the radial direction in domain IIa
$u_{Ba,x}$	particle velocity in the radial direction in domain IIa
$u_{Bb,r}$	particle velocity in the radial direction in domain IIb
$u_{Bb,x}$	particle velocity in the axial direction in domain IIb
u_C	particle velocity in domain III
$u_{C,x}$	particle velocity in the axial direction in domain III
u_f	flow velocity
u_H	particle velocity at the neck the Helmholtz resonator
u_h	particle velocity at a hole
u_{in}	particle velocity at the inlet
u_{m2}	particle velocity at the microphone #2
u_{out}	particle velocity at the outlet
u_a	particle velocity at the upstream of the fiber sample with the first termination condition
u_a'	particle velocity at the upstream of the fiber sample with the second termination condition
u_b	particle velocity at the downstream of the fiber sample with the first termination condition
u_b'	particle velocity at the downstream of the fiber sample with the second termination condition
u_c	particle velocity at the perforations contacting air
u_d	particle velocity at the perforations contacting fiber
V	acoustic domain volume
V_a	volume of void or air
V_t	total volume
V_0	mean flow velocity
V_c	cavity volume of the Helmholtz resonator
x, y, z, r	coordinate axes
Y	porosity of absorbing material

Y_0	Bessel function of the second kind of order zero
Y_1	Bessel function of the second kind of order one
$\tilde{Z}$	$\tilde{\rho}\tilde{c}$, complex characteristic impedance of the absorbing material
Z_H	acoustic impedance of the Helmholtz resonator
Z_p	acoustic impedance of perforations
I, II, III	acoustic domains, I, II, and III
α	end correction coefficient of perforation impedance
β	coefficient
δ	Dirac delta function
$\delta_1, \delta_2, \delta_k$	neck end corrections of the Helmholtz resonator facing air
$\tilde{\delta}_1, \tilde{\delta}_2, \tilde{\delta}_k$	neck end corrections of the Helmholtz resonator facing the absorbing material
ϕ	duct porosity
φ	velocity potential
γ	coefficient
Γ	boundary surface
Γ_i	boundary surface of i^{th} discrete acoustic domain
κ	wavenumber
λ_n	eigenvalues
ρ_0	density of air
ρ_f	filling or bulk density of fibrous material
ρ_m	material density of fibrous material
$\tilde{\rho}$	effective density of the absorbing material
ω	angular velocity
ω_r	resonance angular velocity
ψ'	Fok function
$\psi_{A,n}$	eigenfunctions in domain I
$\psi_{Ba,n}$	eigenfunctions in domain IIa
$\psi_{Bb,n}$	eigenfunctions in domain IIb
$\psi_{C,n}$	eigenfunctions in domain III
$[\Psi]$	modal matrix
$\tilde{\zeta}_p$	non-dimensionalized acoustic impedance of perforated plate
$\tilde{\zeta}_h$	non-dimensionalized acoustic impedance of a hole
∇	del operator

Subscripts

A	domain I
B	domain II
C	domain III
o	air
i	i^{th} discrete acoustic domain
j	j^{th} discrete acoustic domain
n	n^{th} mode

Superscripts

i	inlet
o	outlet
p	perforations
$+$	traveling in the positive direction
$-$	traveling in the negative direction

REFERENCES

Åbom, M. and Bodén, H., 1988, "Error analysis of two-microphone measurements in ducts with flow," *Journal of the Acoustical Society of America* **83**, 2429-2438.

Aly, M. E. and Badawy, M. T. S., 2001, "Sound propagation attenuation in lined annular-variable area ducts using bulk-reacting liners," *Applied Acoustics* **62**, 769-778.

Amédin, C. K., Champoux, Y., and Berry, A., 1997, "Acoustical characterization of absorbing porous materials through transmission measurements in a free field," *Journal of the Acoustical Society of America* **102**, 1982-1994.

Astley, R. J. and Cummings, A., 1987, "A finite element scheme for attenuation in ducts lined with porous material: comparison with experiment," *Journal of Sound and Vibration* **116**, 239-263.

ASTM C522-87, 1997, "Standard test method for airflow resistance of acoustical materials," *American Society for Testing and Materials*, 171-175.

ASTM E1050-98, 1998, "Standard test method for impedance and absorption of acoustical materials using a tube, two microphones and a digital frequency analysis system," *American Society for Testing and Materials*, 951-961.

Beranek, L. L., 1940a, "Precision measurement of acoustic impedance," *Journal of the Acoustical Society of America* **12**, 3-13.

Beranek, L. L., 1940b, "Acoustic impedance of commercial materials and the performance of rectangular rooms with one treated surface," *Journal of the Acoustical Society of America* **12**, 14-23.

Beranek, L. L., 1942, "Acoustic impedance of porous materials," *Journal of the Acoustical Society of America* **13**, 248-260.

Beranek, L. L., 1947a, "Some notes on the measurement of acoustic impedance," *Journal of the Acoustical Society of America* **19**, 420-427.

Beranek, L. L., 1947b, "Acoustical properties of homogeneous, isotropic rigid tiles and flexible blankets," *Journal of the Acoustical Society of America* **19**, 556-568.

Beranek, L. L., 1988, "Noise and Vibration Control," *Institute of Noise Control Engineering*, Washington, DC.

Beranek, L. L. and Ver, I. L., 1992, "Noise and Vibration Control Engineering: Principles and Applications," John Wiley & Sons, Inc.

Bies, D. A., Hansen, C. H., and Bridges, G. E., 1991, "Sound attenuation in rectangular and circular cross-section ducts with flow and bulk-reacting liner," *Journal of Sound and Vibration* **146**, 47-80.

Blackstock, D. T., 2000, "Fundamentals of Physical Acoustics," John Wiley & Sons, Inc., New York, NY.

Bodén, H. and Åbom, M., 1986, "Influence of errors on the two-microphone method for measuring acoustic properties in ducts," *Journal of the Acoustical Society of America* **79**, 541-549.

Bokor, A., 1969, "Attenuation of sound in lined ducts," *Journal of Sound and Vibration* **10**, 390-403.

Bolt, R. H., 1947, "On the design of perforated facings for acoustical materials," *Journal of the Acoustical Society of America* **19**, 917-921.

Braccesi, C. and Bracciali, A., 1998, "Least squares estimation of main properties of sound absorbing materials through acoustical measurements," *Applied Acoustics* **54**, 59-70.

Callaway, D. B. and Ramer, L. G., 1952, "The use of perforated facings in designing low frequency resonant absorbers," *Journal of the Acoustical Society of America* **24**, 309-312.

Champoux, Y. and Stinson, M. R., 1991, "Measurement of the characteristic impedance and propagation constant of materials having high flow resistivity," *Journal of the Acoustical Society of America* **90**, 2182-2191.

Chanaud, R. C., 1994, "Effects of geometry on the resonance frequency of Helmholtz resonators, " *Journal of Sound and Vibration* **178**, 337-348.

Chen, W. H., Lee, F. C., and Chiang, D. M., 2000, "On the acoustic absorption of porous materials with different surface shapes and perforated plates," *Journal of Sound and Vibration* **237**, 337-355.

Cheng, C. Y. R. and Wu, T. W., 1999, "Exhaust muffler design and analysis using a boundary element method based computer program," *SAE* 1999-01-1661, 89-95.

Chung, J. Y. and Blaser, D. A., 1980a, "Transfer function method of measuring in-duct acoustic properties. I. Theory," *Journal of the Acoustical Society of America* **68**, 907-913.

Chung, J. Y. and Blaser, D. A., 1980b, "Transfer function method of measuring in-duct acoustic properties. II. Experiment," *Journal of the Acoustical Society of America* **68**, 914-921.

Craggs, A., 1977, "A finite element method for modeling dissipative mufflers with a locally reactive lining," *Journal of Sound and Vibration* **54**, 285-296.

Crocker, M. J., 1998, "Handbook of Acoustics," John Wiley & Sons, Inc., New York.

Cummings, A. and Astley, R. J., 1996, "Finite element computation of attenuation in bar-silencers and comparison with measured data," *Journal of Sound and Vibration* **196**, 351-369.

Cummings, A. and Chang, I.-J., 1987a, "Acoustic propagation in porous media with internal mean flow," *Journal of Sound and Vibration* **114**, 565-581.

Cummings, A. and Chang, I.-J., 1987b, "Internal mean flow effects on the characteristics of bulk-reacting liners in circular ducts," *Acustica* **64**, 169-178.

Cummings, A. and Chang, I.-J., 1988, "Sound attenuation of a finite length dissipative flow duct silencer with internal mean flow in the absorbent," *Journal of Sound and Vibration* **127**, 1-17.

Cummings, A. and Sormaz, N., 1993, "Acoustic attenuation in dissipative splitter silencers containing mean fluid flow," *Journal of Sound and Vibration* **168**, 209-227.

Cummings, A., 1976, "Sound attenuation in ducts lined on two opposite walls with porous material, with some applications to splitters," *Journal of Sound and Vibration* **49**, 9-35.

Cummings, A., 1986, "The effects of grazing turbulent pipe-flow on the impedance of an orifice," *Acustica* **61**, 233-242.

Davern, W. A., 1977, "Perforated facings backed with porous materials as sound absorbers-an experimental study," *Applied Acoustics* **10**, 85-112.

Davies, P. O. A. L., Harrison, M. F., and Collins, H. J., 1997, "Acoustic modeling of multiple path silencers with experimental validations," *Journal of Sound and Vibration* **200**, 195-225.

Davis, D. D., Stokes, G. M., Moore, D., and Stevens, G. L., 1953, "Theoretical and experimental investigation of mufflers with comments on engine-exhaust muffler design," *NACA report* 1192.

Dean, P. D., 1974, "An in situ method of wall acoustic impedance measurement in flow ducts," *Journal of Sound and Vibration* **34**, 97-130.

Delany, M. E. and Bazley, E. N., 1970, "Acoustical properties of fibrous absorbent materials," *Applied Acoustics* **3**, 105-116.

Dickey, N. S. and Selamet, A., 1996, "Helmholtz resonators: one-dimensional limit for small cavity length-to-diameter ratios, " *Journal of Sound and Vibration* **195**, 512-517.

Dickey, N. S., Selamet, A., and Novak, J. M., 2000, "The effect of high-amplitude sound on the attenuation of perforated tube silencers," *Journal of the Acoustical Society of America* **108**, 1068-1081.

Dickey, N. S., Selamet, A., and Ciray, M. S., 2001, "An experimental study of the impedance of perforated plates with grazing flow," *Journal of the Acoustical Society of America* **110**, 2360-2370.

Dokumaci, E., 1996a, "Matrizant approach to acoustic analysis of perforated multiple pipe mufflers carrying mean flow," *Journal of Sound and Vibration* **191**, 505-518.

Dokumaci, E., 1996b, "A subsystem approach for acoustic analysis of mufflers having identical perforated pipes," *Journal of Sound and Vibration* **193**, 985-1001.

Dokumaci, E., 2001, "A discrete approach for analysis of sound transmission in pipes coupled with compact communicating devices," *Journal of Sound and Vibration* **239**, 679-693.

Fukuda, M., 1986, "Muffler", *United States Patent* 4589517.

Glav, R., 1996a, "The point-matching method on dissipative silencers of arbitrary cross-section," *Journal of Sound and Vibration* **189**, 123-135.

Glav, R., 1996b, "The null-field approach to dissipative silencers of arbitrary cross-section," *Journal of Sound and Vibration* **189**, 489-509.

Glav, R., 2000, "The transfer matrix for a dissipative silencer of arbitrary cross-section," *Journal of Sound and Vibration* **236**, 575-594.

Gogate, G. R. and Munjal, M. L., 1993, "Analytical solution of sound propagation in lined or unlined circular ducts with laminar mean flow," *Journal of Sound and Vibration* **160**, 465-484.

Hetherington, T. W., 1989, "Acoustic muffler", *United States Patent* 4846302.

Hisashige, N., Yokogawa F., and Shinhama M., 1991, "Engine exhaust apparatus," *United States Patent* 5025890.

Howe, M. S., 1979, "The influence of grazing flow on the acoustic impedance of a cylindrical wall cavity," *Journal of Sound and Vibration* **67**, 533-544.

Huff, N. T., 2001, "Materials for absorptive silencer systems," *SAE Noise and Vibration Conference and Exposition*, April 30–May 3, SAE Paper 2001-01-1458 Traverse City, MI.

Ingard, U. and Bolt, R. H., 1951a, "A free field method of measuring the absorption coefficient of acoustic materials," *Journal of the Acoustical Society of America* **23**, 509-516.

Ingard, U. and Bolt, R. H., 1951b, "Absorption characteristics of acoustic material with perforated facings," *Journal of the Acoustical Society of America* **23**, 533-540.

Ingard, U., 1953, "On the theory and design of acoustic resonators, " *Journal of the Acoustical Society of America* **25**, 1037-1061.

Ingard. U., 1954a, "Perforated facing and sound absorption," *Journal of the Acoustical Society of America* **26**, 151-154.

Ingard, U., 1954b, "Sound absorption by perforated porous tiles. I," *Journal of the Acoustical Society of America* **26**, 289-293.

Jang, S.-H. and Ih, J.-G., 1998, "On the multiple microphone method for measuring in-duct acoustic properties in the presence of mean flow," *Journal of the Acoustical Society of America* **103**, 1520-1526.

Jayaraman, K. and Yam, K., 1981, "Decoupling approach to modeling perforated tube muffler components," *Journal of the Acoustical Society of America* **69**, 390-396.

Ji, Z. L. and Selamet, A., 1999, "Boundary element analysis of a three-pass perforated duct muffler," *Proceedings Inter–Noise 99*, December 6–8, Ft. Lauderdale, FL., 557-562.

Ji, Z. L., Ma, Q., and Zhang, Z. H., 1994, "Application of the boundary element method to predicting acoustic performance of expansion chamber mufflers with mean flow," *Journal of Sound and Vibration* **173**, 57-71.

Ji, Z. L., Ma, Q., and Zhang, Z. H., 1995, "A boundary element scheme for evaluation of four-pole parameters of ducts and mufflers with low Mach number non-uniform flow," *Journal of Sound and Vibration* **185**, 107-117.

Jing, X., Sun, X., Wu, J., and Meng, K., 2001, "Effect of grazing flow on the acoustic impedance of an orifice," *American Institute of Aeronautics and Astronautics Journal* **39**, 1478-1484.

Jones, M. G. and Stiede, P. E., 1997, "Comparison of methods for determining specific acoustic impedance," *Journal of the Acoustical Society of America* **101**, 2694-2704.

Jones, M. G., Tracy, M. B., Watson, W. R., and Parrott, T. L., 2002, "Effects of liner geometry on acoustic impedance," *American Institute of Aeronautics and Astronautics*, AIAA-2002-2446.

Kagawa, Y., Yamabuchi, T., and Mori, A., 1977, "Finite element simulation of an axisymmetric acoustic transmission system with a sound absorbing wall," *Journal of Sound and Vibration* **53**, 357-374.

Kakoty, S. K. and Roy, V. K., 2002, "Bulk reaction modeling of ducts with and without mean flow," *Journal of the Acoustical Society of America* **112**, 75-83.

Kang, Y. J. and Jung, I. H., 2001, "Sound propagation in circular ducts lined with noise control foams," *Journal of Sound and Vibration* **239**, 255-273.

Katz, B. F. G., 2000, "Method to resolve microphone and sample location errors in the two-microphone duct measurement method," *Journal of the Acoustical Society of America* **108**, 2231-2237.

Kim, Y.-H. and Yoon, D.-B., 1995, "An experimental study of the acoustic characteristics of perforated pipe in terms of wavenumber and porosity," *Journal of Sound and Vibration* **183**, 115-127.

King, A. J., 1958, "Attenuation of sound in lined air duct," *Journal of the Acoustical Society of America* **30**, 505-507.

Kirby, R. and Cummings, A., 1998, "The impedance of perforated plates subjected to grazing gas flow and backed by porous media," *Journal of Sound and Vibration* **217**, 619-636.

Kirby, R. and Cummings, A., 1999, "Prediction of the bulk acoustic properties of fibrous materials at low frequencies," *Applied Acoustics* **56**, 101-125.

Kirby, R., 2001, "Simplified techniques for predicting the transmission loss of a circular dissipative silencer," *Journal of Sound and Vibration* **243**, 403-426.

Kirby, R., 2003, "Transmission loss predictions for dissipative silencers of arbitrary cross section in the presence of mean flow," *Journal of the Acoustical Society of America* **114**, 200-209.

Ko, S.–H., 1972, "Sound attenuation in acoustically lined circular ducts in the presence of uniform flow and shear flow," *Journal of Sound and Vibration* **22**, 193-210.

Kraai, L. A., Sager, R. L., and Hill, W. E., 1994, "Low backpressure straight-through reactive and dissipative muffler," *United States Patent* 5365025.

Kurze, U. J. and Ver, I. L., 1972, "Sound attenuation in ducts lined with non-isotropic material," *Journal of Sound and Vibration* **24**, 177-187.

Lee, I.-J., Selamet, A., and Huff, N. T., 2003, "Acoustic characteristics of coupled dissipative and reactive silencers," *SAE Noise and Vibration Conference and Exposition*, May 5-8, Traverse City, MI, SAE Paper 2003-01-1643.

Lee, I.-J., Selamet, A., Huff, N. T., and Hrdlicka, M., 2005, "Design of a hybrid silencing systems for a production engine," SAE Noise and Vibration Conference and Exposition, May 16-19, Traverse City, MI, SAE Paper 2005-01-2349.

Lee, F.-C. and Chen, W.-H., 2001, "Acoustic transmission analysis of multi-layer absorbers," *Journal of Sound and Vibration* **248**, 621-634.

Lee, S.-H. and Ih, J.-G., 2003, "Empirical model of the acoustic impedance of a circular orifice in grazing mean flow," *Journal of the Acoustical Society of America* **114**, 98-113.

Luo, H., Tse, C. C., and Chen, Y. N., 1995, "Modeling and applications of partially perforated intruding tube mufflers," *Applied Acoustics* **44**, 99-116.

Manning, W. L., 1939, "Silencer, " *United States Patent* 2166417.

Mclntosh, J. D., Zuroski, M. T., and Lambert, R. F., 1990, "Standing wave apparatus for measuring fundamental properties of acoustic materials in air," *Journal of the Acoustical Society of America* **88**, 1929-1938.

Mechel, F. P., 1990a, "Numerical results to the theory of baffle-type silencers," *Acustica* **72**, 7-20.

Mechel, F. P., 1990b, "Theory of baffle-type silencers," *Acustica* **70**, 93-111.

Mechel, F. P., 1992, "Chapter 8 sound-absorbing materials and sound absorbers," *Noise and Vibration Control Engineering*, Edited by Beranek, L. L. and Vér, I. L., John Wiley and Sons, INC.

Melling, T. H., 1973, "The acoustic impedance of perforates at medium and high sound pressure levels," *Journal of Sound and Vibration* **29**, 1-65.

Meyer, E., Mechel, F., and Kurtze, G., 1958, "Experiments on the influence of flow on sound attenuation in absorbing ducts," *Journal of the Acoustical Society of America* **30**, 165-174.

Morse, P. M., 1939a, "Some aspects of the theory of room acoustics," *Journal of the Acoustical Society of America* **11**, 56-66.

Morse, P. M., 1939b, "The transmission of sound inside pipes," *Journal of the Acoustical Society of America* **11**, 205-210.

Morse, P. M., Bolt, R. H., and Brown, R. L., 1940, "Acoustic impedance and sound absorption," *Journal of the Acoustical Society of America* **12**, 217-227.

Munjal, M. L. and Doige, A. G., 1990, "The two-microphone method incorporating the effects of mean flow and acoustic damping," *Journal of Sound and Vibration* **137**, 135-138.

Munjal, M. L., 1987, "Acoustics of Ducts and Mufflers," John Wiley and Sons, Inc., New York.

Munjal, M. L., 2001, "An error inherent in the use of the two-microphone method for gas pulsation measurement in a reflective environment," *Journal of Sound and Vibration* **242**, 539-541.

Munjal, M. L., Behera, B. K., and Thawani, P. T., 1998, "Transfer matrix model for the reverse-flow, three-duct, open end perforated element muffler," *Applied Acoustics* **54**, 229-238.

Nelson, C. E., 1937, "Silencer", *United States Patent* 2072961.

Nice, M. and Godfrey, D., 2000, "Measurement of characteristic impedance and propagation constant for trim packages," *Proceedings of the First International AutoSEA Users Conf.*, July 27–28, San Diego, CA.

Nice, M.,1999 Internal report, Owens Corning Automotive.

Nichols, R. H., 1947, "Flow-resistance characteristics of fibrous acoustical materials," *Journal of the Acoustical Society of America* **19**, 866-871.

Park, C.-M., Ih, J.-G., Nakayama, Y., and Takao, H., 2003, "Inverse estimation of the acoustic impedance of a porous woven hose from measured transmission coefficients," *Journal of the Acoustical Society of America* **113**, 128-138.

Peat, K. S., 1988; "A numerical decoupling analysis of perforated pipe silencer elements," *Journal of Sound and Vibration* **123**, 199-212.

Peat, K. S., 1991, "A transfer matrix for an absorption silencer element," *Journal of Sound and Vibration* **146**, 353-360.

Peat, K. S. and Pathi, K. L., 1995, "A finite element analysis of the convected acoustic wave motion in dissipative silencers," *Journal of Sound and Vibration* **184**, 529-545.

Peik, P. G., 1935, "Muffler," *United States Patent*, 2014666.

Pierce, A. D., 1991, "Acoustics; An Introduction to Its Physical Principles and Applications," *Acoustical Society of America,* Woodbury, New York.

Rao, K. N. and Munjal, M. L., 1986, "Experimental evaluation of impedance of perforates with grazing flow," *Journal of Sound and Vibration* **108**, 283-295.

Reichert, R. S. and Biringen, S., 2001, "Time-domain simulation of acoustic propagation in a lined duct," *Applied Acoustics* **62**, 1049-1068.

Rienstra, S. W., 1985, "Contributions to the theory of sound propagation in ducts with bulk-reacting lining," *Journal of the Acoustical Society of America* **77**, 1681-1685.

Rschevkin, S. N., 1963 "A Course of Lectures on The Theory of Sound," The Macmillan company, New York.

Salikuddin, M., Syed, A. A., and Mungur, P., 1994, "Acoustic characteristics of perforated sheets with through flow in a high intensity noise environment," *Journal of Sound and Vibration* **169**, 145-177.

Sbardella, L., Tester, B. J., and Imregun, M., 2001, "A time-domain method for the prediction of sound attenuation in lined ducts," *Journal of Sound and Vibration* **293**, 379-396.

Schmidt, U., 1937, "Sound muffling device," *United States Patent* 2101460.

Scott, R. A., 1946a, "The absorption of sound in a homogeneous porous medium," *Proceedings of the Physical Society* **58**, 165-183.

Scott, R. A., 1946b, "An apparatus for accurate measurement of the acoustic impedance of sound-absorbing materials," *Proceedings of the Physical Society* **58**, 253-264.

Scott, R. A., 1946c, "The propagation of sound between walls of porous material," *Proceedings of the Physical Society* **58**, 358-368.

Selamet, A. and Ji, Z. L., 2000, "Circular asymmetric Helmholtz resonators," *Journal of the Acoustical Society of America* **107**, 2360-2369.

Selamet, A., Lee, I.-J., Ji, Z. L., and Huff, N. T., 2001 "Acoustic attenuation performance of perforated concentric absorbing silencers," SAE Noise and Vibration Conference and Exposition, April 30–May 3, Traverse City, MI, SAE Paper 2001-01-1435.

Selamet, A., Radavich, P. M., Dickey, N. S., and Novak, J. M., 1997, "Circular concentric Helmholtz resonator, " *Journal of the Acoustical Society of America* **101**, 41-51.

Selamet, A., Lee, I.-J., and Huff, N. T., 2003, "Acoustic attenuation of hybrid silencers" *Journal of Sound and Vibration* **262**, 509-527.

Selamet, A., Xu, M. B., Lee, I.-J., and Huff, N. T., 2004, "Analytical approach for sound attenuation in perforated dissipative silencers," *Journal of the Acoustical Society of America* **115**, 2091-2099.

Selamet, A., Xu, M. B., Lee, I.-J., and Huff, N. T., 2005a, "Helmholtz resonator lined with absorbing material," *Journal of the Acoustical Society of America* **117**, 725-733.

Selamet, A., Xu, M. B., Lee, I.-J., and Huff, N. T., 2005b, "Analytical approach for sound attenuation in perforated silencers with inlet/outlet extensions," *Journal of the Acoustical Society of America* **117**, 2078-2089.

Seybert, A. F. and Ross, D. F., 1977, "Experimental determination of acoustic properties using a two-microphone random-excitation technique," *Journal of the Acoustical Society of America* **61**, 1362-1370.

Seybert, A. F. and Soenarko, B., 1981, "Error analysis of spectral estimates with application to the measurement of acoustic parameters using random fields in ducts," *Journal of the Acoustical Society of America* **69**, 1190-1199.

Smith, C. D. and Parrott, T. L., 1983, "Comparison of three methods for measuring acoustic properties of bulk materials," *Journal of the Acoustical Society of America* **74**, 1577-1582.

Song, B. H. and Bolton, J. S., 2000, "A transfer-matrix approach for estimating the characteristic impedance and wave numbers of limp and rigid porous materials," *Journal of the Acoustical Society of America* **107**, 1131-1152.

Sterrett, D. E., Pekrul, E. C., and Turner, T. P., 1998, "Multi-chamber muffler with selective sound absorbent material placement," *United States Patent* 5783782.

Sullivan, J. W. and Crocker, M. J., 1978, "Analysis of concentric-tube resonators having unpartitioned cavities," *Journal of the Acoustical Society of America* **64**, 207-215.

Sullivan, J. W., 1979a, "A method for modeling perforated tube muffler components. I. Theory," *Journal of the Acoustical Society of America* **66**, 772-778.

Sullivan, J. W., 1979b, "A method for modeling perforated tube muffler components. II. Applications," *Journal of the Acoustical Society of America* **66**, 779-788.

Sun, X., Jing, X., Zhang, H., and Shi, Y., 2002, "Effect of grazing-bias flow interaction on acoustic impedance of perforated plates," *Journal of Sound and Vibration* **254**, 557-573.

Tack, D. H. and Lambert, R. F., 1965, "Influence of shear flow on sound attenuation in a lined duct," *Journal of the Acoustical Society of America* **14**, 655-666.

Takahashi, D., 1997, "A new method for predicting the sound absorption of perforated absorber systems," *Applied Acoustics* **51**, 71-84.

Tanaka, H., Sekiya, M., and Uchikawa, F., 1987, "Muffler for exhaust gas from internal combustion engine," *United States Patent* 4700805.

Tang, P. K. and Sirignano, W. A., 1973, "Theory of a generalized Helmholtz resonator, " *Journal of Sound and Vibration* **26**, 247-262.

Tao, Z., Herrin, D. W., and Seybert, A. F., 2003, "Measuring bulk properties of sound-absorbing materials using the two-source method," *SAE Noise and Vibration Conference and Exposition*, May 5-8, Traverse City, MI, SAE Paper 2003-01-1586.

Tarnow, V., 1997, "Calculation of the dynamic air flow resistivity of fiber materials," *Journal of the Acoustical Society of America* **102**, 1680-1688.

Tarnow, V., 2002, "Measured anisotropic air flow resistivity and sound attenuation of glass wool," *Journal of the Acoustical Society of America* **111**, 2735-2739.

Thawani, P. T. and Jayaraman, K., 1983, "Modeling and applications of straight-through resonators," *Journal of the Acoustical Society of America* **73**, 1387-1389.

Udell, R. R., 1990, "Noise attenuation apparatus," *United States Patent* 4930597.

Utsuno, H., Tanaka, T., Fujikawa, T., and Seybert, A. F., 1989, "Transfer function method for measuring characteristic impedance and propagation constant of porous materials," *Journal of the Acoustical Society of America* **86**, 637-643.

Wang, C. N., 1999, "Numerical decoupling analysis of a resonator with absorbent material," *Applied Acoustics* **58,** 109-122.

Wang, C.-N. and Liao, C.-Y., 1998, "Boundary integral equation method for evaluating the performance of straight-through resonator with mean flow," *Journal of Sound and Vibration* **216**, 281-294.

Wang, C.-N. and Torng, J.-H, 2001, "Experimental study of the absorption characteristics of some porous fibrous materials," *Applied Acoustics* **62**, 447-459.

Wang, C.-N., 1999, "Numerical decoupling analysis of a resonator with absorbent material," *Applied Acoustics* **58**, 109-122.

Wang, C.-N., Tse, C.-C., and Chen, Y.-N., 1993, "Analysis of three dimensional muffler with boundary element method," *Applied Acoustics* **40**, 91-106.

Wassilieff, C., 1987, "Experimental verification of duct attenuation models with bulk reacting linings," *Journal of Sound and Vibration* **114**, 239-251.

Wilson, D. K., 1997, "Simple, relaxational models for the acoustical properties of porous media," *Applied Acoustics* **50**, 171-188.

Wolfhugel, G., 1983, "Muffler", *United States Patent* 4396090.

Woodcock, R. and Hodgson, M., 1992, "Acoustic methods for determining the effective flow resistivity of fibrous materials," *Journal of Sound and Vibration* **153**, 186-191.

Wu, T. W., Zhang, P., and Cheng, C. Y. R., 1998, "Boundary element analysis of mufflers with an improved method for deriving the four-pole parameters," *Journal of Sound and Vibration* **217**, 767-779.

Wu, T. W., Cheng, C. Y. R., and Zhang, P., 2002, "A direct mixed-body boundary element method for packed silencers," *Journal of the Acoustical Society of America* **111**, 2566-2572.

Wu, T. W., Cheng, C. Y. R., and Tao, Z., 2003, "Boundary element analysis of packed silencers with protective cloth and embedded thin surfaces," *Journal of Sound and Vibration* **261**, 1-15.

Wu, T. W., Zhang, P., and Cheng, C. Y. R., 1998, "Boundary element analysis of mufflers with an improved method for deriving the four-pole parameters," *Journal of Sound and Vibration* **217**, 767-779.

Xu, M. B., Zhang, X. M., and Zhang, W. H., 1999, "The effect of wall joint on the vibrational power flow propagation in a fluid-filled shell," *Journal of Sound and Vibration* **224**, 395-410.

Xu, M. B., Selamet, A., Lee, I.-J., and Huff, N. T., 2004, "Sound attenuation in dissipative expansion chambers," *Journal of Sound and Vibration* **272**, 1125-1133.

Yaniv, S. L., 1973, "Impedance tube measurement of propagation constant and characteristic impedance of porous acoustical material," *Journal of the Acoustical Society of America* **54**, 1138-1142.